34299

National Library of Canada | Bibliothèque nationale du Canada

CANADIAN THESES ON MICROFICHE | THÈSES CANADIENNES SUR MICROFICHE

NAME OF AUTHOR/*NOM DE L'AUTEUR* Richard George Bramm

TITLE OF THESIS/*TITRE DE LA THÈSE* A Grain-Size Sampling Theory and Its Application to the Photographic Grid Sampling of Terrace Gravels

UNIVERSITY/*UNIVERSITÉ* The University of Alberta

DEGREE FOR WHICH THESIS WAS PRESENTED/*GRADE POUR LEQUEL CETTE THÈSE FUT PRÉSENTÉE* M.Sc

YEAR THIS DEGREE CONFERRED/*ANNÉE D'OBTENTION DE CE GRADE* 1977

NAME OF SUPERVISOR/*NOM DU DIRECTEUR DE THÈSE* Dr. Ian Campbell

Permission is hereby granted to the NATIONAL LIBRARY OF CANADA to microfilm this thesis and to lend or sell copies of the film.

The author reserves other publication rights, and neither the thesis nor extensive extracts from it may be printed or otherwise reproduced without the author's written permission.

L'autorisation est, par la présente, accordée à la BIBLIOTHÈQUE NATIONALE DU CANADA de microfilmer cette thèse et de prêter ou de vendre des exemplaires du film.

L'auteur se réserve les autres droits de publication; ni la thèse ni de longs extraits de celle-ci ne doivent être imprimés ou autrement reproduits sans l'autorisation écrite de l'auteur.

DATED/*DATÉ* Oct 21/77 SIGNED/*SIGNÉ* Richard George Bramm

PERMANENT ADDRESS/*RÉSIDENCE FIXE* 11-10839 University Ave.
Edmonton, Alberta
T6E 4R1

NL-91 (3-74)

National Library of Canada

Cataloguing Branch
Canadian Theses Division

Ottawa, Canada
K1A 0N4

Bibliothèque nationale du Canada

Direction du catalogage
Division des thèses canadiennes

NOTICE

The quality of this microfiche is heavily dependent upon the quality of the original thesis submitted for microfilming. Every effort has been made to ensure the highest quality of reproduction possible.

If pages are missing, contact the university which granted the degree.

Some pages may have indistinct print especially if the original pages were typed with a poor typewriter ribbon or if the university sent us a poor photocopy.

Previously copyrighted materials (journal articles, published tests, etc.) are not filmed.

Reproduction in full or in part of this film is governed by the Canadian Copyright Act, R.S.C. 1970, c. C-30. Please read the authorization forms which accompany this thesis.

THIS DISSERTATION
HAS BEEN MICROFILMED
EXACTLY AS RECEIVED

AVIS

La qualité de cette microfiche dépend grandement de la qualité de la thèse soumise au microfilmage. Nous avons tout fait pour assurer une qualité supérieure de reproduction.

S'il manque des pages, veuillez communiquer avec l'université qui a conféré le grade.

La qualité d'impression de certaines pages peut laisser à désirer, surtout si les pages originales ont été dactylographiées à l'aide d'un ruban usé ou si l'université nous a fait parvenir une photocopie de mauvaise qualité.

Les documents qui font déjà l'objet d'un droit d'auteur (articles de revue, examens publiés, etc.) ne sont pas microfilmés.

La reproduction, même partielle, de ce microfilm est soumise à la Loi canadienne sur le droit d'auteur, SRC 1970, c. C-30. Veuillez prendre connaissance des formules d'autorisation qui accompagnent cette thèse.

LA THÈSE A ÉTÉ
MICROFILMÉE TELLE QUE
NOUS L'AVONS REÇUE

THE UNIVERSITY OF ALBERTA

A GRAIN-SIZE SAMPLING THEORY AND ITS APPLICATION TO THE PHOTOGRAPHIC GRID SAMPLING OF TERRACE GRAVELS

by

© RICHARD GEORGE BRAMM

A THESIS

SUBMITTED TO THE FACULTY OF GRADUATE STUDIES IN

PARTIAL FULFILMENT OF THE REQUIREMENTS FOR THE DEGREE

OF MASTER OF SCIENCE

DEPARTMENT OF GEOGRAPHY

EDMONTON, ALBERTA

FALL, 1977

UNIVERSITY OF ALBERTA

FACULTY OF GRADUATE STUDIES AND RESEARCH

The undersigned certify that they have read, and recommend to the Faculty of Graduate Studies for acceptance, a thesis entitled "A Grain-Size Sampling Theory and Its Application to the Photographic Grid Sampling of Terrace Gravels," submitted by Richard George Bramm in partial fulfilment of the requirements for the degree of Master of Science.

K. R. Samaha

Supervisor

John Shaw

External Examiner

Date October 21, 1977

ABSTRACT

Grain-size sampling of densely packed particulate materials by customary bulk sieve analysis is sometimes very difficult. In an attempt to find an equivalent alternative to bulk sieve analysis this thesis examines a probabalistic grain-size sampling theory proposed by Kellerhals et al (1975) here designated as the numerical method, and four related empirical sampling experiments.

Three of the experiments incorporate results found within the literature. Data from Kellerhals' et al (1975) and Friedman's (1962) grid-by-number thin section experiments and McGinn's (1971) grid-by-number gravel bar investigation all tend to confirm the applicability of the numerical method and grid-by-number as a solution to this sampling problem.

The fourth experiment involved the grid-by-number investigation of terrace gravels. It is shown that a terrace gravel surface may in some circumstances be treated as a thin section surface. The statistical results of this final study strongly confirm numerical method predictions.

Generally, the results of these experiments indicate that for a wide variety of sampling situations the grid-by-number sampling technique in conjunction with the numerical method can provide at least median and mean values equivalent to those obtained by sieving.

INTRODUCTION

Grain-size sampling of densely packed particulate materials such as clastic sediments has usually depended upon customary bulk sieve analysis. In a number of sampling situations the application of this standard technique is difficult. For instance, the disaggregation of a sandstone for sieve analysis or the collection of the large gravel samples that are necessary for representativeness may be so laborious as to be impractical. What is required and what has long been sought is an alternative system of sampling which avoids these impediments and yields grain-size distributions which are the same as those derived by bulk sieve analysis.

Central to this thesis is the empirical investigation of one grain-size sampling theory which possibly provides an equivalent alternative to bulk sieve analysis. The probabalistic sampling theory proposed by Kellerhals et al (1975), here designated as the numerical method, employs a computer program to simulate grid-by-number sampling of a randomly selected thin section obtained from an isotropic material composed of identical ellipsoidal grains. For a given uniform material the numerical method predicts the relationships among true axial dimensions, square mesh sieve size and k values of the constituent equi-sized ellipsoidal grains. Furthermore, the probabalistic association of these ellipsoidal properties and the mean values of the major and minor apparent axial cumulative distributions are given.

Mathematical models of complex natural structures and processes are generally idealizations. The numerical method assumes that the material being sampled is uniform, while virtually all clastic sediments

are nonuniform. For the numerical method to be useful it must be shown that its predictions are confirmed for the sampling of nonuniform materials. A number of sampling experiments employing nonuniform materials can be designed to test specific numerical method relationships. Fortunately, experimental data found within the literature can be utilized in some instances for this purpose. The thin section experiment accompanying the Kellerhals et al (1975) paper is reviewed and further analyzed. Data from Friedman's (1962) thin section and McGinn's (1971) gravel bar experiments are reexamined. In the three experiments numerical method predictions are tested through the comparison of grid-by-number and sieve distributions.

Other possibilities remain for checking numerical method predictions. This study presents the results of a fourth experiment which employs terrace gravels. These gravels are often exposed in cut-banks in which the face of the deposit is almost vertical. Proving that a thin section surface and a terrace gravel photograph are equivalent is essential for this sampling experiment and as such is the subject of an extensive discussion. The terrace gravel experiment involves the grid-by-number sampling and subsequent measurement of true axes in the field and apparent axes from photographs of the same clasts. The numerical method predictions based on the true and apparent axial cumulative distributions are then examined.

ACKNOWLEDGEMENTS

To my mind, my thesis is more than what is presented here; it is all those things which happened along the way to make it possible. I would like to acknowledge a few of the many people who have helped me in the last couple of years.

My constant conceptual companion most surely was my supervisor, Dr. Ian Campbell. As well as offering many critical suggestions and unwavering enthusiasm, he had faith in my curiosity and my ability to find the right path amongst a plurality of alternatives.

Dr. John Shaw and Rod McGinn have already been contibutors in the area of research investigated by this thesis. It was my good fortune to be able to talk with them on numerous occasions. These conversations were essential to my understanding of my thesis problem.

I would like to thank all those who took the time to ask me what I was investigating. My attempts at giving the basics and sometimes the details often led to new insights. As well, I would like to acknowledge the typists who worked on the manuscript, Karen Hawryluk and Jill Bell. Their patience in dealing with the profusion of terms with subscripts is most appreciated.

Finally, I would like to thank my wife, Susan. Without her support this thesis would never have been written.

TABLE OF CONTENTS

	Page
ABSTRACT	iv
INTRODUCTION	v
ACKNOWLEDGEMENTS	vii
TABLE OF CONTENTS	viii
LIST OF TABLES	xi
LIST OF FIGURES	xiii
LIST OF TERMS	xv
CHAPTER ONE SURFACE SAMPLING EQUIVALENCE PROBLEMS	1
1.1 General Introduction	1
1.2 Properties of a Densely Packed Granular Material	2
1.2.0 Introduction	2
1.2.1 Sorting	2
1.2.2 Fabric	2
1.2.3 Induration	3
1.2.4 Grain Shape	3
1.3 Comparison of Gravel Bar, Terrace Gravel and Thin Section Surfaces	3
1.3.0 Introduction	3
1.3.1 Inter Grain Contact	5
1.3.2 Three Contact Modes	6
1.3.3 Graphic Experiment 1	7
1.3.4 Graphic Experiment 2 and Description of Overlapping Grain Surface (OGS) and Embedded Grain Surface (EGS)	16
1.3.5 Comparison of Apparent OGS, Apparent EGS and Thin Section	25
1.3.6 Grain-size Measurement on Apparent OGS and EGS and Thin Section	26
1.4 Sampling Procedures	27
1.4.0 Introduction	27
1.4.1 Step I Collection of Sample	28
1.4.2 Step II Grain-size Measurement and Step III Frequencies	28
1.4.3 The Concept of Geometric Equivalence and Its Importance	29
1.4.4 Determination of Conversion Factors for Steps I and III	30
1.4.5 Combined Conversion Factors for Nine Sampling Procedures	35
1.4.6 Geometric Equivalence and Equivalent Grain-size Measures	37
1.5 Grid-by-Number Sampling of the Surface Layer of Exposed Gravel Bars	37
1.5.0 Introduction	37
1.5.1 Comparison of Bulk Sieve and Grid-by-Number (B_t) Distributions	38

1.5.2 Comparison of Grid-by-Number (B_t) and (b_t) Distributions 41
1.5.3 Comparison of Bulk Sieve and Grid-by-Number (b_t) Distributions 43
1.5.4 Relative Coarseness of Grid-by-Number (B_t) Distributions 43

CHAPTER TWO THE NUMERICAL METHOD AND THREE EMPIRICAL TESTS 45

2.1 General Introduction 45
2.2 The Numerical Method 46
2.2.0 Introduction 46
2.2.1 Computation 46
2.2.2 Relationship among D_s, B and k_2 48
2.2.3 Apparent Axial Distributions a^2 and b 50
2.3 Three Empirical Experiments 55
2.3.0 Introduction 55
2.3.1 Experiment 1 55
2.3.2 Experiment 2 58
2.3.3 Experiment 3 61
2.3.4 Conclusion 67

CHAPTER THREE TERRACE GRAVEL EXPERIMENT METHODOLOGY 68

3.1 General Introduction 68
3.2 The Study Area 68
3.3 Field Methods 71
3.3.0 Introduction 71
3.3.1 Site Selection 71
3.3.2 Grid Placement, Grain Selection and Measurement 72
3.4 Data Analysis 77
3.4.0 Introduction 77
3.4.1 Primary Data Analysis 77
3.4.2 The Wilcoxon Matched Pairs Signed Ranks Test 78
3.4.3 Testing Procedures A to F 79

CHAPTER FOUR TERRACE GRAVEL EXPERIMENT RESULTS AND DISCUSSION 83

4.1 General Introduction 83
4.2 The Data Used in the Wilcoxon Tests 83
4.3 Experimental Results and Discussion 83
4.3.0 Introduction 83
4.3.1 Testing Procedure A 83
4.3.2 Testing Procedure B 86
4.3.3 Testing Procedure C 89
4.3.4 Testing Procedure D 89
4.3.5 Testing Procedure E 89
4.3.6 Testing Prodecure F 91
4.3.7 Conclusion 95

CHAPTER FIVE SUMMARY AND CONCLUSIONS 98

5.1 General Introduction 98
5.2 The Four Empirical Experiments and the Numerical Method 98
5.3 Photographic Sampling of Gravel Surfaces 100
5.3.0 Introduction 100
5.3.1 Photographic Sampling of an Apparent OGS 100
5.3.2 Photographic Sampling of an Apparent EGS 101
5.3.3 General Features of Apparent Surface Photographic Sampling 102
5.3.4 Advantages of Photographic Sampling 103

BIBLIOGRAPHY 104

APPENDIX I Important Ø Values of all True and Apparent Axial Distributions 106

APPENDIX II Median and Mean Ø Values for all True Axial Distributions 112

APPENDIX III Grid Camera Bracket 114

APPENDIX IV Field and Data Analysis Procedures Used to Obtain the Predicted Median and Mean Sieve Diameters, d_{sp50} and $\bar{d}_{sp}$ 116

LIST OF TABLES

Table		Page
1	Results of Graphic Experiment 1	11
2	Maximization and Minimization of $\frac{MPD}{ASD}$ %	14
3	Results of Graphic Experiment 2	18
4	Thin Section Sampling Procedures and Combined Conversion Factors	36
5	B Values Calculated by Equation (3), D_s=1.0, k_2 range 0.001 to 1.0	51
6	Axial Inequalities for Ellipsoids with Common k Values, 0.55-0.75	53
7	Comparison Between Predicted and Actual Median Sieve Sizes, d_{sp50} and $D_{sieve50}$ (adopted from Kellerhals et al, 1975, Table 1)	57
8	The Ratio $\bar{a}_t:\bar{D}_{sieve}$ Based on Thin Section Grid-by-Number Analysis and Bulk Sieve Analysis (adopted from Friedman, 1962, Table 2a)	59
9	Some k_1, k_2 Pairs for which $\bar{a}$: D_s=1:1 or 1.16:1	60
10	Ratios. Sample Weight Q:D_{sieve2}, $\bar{B}_t:\bar{D}_{sieve2}$, $\bar{Q}_{sieve}:\bar{D}_{sieve2}$ and $\bar{B}_t:\bar{Q}_{sieve}$ (adopted from McGinn, 1971, Appendix I)	64
11	Matched Pair Groups	82
12	Wilcoxon Test Comparison of True and Apparent Axial Distribution Parameters	84
13a	C_{p50}, a_{p50}, b_{p50}, D_{sp50} and d_{sp} Values in mm. for the 20 Grids	87
13b	$\bar{C}_p$, $\bar{a}_p$, $\bar{b}_p$, $\bar{D}_{sp}$ and $\bar{d}_{sp}$ Values in mm. for the 20 Grids	88
14	Ranges of $\frac{(\bar{a}-B)100}{B} = X$ and $\frac{(\bar{b}-C)100}{C} = Y$ in Tables 13a and b	89

15	Wilcoxon Test (two-tailed) and Arithmetic and Weighted Mean Results for Four Average k_2 Estimate Methods	89
16	Ø Values for 8 Sets of Matched Pairs which are Predicted to be Equivalent	92
17	Analysis of Matched Pair Differences within Matched Pair Groups	93
18	Grids with Large Differences (.4, .5, .6) in Table 17	94
19	Summary of Testing Procedures B, C, and E	96
20	Variations among the Four Empirical Experiments	99

LIST OF FIGURES

Figure		Page
1	Ellipsoidal Grain and Associated Contact Planes	6
2	Ellipsoidal Cross-Sections Illustrating Three Contact Modes	7
3	The Minimizing Plane Dimension (MPD) and Apparent Surface Dimension (ASD) of Oriented Ellipse $\frac{\text{Minor axis}}{\text{Major axis}} = 0.75$	9
4	Graphic Experiment 1, Contact Mode Behavior of Circular and Elliptical Plane Figures	10
5	Graphic Summary of Table 1 Data	13
6	Graphic Experiment 2, Oriented Ellipses with One Point of Boundary on the Surface Plane	19
7	Limits of Total Representation of Elliptical Grains on a Surface Plane (refer Table 3)	20
8	An Apparent OGS	22
9	An Apparent EGS	24
10	Sample of Densely Packed Cubes of Three Sizes (from Kellerhals and Bray 1971, p.1170)	32
11	Axonometric Pictorial of an Ellipsoid Intersected by a Plane	47
12a,b,c	The Relationship of an Ellipse to a Square Hole: Three Cases	49
13	Graph of Table 5 Data	51
14a,b	Difference Between the Sample Mean of Apparent Axes and the Corresponding True Axes (from Kellerhals *et al* 1975, p.88)	52
15a	Regions where $\bar{a} > D_s$ and $D_s > \bar{a}$ (adapted from Kellerhals *et al* 1975, Figure 5a)	60
15b	$\bar{a}:D_s$ Values for k_1, k_2 Pairs Within the Common Range (refer Table 6)	60

16	The Study Area, Whitemud and Weed Creeks near Edmonton, Alberta	69
17a	A Grid and Associated Terrace Gravels	73
17b	A Grid and Its Fixed Frame of Reference	73
18a	Grid and Unsprayed Terrace Gravel Surface	76
18b	Grid and Sprayed Terrace Gravel Surface	76
19	Grid Photograph Taken by means of Grid Camera Bracket and Cable Shutter Release	115

LIST OF TERMS

MPD	denotes the minimizing plane dimension which is the line resulting from the intersection of the minimizing plane and the plane produced by sectioning.
ASD	denotes the apparent surface dimension which corresponds to the minor apparent axis of the grain's outline trace on the apparent surface
c.g.	denotes the center of gravity
γ	denotes the angle in degrees between the major axis and the line of sight passing through the center of gravity
OGS	denotes the overlapping grain surface which consists of an assemblage of surface grains belonging to all three contact modes. A familiar example is the surface of exposed gravel bars.
EGS	denotes the embedded grain surface which consists of an assemblage of surface grains belonging to contact modes 2 and 3. A familiar example is the near vertical face associated with terrace gravels.
Δ	denotes the center of gravity - surface plane distance up to and including one radius
n	denotes a number or size of unspecified value or magnitude
D	denotes the linear size of cubic grains
V	denotes the specimen volume
S	denotes a smooth planar specimen surface
A	denotes the area of S

a_n denotes the total area of S covered by cubic grains with linear size D_n

l_n denotes the combined lengths of cubic grains with linear size D_n which are touched by a transect placed on S

g_n denotes the number of cubic grains with linear size D_n which fall under the intersections of a grid placed on S

L_d denotes the maximum dimension of a square hole of side length D_s. This dimension is along the two diagonals whose length $L_d = \sqrt{2D_s^2}$

t Subscript t signifies that the term's value depends upon the measurement of surface grain true axes.

p Subscript p signifies that the term's value depends upon both experimental data and numerical method predictions.

sieve Subscript sieve signifies that the term's value depends upon the results of customary bulk sieve analysis. In the case of quadrant-by-weight the sieve subscript denotes that this distribution has been converted to its volume-by-weight equivalent.

True Axial Terms

Group 1 A,B, and C denote the major (large), intermediate, and minor (small) axes respectively of an ellipsoid.

Group 1_t A_t, B_t, C_t denote the field measurement of a grain's true A, B, and C axes.

AB_t, ABC_t, and BC_t denote different arithmetic means derived from a grain's A_t, B_t and C_t (ABC_t is the triaxial mean of a grain).

A_{t50}, AB_{t50}, B_{t50}, ABC_{t50}, BC_{t50}, and C_{t50} denote various medians of grid-by-number distributions based on field measurements of true axes.

$\overline{A}_t$, $\overline{AB}_t$, $\overline{B}_t$, $\overline{ABC}_t$, $\overline{BC}_t$, and $\overline{C}_t$ denote various means of grid-by-number distributions based on field measurements of true axes.

Group 1_p C_{p50} and $\overline{C}_p$ denote the predicted median and mean minor axis length whose values are based on apparent axial values and numerical method predictions.

Example computation of C_{p50}: Using $k_2 = \frac{b_{t50}}{a_{t50}}$ in Figure 14b), $\frac{(\overline{b}-C)100}{C} = Y$, $C_{p50} = (1.0-Y)(b_{t50})$

$\overline{C}_p$, the mean counterpart of C_{p50} can be calculated in the same way except $\overline{b}_t$ and $\overline{a}_t$ are used.

Apparent Axial Terms

Group 2 a and b denote the major and minor axes of an ellipse or the major and minor apparent axes of an ellipsoid.

$\overline{a}$ and $\overline{b}$ denote the means of apparent axial distributions based on a and b.

Group 2_t a_t and b_t denote the major and minor apparent axes respectively of a surface grain associated with either an apparent or thin section surface.

ab_t denotes the arithmetic mean derived from a_t and b_t.

a_{t50}, ab_{t50}, and b_{t50} denote various medians of grid-by-number distributions based on measurements of surface grain apparent axes.

$\overline{a}_t$, $\overline{ab}_t$, and $\overline{b}_t$ denote various means of grid-by-number distributions based on measurements of surface grain apparent axes.

Group 2_p a_{p50} and $\overline{a}_p$ denote the predicted median and mean apparent major axis length whose values are based on true axial values and numerical method predictions.

Example computation of a_{p50}: Using $k_1 = \frac{B_{t50}}{A_{t50}}$ and $k_2 = \frac{C_{t50}}{B_{t50}}$ in Figure 14a), $\frac{(\overline{a}-B)100}{B} = X$; then $a_{p50} = B_{t50}(\frac{X}{100} + 1)$

$\overline{a}_p$, the mean counterpart of a_{p50} can be calculated in the same way except $\overline{A}_t$, $\overline{B}_t$, and $\overline{C}_t$ are used.

b_{p50} and $\overline{b}_p$ denote the predicted median and mean minor apparent axis length whose values are based on true axial values and numerical method predictions.

Example computation of b_{p50}: Using $k_2 = \frac{C_{t50}}{B_{t50}}$ in Figure 14b), $\frac{(\overline{b}-C)100}{C} = Y$; $b_{p50} = C_{t50}(\frac{Y}{100} + 1)$.

$\overline{b}_p$, the mean counterpart of b_{p50} can be calculated in the same way except $\overline{B}_t$ and $\overline{C}_t$ are used.

Sieve Terms

Group 3 D_s denotes the square mesh sieve diameter (the side length of a square hole).

Group 3_{sieve} D_{sieve} denotes the volume-by-weight sampling procedure (customary bulk sieve analysis).

$D_{sieve50}$ denotes the median of a grain-size distribution produced by bulk sieve analysis.

$\overline{D}_{sieve}$ denotes the mean of a grain-size distribution produced by bulk sieve analysis

D_{sieve2} denotes the bulk sieve analysis of the coarse ($\geq$ 8mm.) portion of the subsurface sample.

$\overline{D}_{sieve\ 2}$ denotes the mean of the grain-size distribution obtained from D_{sieve2}.

Q denotes the quadrant (area)-by-weight sampling procedure whereby all surface grains ($\geq$ 8mm.) within a specified area are removed and sieved.

$\overline{Q}$ denotes the mean of the grain-size distribution obtained from Q.

Q_{sieve} denotes the distribution resulting from the conversion of Q to volume-by-weight by the weighting factor $\frac{1}{D}$.

$\overline{Q}_{sieve}$ denotes the mean of the Q_{sieve} grain-size distribution.

Group 3_p d_{sp50} and $\overline{d}_{sp}$ denote the predicted median and mean sieve diameter whose values are based on apparent axial values and numerical method predictions.

Example computation of d_{sp50}: $d_{sp50}=\frac{C_{p50}}{2k_2}\ [2(1+k_2^2)]^{\frac{1}{2}}$,

where $k_2=\frac{b_{t50}}{a_{t50}}$

$\overline{d}_{sp}$ is calculated in the same way except $\overline{b}_t$, $\overline{a}_t$, and $\overline{C}_p$ are used.

D_{sp50} and $\overline{D}_{sp}$ denote the predicted median and mean sieve diameter whose values are based on true axial values and numerical method predictions.

Example computation of D_{sp50}: $D_{sp50}=\frac{C_{t50}}{2k_2}\ [2(1+k_2^2)]^{\frac{1}{2}}$,

where $k_2=\frac{C_{t50}}{B_{t50}}$

$\overline{D}_{sp}$ is calculated in the same way except $\overline{B}_t$ and $\overline{C}_t$ are used.

k Value Estimates

Group 4

$$k_1 = \frac{B}{A}$$

$$k_2 = \frac{C}{B}$$

Group 4_t

$$k_1 = \frac{B_t}{A_t} \text{ or } \frac{B_{t50}}{A_{t50}} \text{ or } \frac{\overline{B}_t}{\overline{A}_t}$$

$$k_2 = \frac{C_t}{B_t} \text{ or } \frac{C_{t50}}{B_{t50}} \text{ or } \frac{\overline{C}_t}{\overline{B}_t} \text{ or } \frac{b_{t50}}{a_{t50}} \text{ or } \frac{\overline{b}_t}{\overline{a}_t}$$

CHAPTER ONE

SURFACE SAMPLING EQUIVALENCE PROBLEMS

1.1 General Introduction

Central to this thesis is the examination of the Kellerhals et al(1975) numerical method and four grain-size sampling experiments which test its predictions. This introductory chapter discusses four topics of critical importance to the numerical method and its empirical tests:

1) The numerical method assumes a densely packed granular material. It is essential that properties of this material relevant to grain-size sampling be identified and defined.
2) The numerical method makes grain-size predictions specifically for thin section surfaces. While two of the experiments utilize thin sections the other two use gravel surfaces, one associated with the surface layer of exposed gravel bars, the other with terrace gravels. It is necessary to evaluate the characteristics of these surfaces relative to that of a thin section.
3) Sampling procedures which require only the surface of a deposit are quite different from the standard volumetric procedure, bulk sieve analysis. A surface sampling procedure should be geometrically equivalent to this standard.

4) In customary bulk sieve analysis the square mesh sieve size D_s, is the grain-size measure. The relationships between D_s and true or apparent axial grain-size measures frequently used in surface sampling procedures are investigated.

1.2 Properties of a Densely Packed Granular Material

1.2.0 Introduction

Granular materials may be described as being densely packed or dilutely distributed (Kellerhals et al 1975). Earth sciences are usually concerned with densely packed grains in contact, while dilutely distributed granular materials are of greater interest to biologists. Since only densely packed material is examined here, henceforth it is simply termed material. The following discussion defines those textural characteristics of a material relevant to grain-size analysis.

1.2.1 Sorting

The constituent grains of an homogeneous material (Kellerhals and Bray, 1971, p.1175) may vary in size. Sorting is a measure of the degree of grain-size similarity.

1.2.2 Fabric

Isotropic means having the same properties in all directions. As used here, a material possesses an isotropic fabric when the axes of constituent grains are randomly oriented. Conversely, when there is a definite axial orientation the fabric is anisotropic.

1.2.3 Induration

Induration is the process whereby a material is hardened into rock by exposure to heat, pressure or a cementing agent. Once indurated it becomes very difficult to disaggregate into constituent grains.

1.2.4 Grain Shape

Grain shape can be defined in terms of the ratio of the three axial dimensions. Using values for the large axis A, intermediate axis B, and the small axis C, the Zingg grain shape ratios $k_1=\frac{B}{A}, k_2=\frac{C}{B}$, can be obtained (Kellerhals et al 1975). Depending upon the values of k_1 and k_2 a grain shape falls within one of four general classes a) tabular, oblate or discoidal b) equant, equiaxal or spherical c) bladed or triaxial d) prolate or rod-shaped (Whitten et al 1972).

A wide range of sedimentary grains may be approximated by ellipsoids (Allen 1969; Kellerhals et al 1975). According to the latter reference the common range of k values for these ellipsoids is 0.55-0.75. Allen (1969) states that the shapes of these triaxial ellipsoids may be approximated by $k_1=0.667$, $k_2= 0.50$. It is acknowledged that there is some discrepancy between these two sources, although this may be unimportant.

1.3 Comparison of Gravel Bar, Terrace Gravel and Thin Section Surfaces

1.3.0 Introduction

Many textural properties of a material can be investigated by observing its surface. These properties include degree of sorting and homogeneity, presence of matrix, fabric and grain size. It is this latter property which is of concern here.

In the following discussion, it is assumed that the material, the constituent grains, and the surface have certain basic properties.

Material

The material is homogeneous, nonindurated and isotropic.

Grains

The constituent grains of this material are ellipsoidal in shape and have common k values 0.55-0.75. The grains may be of any size and the density of each grain mass is uniform.

Surface

The surface being sampled is approximately planar. The ideal plane associated with this surface is defined as the surface plane. If the surface is viewed from a given point on a line of sight normal to the surface plane, it is defined as the apparent surface. Grains observed on the apparent surface are termed surface grains. The apparent grain surface is defined as that part of the actual grain surface of a surface grain which can be viewed on the apparent surface. An apparent grain surface is bounded by its outline trace. This is formed when an apparent grain surface appears to contact apparent grain surfaces of other adjacent surface grains.

Employing these assumptions it is proposed that:

1) there are three types of surfaces; overlapping grain surface (OGS), embedded grain surface (EGS) and thin section surface.
2) the surface associated with the surface layer of gravel bars possesses an OGS and that of a near vertical face of a terrace gravel deposit possesses an EGS.
3) grain-size analysis procedures developed for thin sections can be used on a terrace gravel EGS.

1.3.1 Inter Grain Contact

The actual grain surface of a surface grain has one or more point contacts with at least one other grain. It is assumed that each contact point participates in supporting the grain in its present surface position. In well-sorted material the number of contact points tends to be low; conversely, if there is a matrix and the surface grain is relatively large, the number of contact points is probably much greater. A surface grain may be in contact with both matrix grains and similar sized grains.

There are three basic classes of contact in which the surface grain may be involved; single point contact, two point contact, and three or more point contact. In the second class a straight line may be envisaged to link the two points. In the third class any three contact points can function as vertices of a triangular shaped figure. This figure forms a three point contact plane.

The number of three point contact planes which can be formed from a set of n contact points can be determined by using C(n,r) which is the number of r-subsets of a set of n elements.

$$C(n,r) = \frac{n!}{(n-r)!r!} \text{ where } n,r \in N_o,\ r \leq n \quad (1)$$

In this case $r=3 \therefore C(n,3) = \frac{n!}{(n-3)!3!}$

A three point contact plane may be extended until it is bounded by the actual grain surface. This plane is termed the extended three point contact plane. It divides the grain volume and the actual grain surface into two parts. Every three point contact plane has an extended three point contact plane counterpart. Since a grain may have vast numbers of contact points, especially when there is a matrix, many extended three point contact planes which can be formed may be coplanar (Figure 1).

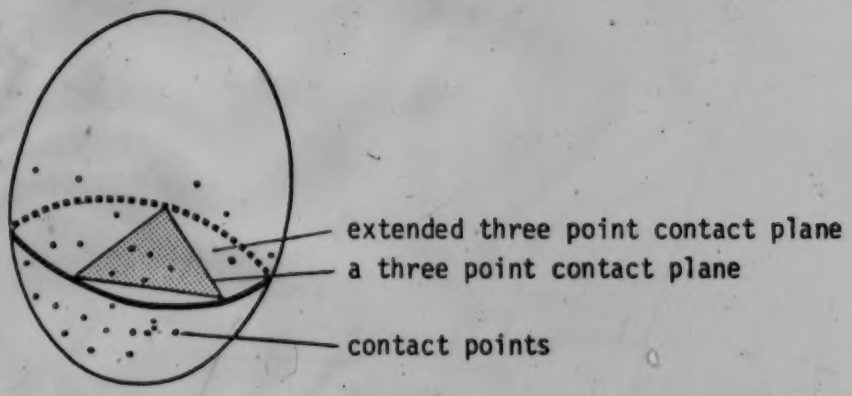

Figure 1 Ellipsoidal Grain and Associated Contact Planes

For a given surface grain, there is one particular extended three point contact plane (or group of coplanar planes), the minimizing plane, which minimizes the volume of the part bearing all or the greatest portion of the apparent grain surface (1.3.0). This part bearing most of the apparent grain surface is termed the top part, the other, the bottom part.

1.3.2 Three Contact Modes

The center of gravity of a grain is that point through which the resultant attraction of gravity acts regardless of the grain's position. If the grain could be suspended or poised from this center, it would be in equilibrum in any orientation. Employing the grain assumptions in 1.3.0 the center of gravity is located in the center of each grain.

With reference to 1.3.1 it may be seen that the center of gravity may lie in the top part, bottom part or on the minimizing plane. These represent the three modes of contact a surface grain may have (Figure 2).

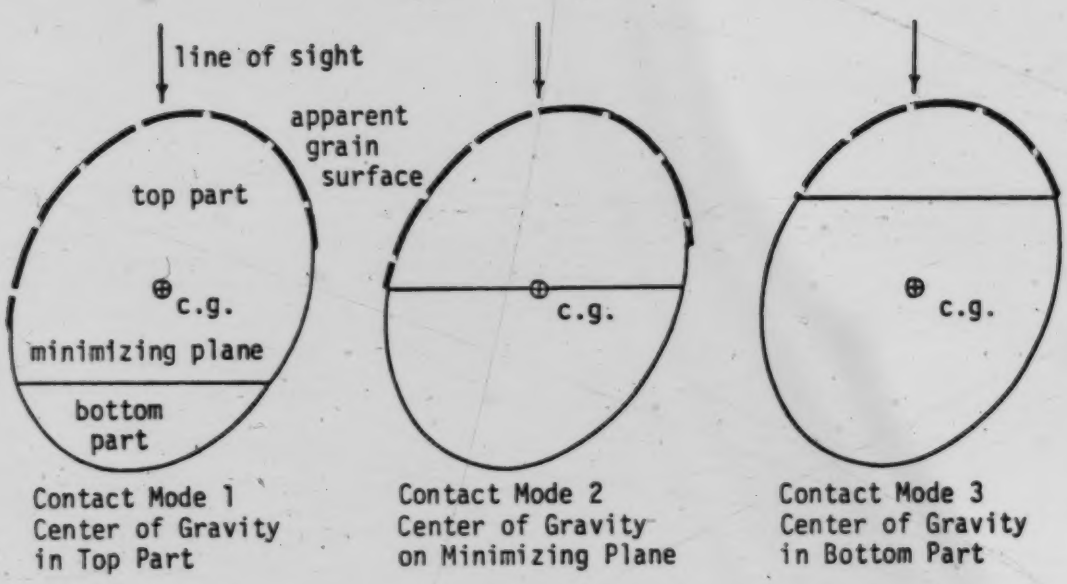

Figure 2 Ellipsoidal Cross-Sections Illustrating Three Contact Modes

The single point contact class may be considered a special case of contact mode 1, where the entire volume of the grain is the top part. For the two point contact class, it is conceivable that the grain is balanced and resting on two point contacts (e.g., a spherical grain resting in a V-shaped channel).

It is likely that these two special mode 1 cases are rarely observed in nature for such reasons as grain surface roughness, instability and presence of matrix.

1.3.3 Graphic Experiment 1

For an ellipsoidal grain the axial dimensions of its outline trace (1.3.0) and minimizing plane are dependent basically upon its k values, orientation and contact mode. Subsection 1.3.3 investigates this complex topic with a number of simplifying assumptions and a small graphic experiment.

Three grain shapes are investigated, a sphere ($k_1=k_2=1$) and two ellipsoids ($k_1=k_2=0.75$ and $k_1=k_2=0.55$). The sphere is included because it is the simplest case; the ellipsoids, because their k values are the upper and lower limits of those commonly observed.

In all cases the ellipsoids are oriented such that the A axis is perpendicular to the line of sight associated with the apparent surface (1.3.0). This axis functions as an axis of rotation for the B and C axes which it intersects in the center of the grain (center of gravity). The B axis forms angles (0^0,22.5^0,45^0,67.5^0,90^0) with this line of sight.

The spherical and oriented ellipsoidal grains are analyzed with respect to their behavior in each of the three contact modes. For contact modes 1 and 3 the center of gravity is arbitrarily situated 0.24 X B above and below respectively, the minimizing plane. In all three contact modes the actual grain surface associated with the bottom part is never visible (buried) and the minimizing plane is normal to the line of sight.

Combining these different grain k values, orientations and contact modes many variations are possible. These are examined by halving each grain so that the resulting planes are perpendicular to the axis of rotation. This sectioning procedure produces three distinct plane figures, one circle ($\frac{\text{minor axis}}{\text{major axis}} = 1.0$), and two ellipses ($\frac{\text{minor axis}}{\text{major axis}} = 0.75$ and 0.55). For the ellipses, the major axis corresponds to B, the minor axis to C, of the parent ellipsoid. Each of these figures have two measurable dimensions whose values depend upon the specific characteristics of the parent grain:

1) The minimizing plane dimension (MPD) is the line resulting

from the intersection of the minimizing plane and the plane produced by sectioning (Figure 3).

2) The apparent surface dimension (ASD) corresponds to the minor apparent axis b, of the grain's outline trace on the apparent surface. The ASD is determined with reference to the line of sight which passes through the center of gravity. The length of the ASD is the sum of the length of those two lines on the plane that are perpendicular to and lie on either side of the line of sight, are in the top part or on the MPD, and have maximum possible length (Figure 3).

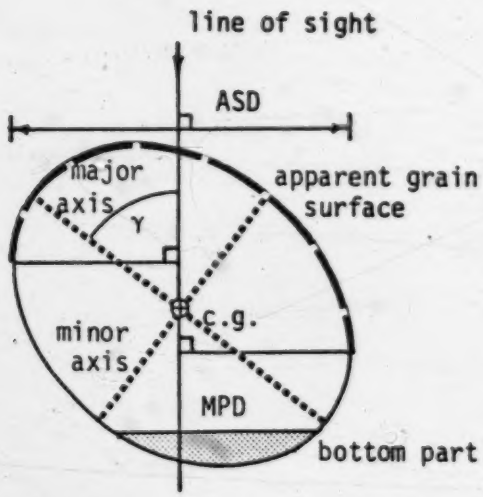

Figure 3 The Minimizing Plane Dimension (MPD) and Apparent Surface Dimension (ASD) of Oriented Ellipse
$\frac{\text{Minor axis}}{\text{Major axis}} = 0.75$

major axis = B axis of parent ellipsoid
minor axis = C axis of parent ellipsoid

c.g. center of gravity
γ angle in degrees between the major axis and the line of sight passing through the center of gravity.

In the small graphic experiment (Figure 4) the major axes of the circular and elliptical sectioning planes are made equal. Because the axes of a circle are equal any change in their orientation makes no dimensional difference. For each case the $\frac{\text{MPD}}{\text{ASD}}$ percent is calculated (Table 1). Since a surface grain's apparent grain surface and minimizing plane are both elliptical figures, in each case the $\frac{\text{MPD}}{\text{ASD}}$ percent quantitatively relates b to the corresponding axis of its

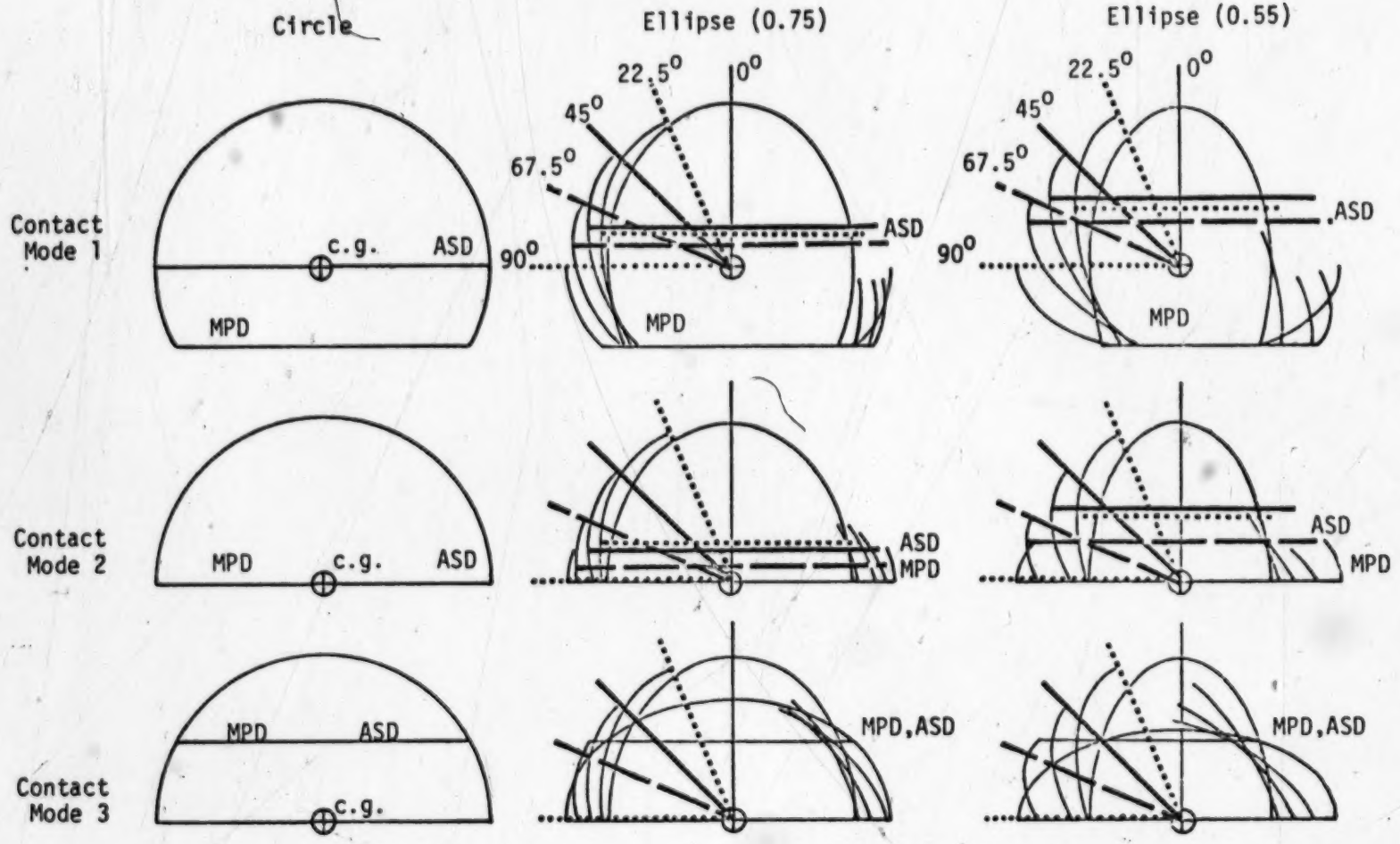

Figure 4 Graphic Experiment 1, Contact Mode Behavior of Circular and Elliptical Plane Figures

Table 1
Results of Graphic Experiment 1

Contact Mode	γ (Degrees)	Circle ASD (mm)	Circle MPD (mm)	Circle MPD/ASD %	Ellipse (0.75) ASD (mm)	Ellipse (0.75) MPD (mm)	Ellipse (0.75) MPD/ASD %	Ellipse (0.55) ASD (mm)	Ellipse (0.55) MPD (mm)	Ellipse (0.55) MPD/ASD %
1	0	52.5	46	87.6	39.0	35.5	91.0	29.5	25.5	86.4
Center of	22.5				41.5	36	86.7	33	26	78.8
Gravity in	45				46.5	38.5	82.8	42.5	29	68.2
Top Part	67.5				50.5	41.5	82.2	49	30	61.2
	90				52	43	82.7	52	26	50
							85.08			68.92
2	0	52.5	52.5	100	39.5	39.5	100	29.5	29.5	100
Center of	22.5				40.5	40.5	100	32	31	97.0
Gravity on	45				46	45	97.8	39.5	36	91.1
Minimizing	67.5				49.5	49	99	47	45	95.7
Plane	90				52	52	100	52	52	100
							99.36			96.76
3	0	45	45	100	34	34	100	25.5	25.5	100
Center of	22.5				35.5	35.5	100	26	26	100
Gravity in	45				36.5	36.5	100	29	29	100
Bottom Part	67.5				38.5	38.5	100	29	29	100
	90				36.5	36.5	100	24.5	24.5	100
							100			100

minimizing plane.

For contact mode 1 grains, the mean $\frac{MPD}{ASD}$ percent decreases with decreasing $\frac{\text{minor axis}}{\text{major axis}}$ value (Table 1). For the ellipse (0.55) in particular, minimum percent values are achieved when the major axis parallels the MPD. Brief consideration of Figure 4 suggests that as the center of gravity - minimizing plane distance increases so the $\frac{MPD}{ASD}$ percent values tend to decrease.

For contact mode 2 grains, the mean $\frac{MPD}{ASD}$ percent is nearly 100 for the three planes, in all tested orientations (Table 1). The $\frac{MPD}{ASD}$ percent for the circle is 100 but decreases slightly with decreasing $\frac{\text{minor axis}}{\text{major axis}}$ value (ellipses 0.75 and 0.55 have mean $\frac{MPD}{ASD}$ percent values of 99.36 and 96.76 respectively). The minimum $\frac{MPD}{ASD}$ percent is reached for the ellipse (0.55) at an orientation of 45^{o}.

For contact mode 3 grains, the $\frac{MPD}{ASD}$ percent is uniformly 100 (Table 1). Careful examination of Figure 4 diagrams reveal that if the center of gravity is closer to the minimizing plane, the $\frac{MPD}{ASD}$ percent value drops slightly for the two ellipses (particularly ellipse 0.55), but not for the circle. For ellipses 0.75 and 0.55 noticeable reductions in $\frac{MPD}{ASD}$ percent begin when the center of gravity is 0.10 and 0.17 X B respectively, below the MPD.

Figure 5 displays Table 1 data as well as a few additional contact mode 3 data points. Table 2 summarizes the trends in Table 1 and Figure 5. Table 2 is based entirely on results from ellipses whose major and minor axes correspond to parent grain axes B and C. These results are equally valid if the rotational axis perpendicular to the line of sight is B or C, rather than A. While this seems to extend the range of application for the results, the initial experimental assumptions prevent the

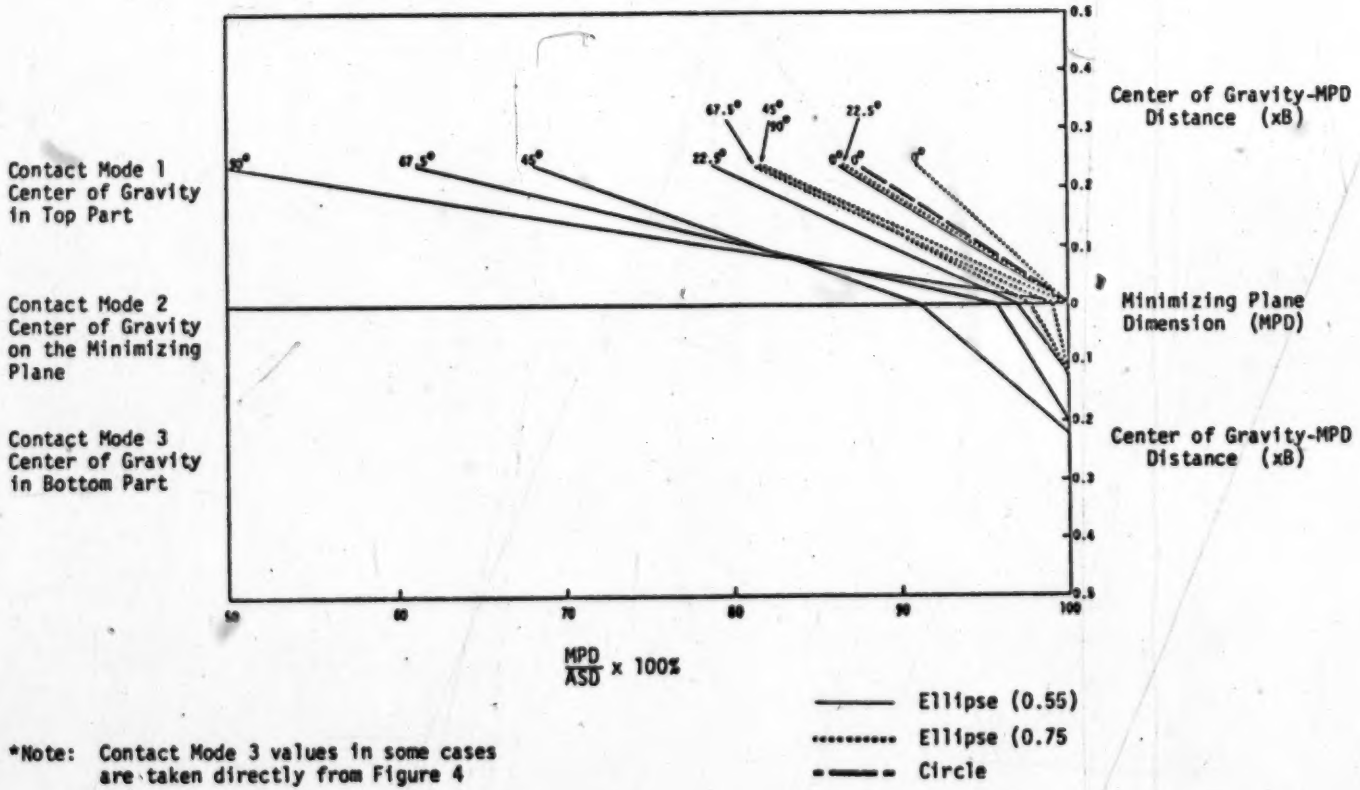

*Note: Contact Mode 3 values in some cases are taken directly from Figure 4

Figure 5

Graphic Summary of Table 1 Data

Table 2
Maximization and Minimization of $\frac{MPD}{ASD}$ %

Contact Mode	Maximization of $\frac{MPD}{ASD}$ %			Minimization of $\frac{MPD}{ASD}$ %		
	$\frac{\text{Minor Axis}}{\text{Major Axis}}$ %	γ (Degrees)	Center of Gravity - MPD Distance	$\frac{\text{Minor Axis}}{\text{Major Axis}}$ %	γ (Degrees)	Center of Gravity - MPD Distance
1 Center of Gravity in Top Part	Maximize	0	Minimize	Minimize	90	Maximize
2 Center of Gravity on Minimizing Plane	Maximize	0 or 90	———	Minimize	45	———
3 Center of Gravity in Bottom Part	Maximize	0 or 90	Maximize	Minimize	45	Minimize

determination of the major and minor axes for both the minimizing plane and trace outline, except for a few special situations. The $\frac{MPD}{ASD}$ percent values (Figure 5), however, and observed trends (Table 2) not only compare axial lengths but, indirectly, shapes and areas of the minimizing plane and the apparent grain surface which is bounded by the trace outline. This is particularly evident for the spherical grain. When in contact mode 1 the $\frac{MPD}{ASD}$ percent is 87.6 (Table 1). Since both the minimizing plane and the apparent grain surface are circular the diameter of the minimizing plane is 87.6 percent of the apparent grain surface. Thus the minimizing plane area is also much smaller. In contact modes 2 and 3 the $\frac{MPD}{ASD}$ percent is 100 implying that for a spherical grain the minimizing plane and apparent grain surface coincide in shape and area in contact modes 2 and 3.

Similar reasoning can be applied to ellipsoidal grains. Table 2 and Figure 5 reveal that as ellipses decrease in circularity, the greater the potential for orientation to have a minimizing effect on the $\frac{MPD}{ASD}$ percent. Figure 5 demonstrates that even for an ellipse (0.55) in any orientation, the minimizing effect is less than 9 percent for mode 2 ($\frac{MPD}{ASD}$ percent for a circle is 100 and for an ellipse (0.55) at 45^{o} is 91.1) and quickly vanishes in mode 3. In contact mode 1, the effect of small $\frac{\text{minor axis}}{\text{major axis}}$ values and orientation on minimizing the $\frac{MPD}{ASD}$ percent is greatest.

The above discussion provides evidence that ellipses, including those whose $\frac{\text{minor axis}}{\text{major axis}}$ value is equivalent to common k values, are similar to circles with respect to their $\frac{MPD}{ASD}$ percent behavior for a given contact mode. In contact mode 1, for both spheres and ellipsoids

the apparent grain surface area and axial dimensions are greater than those of the minimizing plane.. For contact mode 2, the apparent grain surface - minimizing plane correspondence is exact for spheres and very close or exact for ellipsoids, especially with high k values. For contact mode 3, coincidence is always exact for spheres and eventually for any ellipsoid (the greater the center of gravity - minimizing plane distance, the more probably coincidence is exact for any k value and orientation).

1.3.4 Graphic Experiment 2 and Description of Overlapping Grain Surface (OGS) and Embedded Grain Surface (EGS)

Where a material (1.3.0) has an approximately planar surface consisting of an assemblage of grains in one or more contact modes, this material may have two distinct types of surfaces; overlapping grain surface (OGS) and embedded grain surface (EGS). These are defined in terms of which contact modes are associated with the surface. Graphic experiment 2 reveals their characteristics for a material consisting of ellipsoidal grains.

An OGS consists of an assemblage of grains belonging to all three contact modes. The characteristics of this surface may be appreciated by first considering all grains to be spheres. Following this discussion the more complex ellipsoidal grain situation is examined.

It is assumed that a material consists of identical spherical grains and the minimizing plane of each surface grain is coplanar with the surface plane. Since this is an OGS, there are surface grains associated with all three contact modes.

Assuming that there are equal numbers of grains present at

any center of gravity - surface plane distance (Δ) up to and including one radius, then all spheres within this Δ range touch the surface plane and are represented by their respective minimizing planes. Beyond one radius, the spheres abruptly cease to touch the surface plane and are no longer represented on it.

Another consequence of the equal numbers assumption is that contact modes 1 and 3 grains are equally numerous. Contact mode 2 grains are very rare in comparison because they represent the special case where Δ is zero.

In the OGS spherical grain case, orientation effects are non-existent. For ellipsoids this is not so. Since the ellipsoid may have three different axial values, grain contact with the surface plane is dependent on both Δ and grain orientation. In the following discussion, assumptions similar to those in OGS spherical grains are employed, the primary exception being that the material consists of equi-sized ellipsoidal grains.

Graphic experiment 2 demonstrates the dependence of surface plane representation of ellipsoids on Δ and orientation. In this experiment, which is analogous to the one in 1.3.3, two ellipsoids ($k_1=k_2=0.75$ and $k_1=k_2=0.55$) are investigated. They are oriented such that the A axis is perpendicular to the line of sight associated with the apparent surface. This axis functions as an axis of rotation for the B and C axes which it intersects in the center of the grain (center of gravity). The angle γ between the line of sight and major axis has five values (0^o,22.5^o,45^o,67.5^o,90^o). These oriented ellipsoidal grains are examined with respect to their behavior in contact mode 3. The grains are situated so that for a particular orientation only one point on their surface touches the surface plane.

As in 1.3.3 each ellipsoidal grain is halved forming two distinct ellipses ($\frac{\text{minor axis}}{\text{major axis}} = \frac{C}{B} = 0.75$ and 0.55). Each type of ellipse is drawn (Figure 6) in its five different orientations and with only one point on its boundary touching the surface plane. Δ is then measured for each of these orientations (Table 3) and plotted (Figure 7).

Table 3 Results-Graphic Experiment 2

γ(degrees)	Ellipse (0.75) Δ=%B	Ellipse (0.55) Δ=%B
90.0	37.5	28.0
67.5	40.0	31.8
45.0	43.8	40.5
22.5	48.6	47.6
0	0	50.0

Figure 7 shows that as the orientation of both elliptical types changes from $\gamma=90^{o}$ (Δ=0.5 x C axis) to $\gamma=0^{o}$ (Δ=0.5 x B axis) Δ increases. Closer scrutiny of the two curves in Figure 7 uncover their nature as the limits of total surface plane representation for a given elliptical shape. All ellipses with Δ and γ values less than or equal to their respective curves, touch the surface plane and therefore are represented on it. For combinations exceeding curve values the converse is true.

If it is assumed that there are equal numbers of ellipses at any given γ, and all orientations of B about A are equi-probable, then Figure 7 curves correspond to surface plane representation frequency curves, the frequency of representation being dependent upon Δ and γ. Figure 7 illustrates that representation on the surface plane is total up to a critical Δ (50 percent C), then steadily declines to a point of zero representation (50 percent B). Furthermore, the more circular in

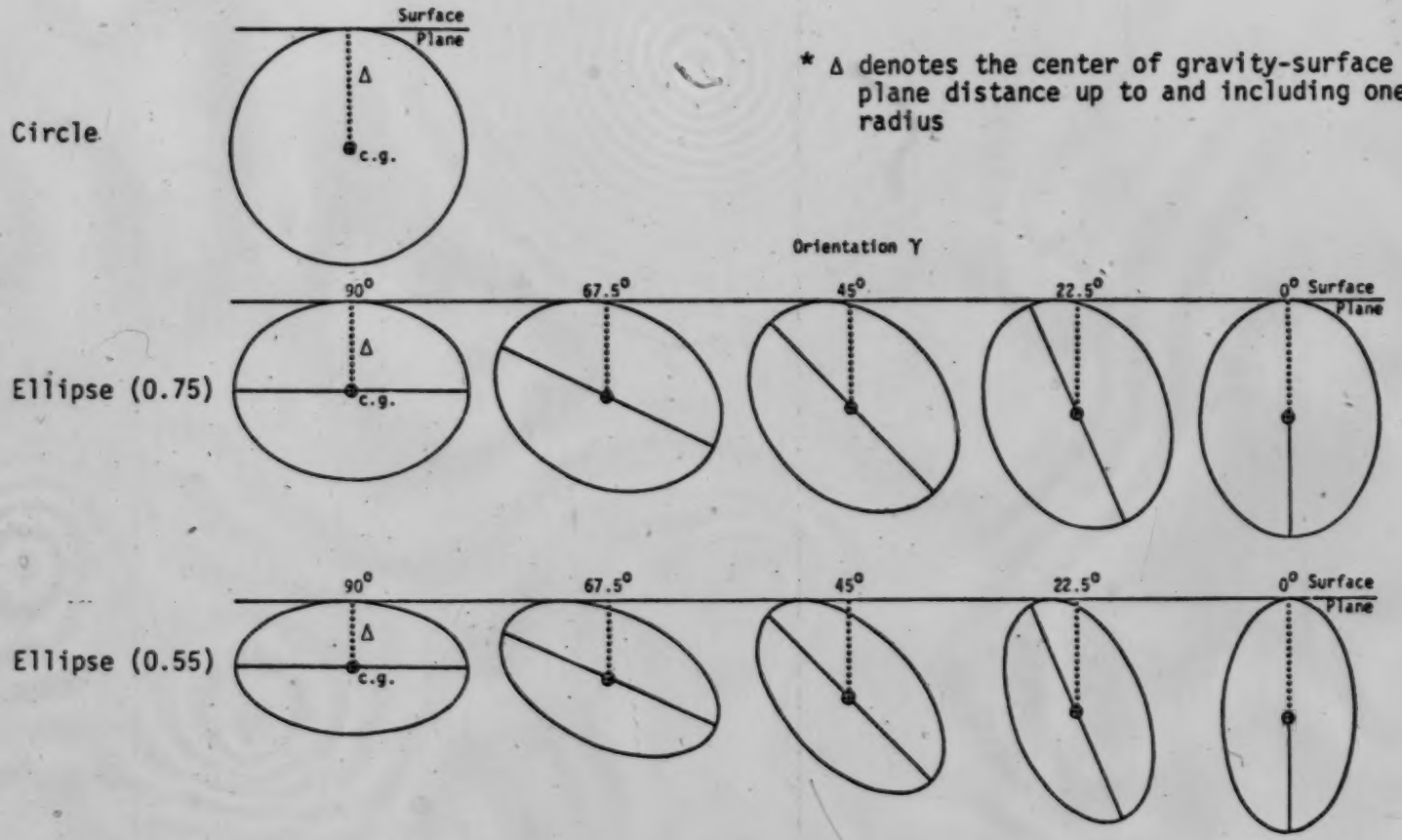

Figure 6 Graphic Experiment 2, Oriented Ellipses with One Point of Boundary on the Surface Plane

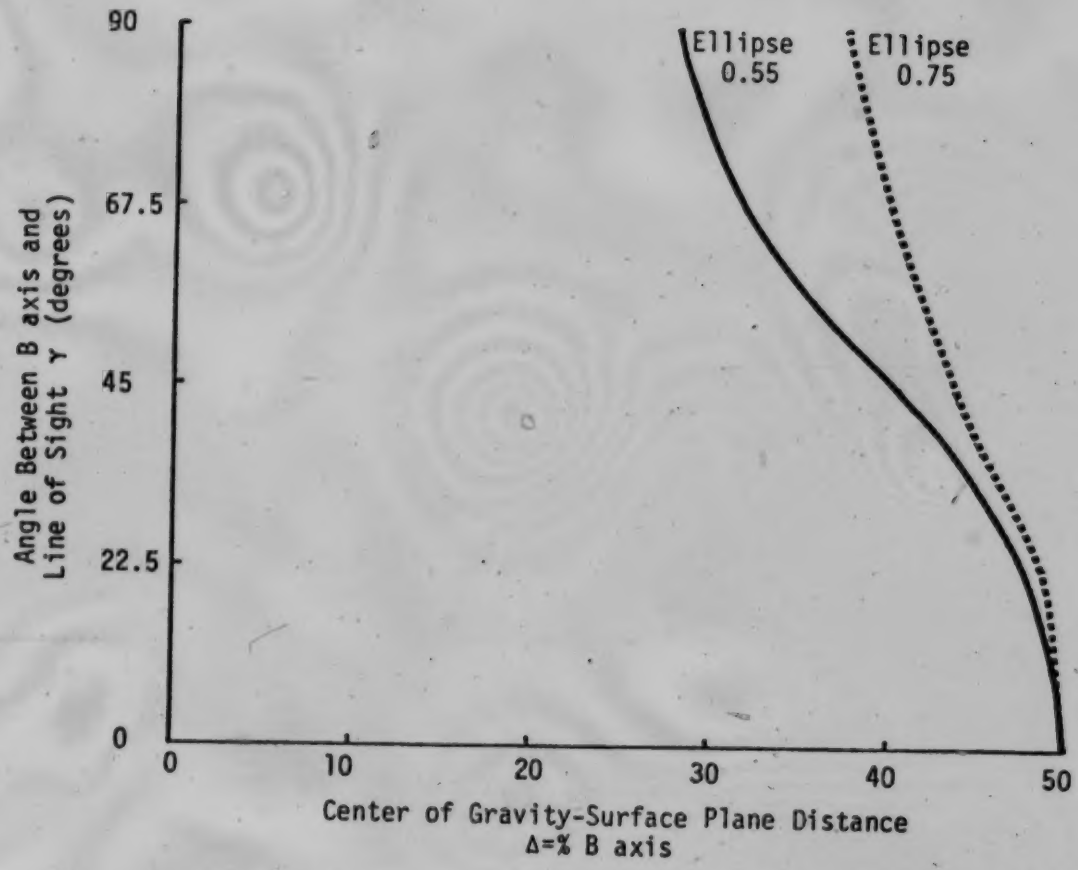

Figure 7
Limits of Total Representation of Elliptical Grains on a Surface Plane (refer Table 3)

form the ellipse the greater the Δ before orientation - induced decline is initiated. As in 1.3.3 identical findings are produced if the axis of rotation is B or C instead of A.

The results of this graphic experiment also hold true for the parent ellipsoids. More generally, it is expected that similar Δ-orientation dependent behavior is exhibited by ellipsoids in which any orientation is equi-probable. If so, the more spherical the ellipsoidal form, the greater the Δ (maximum 50 percent A axis) before orientation - surface plane representation effects are initiated.

The above observations are based on an experiment using only contact mode 3 ellipsoids. It is clear that for both contact modes 1 and 3 grain representation on the surface plane is dependent upon identical Δ-orientation combinations. Certain grains do not touch the surface plane because they are buried; identical potential contact mode 1 grains are not possible because they are not supported, assuming that the minimizing plane of all grains of this surface are coplanar with the surface plane. Therefore, the surface plane representation frequency curves for contact modes 1 and 3 are symmetric about the surface plane.

These statements remain applicable if a material bearing an OGS contains numerous various sized ellipsoids. Instead of the surface plane being touched by identically shaped grains in different Δ-orientation combinations, the surface plane is shared by representatives of each size. This complex situation closely corresponds to OGS observed in nature. A familiar example is the surface of exposed gravel bars which usually consists of ellipsoidal shaped pebbles and cobbles. Contact mode 1 clasts rest upon and thus overlap contact modes 2 and 3 material (Figure 8).

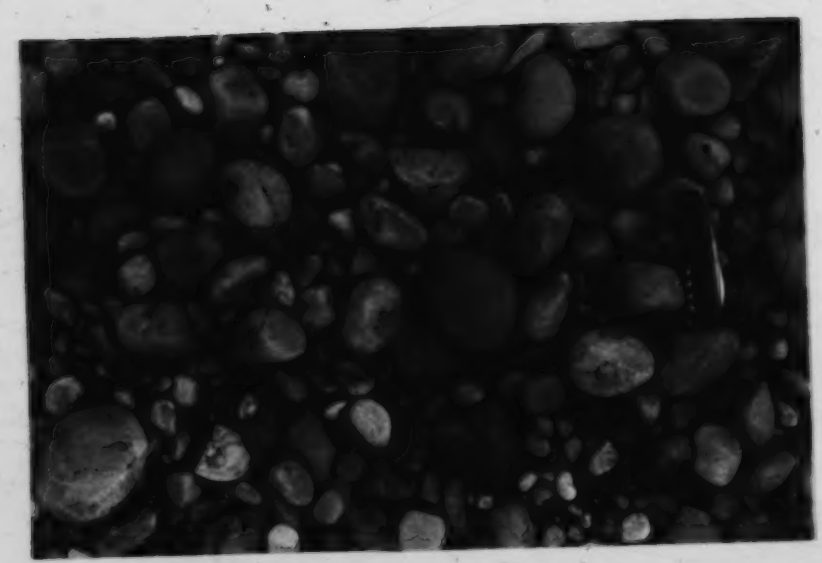

Figure 8 An Apparent OGS

An EGS consists of an assemblage of surface grains belonging to contact modes 2 and 3. Assuming that the minimizing plane of each surface grain is coplanar with the surface plane and the material consists of numerous size fractions of ellipsoidal grains, the behavior of the contact mode 2 and 3 surface grains is identical to that for OGS. Thus contact mode 2 grains are rare in comparison to contact mode 3 grains and the surface plane representation of these latter grains is dependent upon Δ and orientation.

Both artificial and natural materials may possess an EGS. Usually these materials have a matrix. The surface of the matrix is generally equatable with the surface plane of the EGS.

Artificial materials possessing an EGS, typically are indurated. A familiar example of EGS is a paved road surface of sand and gravel mixed with asphalt. During paving the asphalt is soft and the grains are embedded by rolling. Subsequent to hardening some grains may become contact mode 1 grains due to the disappearance of some of the surrounding asphalt matrix. This creates an ephemeral OGS, since these grains are easily dislodged.

In nature, gravels which have fine sand, silt or clay matrixes can maintain near vertical faces, as is often the case with terrace gravels. Investigation of these faces reveals that they are EGS. The explanation for this is quite similar to that for road surfaces. If a grain on a vertical face loses some of its supporting point contacts (matrix or similar sized grains) and becomes a contact mode 1 grain, the grain weight is unsupported and it tumbles out of its mold (Figure 9).

Figure 9 An Apparent EGS

1.3.5 Comparison of Apparent OGS, Apparent EGS and Thin Section

If a randomly chosen plane is extended through a material (1.3.0) consisting of ellipsoidal grains, the frequency of grain representation on this plane is the same as discussed in 1.3.4 (OGS Ellipsoidal Grains). If the material is cut along this plane, a planar surface results consisting of intersected grains and matrix, if present. Referring to 1.3.4, the cutting plane is equivalent to the surface plane, and the intersected surfaces of the ellipsoids are equivalent to minimizing planes coplanar with the surface plane. This planar surface can be considered a thin section.

For OGS, the surface plane contains minimizing planes of all three contact mode grains. As discussed in 1.3.3, the minimizing plane and apparent grain surface of contact mode 1 grains do not coincide. Coincidence is far more probable for contact mode 2 and particularly for contact mode 3. Since nearly half of OGS grains are in contact mode 1 (1.3.4), and they lack coincidence, an apparent OGS is not equivalent to a thin section corresponding to the surface plane. More generally, since all thin sections cut from this material should have equivalent grain representation, the apparent OGS is not equivalent to any thin section surface.

For EGS the surface plane contains minimizing planes of only contact modes 2 and 3 grains. Coincidence between the apparent grain surfaces and their minimizing planes is very good, particularly as Δ increases (1.3.3; 1.3.4). This seems to ensure apparent EGS comparability with its associated thin section surface, though it may be argued that the center of gravity of grains represented on a thin section are on

either side, or on the cutting plane. In contrast, EGS grains have their center of gravity on or to only one side of the surface plane. The effect of this is negligible for the following reason. As discussed in 1.3.4, surface plane representation frequency curves for an OGS are symmetric about the surface plane. This also applies to thin sections. Since contact mode 1 grains are non-existent in an EGS, the 'gaps' are filled by contact mode 3 grains. On the basis of surface plane representation symmetry, it is probable that the replacement contact mode 3 grains will be represented on the surface plane in a very similar manner. Therefore, the net result is an apparent EGS which is equivalent to any thin section cut through the material.

1.3.6 Grain-Size Measurement on Apparent OGS and EGS and Thin Section

If the apparent surface of a material (1.3.0) is used for grain-size analysis it is necessary to assign linear dimensions to the trace outlines of the surface grains. There are a variety of measures which may be employed (Kellerhals *et al* 1975).

Apparent Axis Measurements

a) major apparent axis a
b) minor apparent axis b
c) some combination of a and b

Chord Length Measurements

a) chord length of a grain falling along a predetermined line
b) maximum chord length in a predetermined direction

For an apparent OGS approximately one half of the surface grains are contact mode 1. The fabric may be anisotropic such that true axial values may be obtained directly by measurement of the apparent axes of contact mode 1 grains. At least one true axis must be parallel with the surface plane.

a) If only one true axis of the surface grain is parallel to the surface plane and its direction on the plane is fixed, measurement of the corresponding apparent axis, provides the true axial value.

b) If one true axis of the surface grain is normal to the surface plane, then the other two are parallel to the plane. Association of the two apparent axial values with the corresponding true ones may be done on the basis of relative size, preferential direction or both.

Particularly for contact mode 3 grains it is improbable that an apparent axis corresponds with a true one. Because these grains are the primary constituents of an apparent EGS this fact must be recognized by all grain-size analysis procedures utilizing this apparent surface. Thin section surfaces and the apparent EGS of a material are essentially equivalent (1.3.5), and it is reasonable to assume that thin section grain-size analysis may be applied to an apparent EGS.

1.4 Sampling Procedures

1.4.0 Introduction

Section 1.4 examines all possible sampling procedures which can be used on thin section surfaces and the apparent EGS of terrace gravels. When the constraint imposed by the necessity for geometric equivalence of a sampling technique to bulk sieve analysis is taken into account, very few of these sampling procedures remain applicable.

Kellerhals *et al* (1975, p.80) state that all grain-size analysis procedures in geology may be classified according to three basic steps and associated choices. These steps are:

Step I Collection of sample

Step II Assignment of linear dimensions to grains

Step III Allocation of frequencies

In the following discussion this clear and comprehensive system of steps and choices is adopted.

1.4.1 Step I Collection of Sample

The basic choices associated with collecting a sample are fixed by the number of dimensions (i.e., zero, one, two, three) of the total sample volume (sum of the volumes of all grains in a sample) determined by the experimenter, and the number of dimensions dependent on grain size.

1) Volumetric (Bulk) Sample: The sample consists of a volume of the material under investigation. Three dimensions are predetermined by the operator. Standard sieve analysis uses this method.
2) Areal Sample: Every grain in a given area is examined. Two dimensions are predetermined by the operator.
3) Transect Sample (line counting): A line is placed through the material. The operator predetermines one dimension.
4) Grid Sample (point counting): Only dimensionless points are predetermined within the material.

Only methods 2), 3), and 4) are applicable to thin section analysis.

1.4.2 Step II Grain-Size Measurement and Step III Frequencies

In 1.3.6 various methods are presented for assigning linear dimensions to trace outlines of surface grains on apparent surfaces. These methods are also applicable to trace outlines on thin sections. These grain-size measures, as well as other methods of assigning linear dimensions to grains, constitute Step II (see Kellerhals et al, 1975, p.80). This step is necessary for computing frequencies, Step III, since frequency determination requires that each grain be a member of a size interval.

1) Frequency by Area: The frequency of each size interval is expressed as the percentage by area of the original sample falling into the interval.

2) Frequency by Length: The frequency of each size interval is expressed as the percentage by length of the original sample falling into the interval.

3) Frequency by Number: The frequency of each size interval is expressed as the percentage by number of the total number of grains in the original sample that fall into the interval (Kellerhals and Bray, 1971, p.1169).

4) Frequency by Weight: The frequency of each size interval is expressed as the percentage by weight of the original sample falling into the interval (Kellerhals and Bray, 1971, p.1169).

Frequency methods 1), 2), and 3) are applicable to the analysis of apparent OGS and EGS and thin sections.

1.4.3 The Concept of Geometric Equivalence and Its Importance

A number of different sampling procedures arise because of the alternative methods which exist in Steps I and III. It is necessary to determine whether these sampling procedures are geometrically equivalent. "Equivalent sampling procedures, applied to a homogeneous and isotropic deposit result, on average, in identical size distributions" (Kellerhals and Bray, 1971, p.1166).

There are several important issues associated with the concept of geometric equivalence.

1) Although many sampling procedures have been used, questions

dealing with their geometric equivalence are rarely adequately explored. This has resulted in the comparison of non equivalent data and in other cases the omission of important results because differences in procedures could not be evaluated (Kellerhals and Bray, 1971, p.1166).

2) Customary bulk sieve analysis (volume-by-weight sampling procedure) is central to the problem of equivalence because most grain-size analyses employ this procedure. As such, most accepted theories of sedimentation are based on data derived from bulk sieve analyses. Thus, it is critical that other sampling procedures, such as those applicable to thin section grain-size analysis, yield comparable grain-size distributions to those that would be achieved by this standard sampling technique.

3) Recognition of the problems associated with geometric equivalence have lead to geometric formulations of this concept and its implications. Ensuing geometric arguments reveal that some sampling procedures are directly equivalent while others must undergo conversion to achieve comparability.

1.4.4 Determination of Conversion Factors for Steps I and III

The following discussion presents conversion factors for Steps I and III. Because of the importance of bulk sieve analysis, conversion factors are determined relative to volume (Step I) and weight (Step III). Since many basic assumptions used to derive these factors are essentially those found in Kellerhals and Bray (1971) the derived factors are identical to those used by them.

Assumptions

A) A homogeneous, isotropic specimen material (1.3.0) consists of densely packed cubes of constant specific weight. These cubes may be referred to as grains (Figure 10).

B) There are n different size fractions each consisting of one or more cubic grains of linear sizes D_1, D_2, D_3, ... D_n.

C) The specimen volume V can be divided into constituent volumes V_1, V_2, V_3, ... V_n, each representing the total volume of the cubes of the corresponding size fraction. These volumes form a ratio $V_1:V_2:V_3$: ... V_n.

D) In a volumetric (bulk) sample all three dimensions are predetermined by the operator (Kellerhals et al 1975). Thus, none of the sample dimensions are dependent on grain size. If V is sampled volumetrically the ratio of the volumes associated with each size fraction is expected to be equal on average to the ratio $V_1:V_2:V_3$: ... V_n.

E) A cut parallel to a side of the cube produces a smooth planar specimen surface S, of area A, in which the exposed area of each surface grain is proportional to the square of its linear size

Employing these assumptions six conversion factors are determined.

1) Areal Sample to Volumetric Sample

It is assumed that the grains of each size fraction cover a total area (a) on S, such that these areas form a ratio $a_1:a_2:a_3$: ... a_n

Grain	Linear Size D	Weight W	Total No. in Sample Volume	Total No. in Sample Surface
	1	1	4610	192
	2	8	576	48
	4	64	72	12

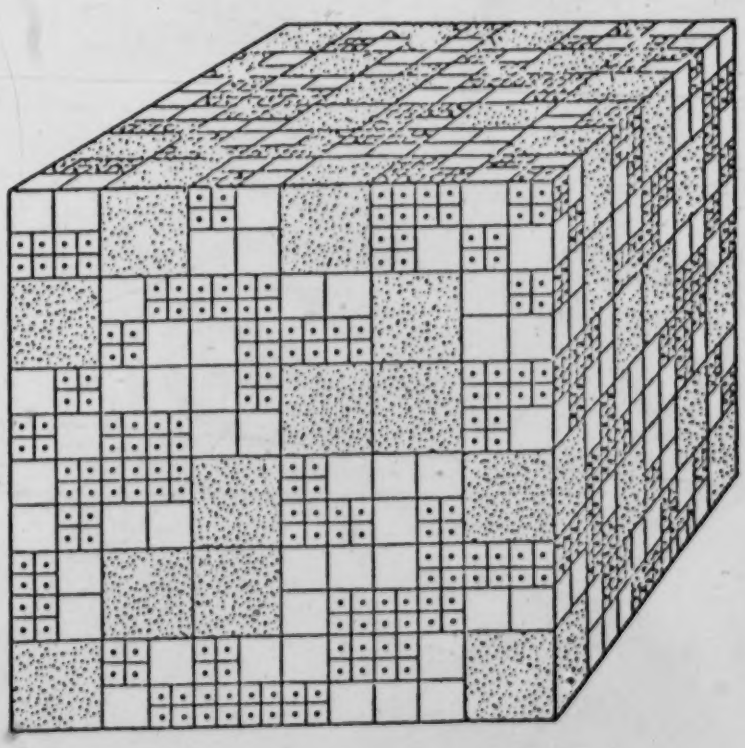

Figure 10
Sample of Densely Packed Cubes of Three Sizes
(from Kellerhals and Bray 1971, p.1170)

which is equal to the ratio of the corresponding volumes $V_1:V_2:V_3: \ldots V_n$ (see Kellerhals and Bray, 1971, p.1175).

Areal collection involves the measurement of every grain on S. Volume values may be derived from this areal sample if the volume of every surface grain is calculated.

The volume of each size fraction is $a_1 \times D_1$, $a_2 \times D_2$, $a_3 \times D_3$, $\ldots a_n \times D_n$. But the volumes of size fractions collected areally will not necessarily form a ratio equal to $V_1:V_2:V_3: \ldots V_n$. Equivalence is achieved by multiplying each size fraction by $\frac{1}{D}$.

Thus $a_1 \times D_1 \times \frac{1}{D_1} : a_2 \times D_2 \times \frac{1}{D_2} : a_3 \times D_3 \times \frac{1}{D_3} : \ldots a_n \times D_n \times \frac{1}{D_n}$

$=a_1:a_2:a_3: \ldots a_n$

$=V_1:V_2:V_3: \ldots V_n$

2) Transect Sample to Volumetric Sample

It is assumed that for any transect which is placed on S, the ratio formed by the combined lengths of those grains in each size fraction which the transect touches, $l_1, l_2, l_3, \ldots l_n$, is $l_1:l_2:l_3: \ldots l_n$ and is equal on average to $V_1: V_2:V_3: \ldots V_n$.

Transect collection involves the measurement of every grain which it touches. Volume values may be derived from a transect sample if the volumes of collected grains are calculated.

The volume of each size fraction is $l_1 \times D_1^2$, $l_2 \times D_2^2$, $\times l_3 \times D_2^3$, $\ldots l_n \times D_n^2$. But the volumes of size fractions collected by transect will not necessarily form a ratio equal to $V_1:V_2:V_3: \ldots V_n$. Equivalence is achieved by multiplying each size fraction by $\frac{l}{D^2}$.

Thus $l_1 \times D_1^2 \times \frac{l_2}{D_1^2} : l_2 \times D_2^2 \times \frac{l_2}{D_2^2} : l_3 \times D_3^2 \times \frac{l_2}{D_3^2} : \ldots l_n \times D_n^2 \times \frac{l_2}{D_n^2}$

$=l_1:l_2:l_3: \ldots l_n$

$=V_1:V_2:V_3: \ldots V_n$

3) Grid Sample to Volumetric Sample

It is assumed that for any origin point and orientation of a grid on S, the ratio formed by the number of those grains in each size fraction falling under grid intersections, $g_1, g_2, g_3, \ldots g_n$, is $g_1:g_2:g_3: \ldots g_n$ and is equal on average to $V_1:V_2:V_3 \ldots V_n$.

Grid collection involves the measurement of each grain falling under each grid intersection. Volume values may be derived from a grid sample if the volumes of the collected grains are calculated.

The volume of each size fraction is $g_1 \times D_1^3$, $g_2 \times D_2^3$, $g_3 \times D_3^3$, $\ldots g_n \times D_n^3$. But the volumes of size fractions collected by grid will not necessarily form a ratio equal to $V_1:V_2:V_3: \ldots V_n$. Equivalence is achieved by multiplying each size fraction by $\frac{1}{D}3$.

Thus $g_1 \times D_1^3 \times \frac{1}{D_1}3 : g_2 \times D_2^3 \times \frac{1}{D_2}3 : g_3 \times D_3^3 \times \frac{1}{D_3}3 : \ldots g_n \times D_n^3 \times \frac{1}{D_n}3$

$= g_1:g_2:g_3: \ldots g_n$

$= V_1:V_2:V_3: \ldots V_n$

In frequency by weight the frequency of each size interval is expressed as the percentage by weight of the original sample falling into the interval (1.4.2). If the grains have a constant specific weight, weight frequencies are identical to volume frequencies (Kellerhals et al, 1975, p.80). Thus for size fractions in the specimen material: $V_1:V_2:V_3: \ldots V_n = W_1:W_2:W_3: \ldots W_n$ where W is the weight of the volume of a given size fraction.

4) Frequency by Area to Frequency by Weight

To convert frequency by area to frequency by weight the calculated area of each size fraction must be converted to a volume. This is performed by multiplying the area of each fraction by its corresponding linear size, D. The resulting volumes are proportional to weights.

5) Frequency by Length to Frequency by Weight

To convert frequency by length to frequency by weight the observed grain numbers of each size fraction must be converted to a volume. This is performed by multiplying the length of each fraction by its corresponding area, D^2. The resulting volumes are proportional to weights.

6) Frequency by Number to Frequency by Weight

To convert frequency by number to frequency by weight the observed grain numbers of each size fraction must be converted to a volume. This is performed by multiplying the number of each fraction by its corresponding volume, D^3. The resulting volumes are proportional to weights.

1.4.5 Combined Conversion Factors for Nine Sampling Procedures

Nine sampling procedures emerge when methods applicable to thin section analysis, within Steps I and III, are combined. For each procedure, the conversion factors derived for densely packed cubes in random arrangement (1.4.4) may also be combined. These combined conversion factors e.g., 1, D, $\frac{1}{D}$ can be used to adjust the value of each size fraction as determined by any of the nine sampling procedures, to its volume-by-weight equivalent. More generally, the results of any procedure can be transformed so as to be equivalent to any other (Table 4).

Three sampling procedures, area-by-area, transect-by-length and grid-by-number have combined conversion factors of one with respect to volume-by-weight, and thus are geometrically equivalent to this standard and to each other. Identical conclusions were reached by Kellerhals et al (1975).

Table 4
Thin Section Sampling Procedures
and Combined Conversion Factors

Steps and Methods	Sampling Procedure	Combined Conversion Factor: Conversion to Volume-by-Weight
I(2) - III(1)	area-by-area	$\frac{1}{D} \times D = 1$
I(3) - III(1)	transect-by-area	$\frac{1}{D^2} \times D = \frac{1}{D}$
I(4) - III(1)	grid-by-area	$\frac{1}{D^3} \times D = \frac{1}{D^2}$
I(2) - III(2)	area-by-length	$\frac{1}{D} \times D^2 = D$
I(3) - III(2)	transect-by-length	$\frac{1}{D^2} \times D^2 = 1$
I(4) - III(2)	grid-by-length	$\frac{1}{D^3} \times D^2 = \frac{1}{D}$
I(2) - III(3)	area-by-number	$\frac{1}{D} \times D^3 = D^2$
I(3) - III(3)	transect-by-number	$\frac{1}{D^2} \times D^3 = D$
I(4) - III(3)	grid-by-number	$\frac{1}{D^3} \times D^3 = 1$

1.4.6 Geometric Equivalence and Equivalent Grain-Size Measures

Most investigators agree that for commonly occurring grain shapes, the square mesh sieve size D_s, and the intermediate axis B (1.2.4) are both acceptable and almost identical measures of actual grain size (Leopold, 1970; Kellerhals and Bray, 1971). Thus, for the three sampling procedures in 1.4.5 which are geometrically equivalent to bulk sieve analysis, measurement of the B axis of the collected grains should yield a grain-size distribution closely similar to the one produced by sieving the specimen.

Under certain conditions, there may be direct axial correspondence between an apparent and true axis for grains on an OGS (1.3.6). If the true axis is B and the corresponding apparent axis is measured, it seems likely that any of the three geometrically equivalent sampling procedures (1.4.5) may be used to derive a grain-size distribution which is nearly identical to the one achieved by sieving.

For thin section and terrace gravel surfaces it is probable that the apparent axes of sampled grains do not correspond with true axial values (1.3.6). While sampling procedures geometrically equivalent to sieve analysis can be employed on these surfaces, some technique must be devised to obtain "the distribution of actual grain size (A,B,C,D, ...) from the corresponding distribution of observed sizes" (a,b, ...) (Kellerhals et al 1975, p.82). These "observed sizes" refer to the linear dimensions assigned to trace outlines of grains on either an apparent surface or a thin section.

1.5 Grid-by-Number Sampling of the Surface Layer of Exposed Gravel Bars

1.5.0 Introduction

Three surface-oriented sampling procedures, area-by-area,

transect-by-length and grid-by-number were shown to be geometrically equivalent to volume-by-weight (1.4.5). It is necessary to determine whether this theorized equivalence can be confirmed by sampling actual deposits.

Much work of this kind has been performed using the surface layer of exposed gravel bars. In these studies of this OGS (1.3.4) most research has compared the grain-size distributions arising from grid-by-number and bulk sieve analysis. The problems associated with collecting a grid-by-number sample of this surface layer (especially when only the apparent surface is examined) and the equivalence of this technique to bulk sieve analysis have many implications to similar terrace gravel grain-size investigations.

1.5.1 Comparison of Bulk Sieve and Grid-by-Number (B_t) Distributions

Kellerhals and Bray (1971) list four grid sampling methods which may be used on the surfaces of exposed gravel bars.

1) A grid is established over the gravel surface and the grains immediately beneath the grid points constitute the sample (see Thornes and Hewitt, 1967; Kellerhals and Bray, 1971; McGinn, 1971).
2) A survey tape is stretched across the area to be sampled using a set of regularly spaced points (e.g., footmarks) as grid points (Wolman, 1954).
3) A grid system is formed by traversing the sample area collecting the stone immediately beneath the toe after one or more steps (Wolman, 1954).
4) The operator walks along several parallel lines

stopping after each stride, averts his gaze and reaches down over his toe with a finger and the first rock touched is picked up for measurement (Leopold, 1970).

Once a grain was selected by one of the above grid collection techniques, usually one or more of the true axes were measured in the field (henceforth: subscript t signifies that the term's value depends upon the measurement of surface grain true or apparent axes; A_t, B_t, and C_t are terms denoting the field measurement of a grain's true A, B, and C axes; AB_t, ABC_t, BC_t are terms of denoting different arithmetic means derived from a grain's A_t, B_t, and C_t; ABC_t is the triaxial mean of a grain). Wolman (1954), and Kellerhals and Bray (1971) took B_t as being comparable to the square mesh sieve size D_s, and used 50 to 100 axial values to compare bulk sieve and grid-by-number grain size distributions. McGinn (1971), as well as testing B_t, examined the consequences of using grain-size measures AB_t, and ABC_t.

Generally, the results from these comparisons indicated that grid-by-number, using B_t, or ABC_t as a measure of grain size, yields grain-size distributions coarser than those generated by bulk sieve analysis procedures (henceforth: A_{t50}, AB_{t50}, B_{t50}, ABC_{t50}, BC_{t50}, and C_{t50}, are terms denoting various medians of grid-by-number distributions based on field measurements of true axes; $\overline{A}_t$, $\overline{AB}_t$, $\overline{B}_t$, $\overline{ABC}_t$, $\overline{BC}_t$, and $\overline{C}_t$ are terms denoting various means* of grid-by-number distributions based on field measurements of true axes; subscript sieve signifies that the term's value depends upon square mesh grain-size measurement; $D_{sieve50}$ is the term denoting the median of a grain-size distribution produced by sieving; $\overline{D}_{sieve}$ is the term denoting the mean of a grain-size distribution produced by sieving). While Wolman (1954) found that B_{t50} was

*means used in this thesis are Folk and Ward unless otherwise specified

substantially greater than $D_{sieve50}$, Kellerhals and Bray (1971) concluded on the basis of 15 samples, B_{t50} was only slightly greater than $D_{sieve50}$ (grains $\geq$ 8mm). McGinn (1971, Table 4) found that grid-by-number (B_t) and bulk sieve distributions (grains $\geq$ 8mm) were significantly close in only 43.1 percent of the 30 test samples. McGinn also utilized the Wilcoxon Test (Wilcoxon Matched Pairs Signed Ranks Test) to compare the statistical parameters (median, mean, standard deviation, skewness and kurtosis) of each grain-size distribution. The Wilcoxon Test indicated that grid-by-number (B_t) and bulk sieve distributions were not statistically similar except for skewness. As well, the Wilcoxon Test (one-tailed) revealed that $\overline{B}_t > \overline{D}_{sieve}$.

Most researchers agree that there is one major problem with using the surface layer of exposed gravel bars to test the equivalence between grid-by-number and bulk sieve sampling procedures. As Kellerhals and Bray (1971, p.1166) explain:

> "At low to intermediate stages virtually all sand and sometimes the finer gravel fractions are removed from the bed surface of a gravel-bed river. This results in a distinct pavement of the bed with a gravel layer one grain thick ... gravel beds commonly consist of two separate populations, the surface layer and the underlying deposit."

Kellerhals and Bray argued that while the surface layer is very important to hydraulic friction or initiation of bed movement studies, it theoretically cannot be sampled volumetrically. This is because the gravel layer is only one grain thick, thus the thickness dimension of an intended volumetric sample (all three dimensions are predetermined by the operator) cannot be predetermined. This argument justifies the use of a surface oriented technique like grid-by-number but suggests it may be difficult to confirm the equivalence between this technique and customary bulk

sieve analysis. If population differences are ignored completely the grid-by-number (B_t) distribution is substantially coarser than that produced by sieving (Wolman, 1954). Both Kellerhals and Bray (1971) and McGinn (1971) eliminated material less than 8 mm from their bulk sieve analyses in what the former said was, " ... an attempt to compensate for the population differences between the surface layer and the underlying volume.". However, as discussed, both still found grid-by-number (B_t) distributions to be coarser than those of bulk sieve.

1.5.2 Comparison of Grid-by-Number (B_t) and (b_t) Distributions

In some of the above studies, the apparent surface of exposed gravel bars (an example of an apparent OGS, refer 1.3.4) was sampled with grid-by-number.

The surface layer of the exposed gravel bars was photographed so that the line of sight was approximately normal to the surface plane. A grid was superimposed either in the field or on the photograph (slide or print). In either case, the photograph always contained some means (rulers at right angles or the grid) whereby the surface plane could be more precisely normalized. With this done and the grid in place the trace outlines of the surface grains falling beneath the grid intersection points were measured. Generally, only those grains which were > 8mm were used (Thornes and Hewitt, 1967; Kellerhals and Bray, 1971; McGinn, 1971).

The problem remains as to how the trace outlines of the grid selected surface grains should be measured. Pashinsky (1964, p.279) and Leopold (1970, p.1358) observed that the C axis of the surface layer gravels were normal to the surface plane. Although this is an approximation in cases where there is imbrication (Johanson, 1963), basically the surface

layer can be treated as an example of a situation discussed in 1.3.6, case b) and 1.4.6, namely, there is a direct axial correspondence between major and minor apparent axes a and b and true axial values A and B respectively, for contact mode 1 grains of the apparent OGS. Generally, contact mode 1 grains can be recognized on the apparent surface because they tend not to be overlapped. Therefore, it can be expected that measurements of the b axis of the gravel bar contact mode 1 surface grains selected by a grid, would produce a grid-by-number distribution very similar to that of grid-by-number (B_t) (henceforth: a_t and b_t are terms denoting the major and minor apparent axes respectively, of a surface grain associated with either an apparent or thin section surface; ab_t is the term denoting the arithmetic mean derived from a_t and b_t; a_{t50}, ab_{t50}, b_{t50} are terms denoting various medians of grid-by-number distributions based on measurements of surface grain apparent axes; $\overline{a}_t$, $\overline{ab}_t$, $\overline{b}_t$ are terms denoting various means of grid-by-number distributions based on measurements of surface grain apparent axes).

Kellerhals and Bray (1971) and McGinn (1971) compared the grid-by-number distributions based on the measurement of B_t and b_t. The former advanced the tentative correction formula, $b_{t50}=0.88B_{t50}$ based on 14 sample points. McGinn's results revealed that for 30 samples compared in this manner, the grain-size distributions were statistically equivalent in 93.3 percent of the cases. The Wilcoxon Test (McGinn, Table 5) disclosed that grid-by-number (B_t) and grid-by-number (b_t) were significantly close for median, skewness and kurtosis parameters.

Kellerhals and Bray recognized that there was some disagreement between the two sampling procedures, but concluded that the results were closely equivalent. McGinn stated that these grid-by-number procedures produce significantly close results for median and mean values.

1.5.3 Comparison of Bulk Sieve and Grid-by-Number (b_t) Distributions

Both Kellerhals and Bray (1971) and McGinn (1971) examined the relationship between grid-by-number (b_t) and bulk sieve grain-size distributions. Based on 11 sample points, Kellerhals and Bray advance $D_{sieve50}$ (grains greater than 8mm) = $1.0b_{t50}$ + 5mm as a tentative correction formula. McGinn found that these two grain-size distributions were equivalent in 66.7 percent of his 30 samples. The Wilcoxon Test (two-tailed) indicated that the two distributions were significantly similar only for standard deviation and skewness parameters and the Wilcoxon Test (one-tailed) confirmed that $\overline{b}_t$ was greater than $\overline{D}_{sieve}$.

The above results seem to conflict, since Kellerhals and Bray found $D_{sieve50}$ was greater than b_{t50} and McGinn showed that $\overline{b}_t$ was greater than $\overline{D}_{sieve}$. Examination of 1.5.1 and 1.5.2 reveals that these results are consistent with their respective studies. Since Kellerhals and Bray found B_{t50} slightly greater than $D_{sieve50}$ in 1.5.1, and B_{t50} greater than b_{t50} in 1.5.2, it is quite possible that one should find $D_{sieve50}$ greater than b_{t50} (1.5.3). McGinn observed $\overline{B}_t$ was greater than $\overline{D}_{sieve}$ in 1.5.1 but he found in contrast to Kellerhals and Bray B_{t50} was equivalent to b_{t50} (1.5.2). Therefore, McGinn's finding that $\overline{b}_t$ was greater than $\overline{D}_{sieve}$ (1.5.3), is reasonable. Perhaps the C axis of the surface layer gravels McGinn examined were more strongly oriented normal to the surface plane.

1.5.4 Relative Coarseness of Grid-by-Number (B_t) Distributions

The gravel bar experiments reviewed in this section indicate that grid-by-number (B_t) distributions tend to be coarser than their bulk sieve counterparts. This may arise for two reasons:

1) Geometric Non-equivalence

As discussed in 1.5.1 gravel beds often possess two separate populations due to surface paving, a surface pavement one grain thick and a finer underlying deposit. Given these conditions, the geometric equivalence between bulk sieve analysis and grid-by-number would breakdown, since the latter employs exclusively the coarser surface layer. Although these population differences have been recognized and compensated for by only sieving material greater than 8 mm, this compensation may not be sufficient to overcome population differences.

2) Non-equivalence of Grain-size Measures

Discrepancies may arise due to the assignment of linear dimensions to grains. It has generally been assumed that the B axis is comparable to D_s, as a measure of grain-size. If population differences have been compensated for adequately, then the relative coarseness of grid-by-number (B_t) distributions may stem from the B axis having a greater value than their D_s.

CHAPTER TWO

THE NUMERICAL METHOD AND THREE EMPIRICAL TESTS

2.1 General Introduction

This chapter presents Kellerhals et al (1975) numerical method and three empirical experiments which test its predictions for nonuniform materials.

The numerical method, which was explicitly developed for the grain-size sampling of thin sections, incorporates solutions to geometric and grain-size measure equivalence problems discussed in Chapter One. Grid-by-number is taken to be geometrically equivalent to bulk sieve analysis (see 1.4.5). Their equations (3a), (3b), and (3c) embody the belief that B and D_s are systematically related in such a way that equivalence is a special case (see 1.4.6 and 1.5.4).

Kellerhals et al (1975) argue that other attempts at determining grain size from thin sections of densely packed granular materials have run into difficulties for the following reasons:

1) The sampling procedures employed have not been geometrically equivalent to bulk sieve analysis.
2) Many theoretical approaches employ spherical shaped grains or ellipsoids of rotation. Instead, ellipsoids whose k values are within the common range should be observed.
3) Theoretical solutions assume that the grain centers are distributed in space according to the Poisson process. This is reasonable for dilutely distributed phases but not for densely packed granular materials found in sediments. The procedures involved in sampling this

material have resisted analytical study because there is no mathematical definition of a random distribution of grain centers, given a closely packed granular phase of nonoverlapping grains.

2.2 The Numerical Method

2.2.0 Introduction

The comprehensiveness of the numerical method contrasts with the simplicity of the experiments in 1.3. Other than this, any difference depends solely upon which is fixed in position, the plane or ellipsoid. In 1.3 ellipsoids were moved relative to a fixed plane, whereas, in the thin section experiment the fixed plane was transformed into a cutting plane operating on a fixed ellipsoid.

2.2.1 Computation

In the numerical method, distributions of apparent axes a and b were computed by cutting ellipsoids with a large number of planes and determining the lengths of the major and minor axes of the elliptical intercepts between the planes and the ellipsoid. Cutting planes were defined by latitude α, longitude β, and the length r, of the normal from the center of the ellipsoid (origin of the spherical coordinate system) to the cutting plane (Figure 11). All ellipsoids were assumed to have a square mesh diameter D_s=1.0. With Zingg diagram coordinates $k_1=\frac{B}{A}$, $k_2=\frac{C}{B}$, the relationships between D_s and the three axes were given as:

$$A=\frac{2}{k_1}\left[2(1+k_2^2)\right]^{-\frac{1}{2}}D_s \qquad (2)$$

$$B=2\left[2(1+k_2^2)\right]^{-\frac{1}{2}}D_s \qquad (3)$$

$$C=2k_2\left[2(1+k_2^2)\right]^{-\frac{1}{2}}D_s \qquad (4)$$

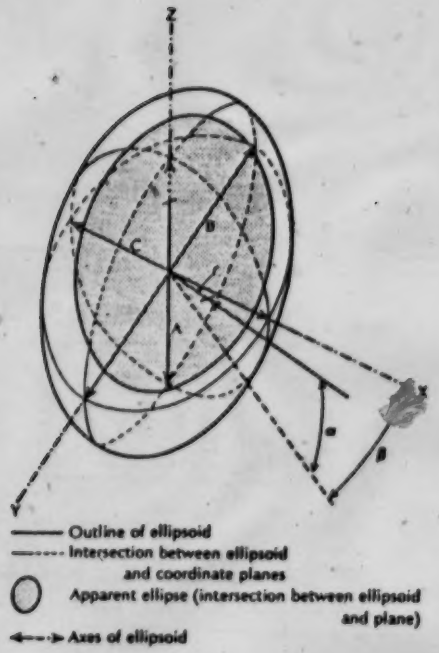

Figure 11 Axonometric Pictorial of an Ellipsoid Intersected by a Plane (The true axes are A=2C and B=1.5C. A line of sight with $\alpha=60^{\circ}$ and $\beta=60^{\circ}$ is used. The plane of intersection is located a distance of 0.5C from the center of the ellipsoid along a line with $\alpha=45^{\circ}$ and $\beta=30^{\circ}$.) (from Kellerhals et al 1975, p.83)

The procedure produced approximately 8000 to 12000 sample ellipses per ellipsoid. The resulting a and b values were arranged in 20 size classes and plotted as histograms, and as cumulative frequency distributions. A total of 49 ellipsoids were sampled using k_1 and k_2 values 0.15, 0.3, 0.5, 0.67, 0.75, 0.85, and 1.0 (see Kellerhals et al, 1975, p.83 for further details on numerical method).

2.2.2 Relationship among D_s, B and k_2

Interpretations of equations (2), (3), and (4) requires the consideration of the following three points:

1) D_s refers to the side length of a square hole, and not the maximum hole size. The maximum dimension of the square hole is along its two diagonals whose length $L_d = \sqrt{2D_s^2}$ (McGinn, 1971, p.30).

2) For an ellipsoid the critical dimensions which determine whether it can possibly pass through a square hole of a given side length D_s, are its B and C axes. These axes form an elliptical plane with $\frac{\text{minor axis}}{\text{major axis}} = \frac{C}{B} = k_2$ of the parent ellipsoid.

3) If the elliptical plane formed in 2) is coplanar with the plane formed by the sides of the square hole, and the center of the square is also that of the ellipse, and the B axis of the ellipse falls along one of the diagonals, then three cases arise:

   a) The boundary of the ellipse in part or completely falls outside the square, thus the parent ellipsoid is retained by the square hole (Figure 12a).

   b) The boundary of the ellipse touches the square at four points but never falls outside, thus the parent

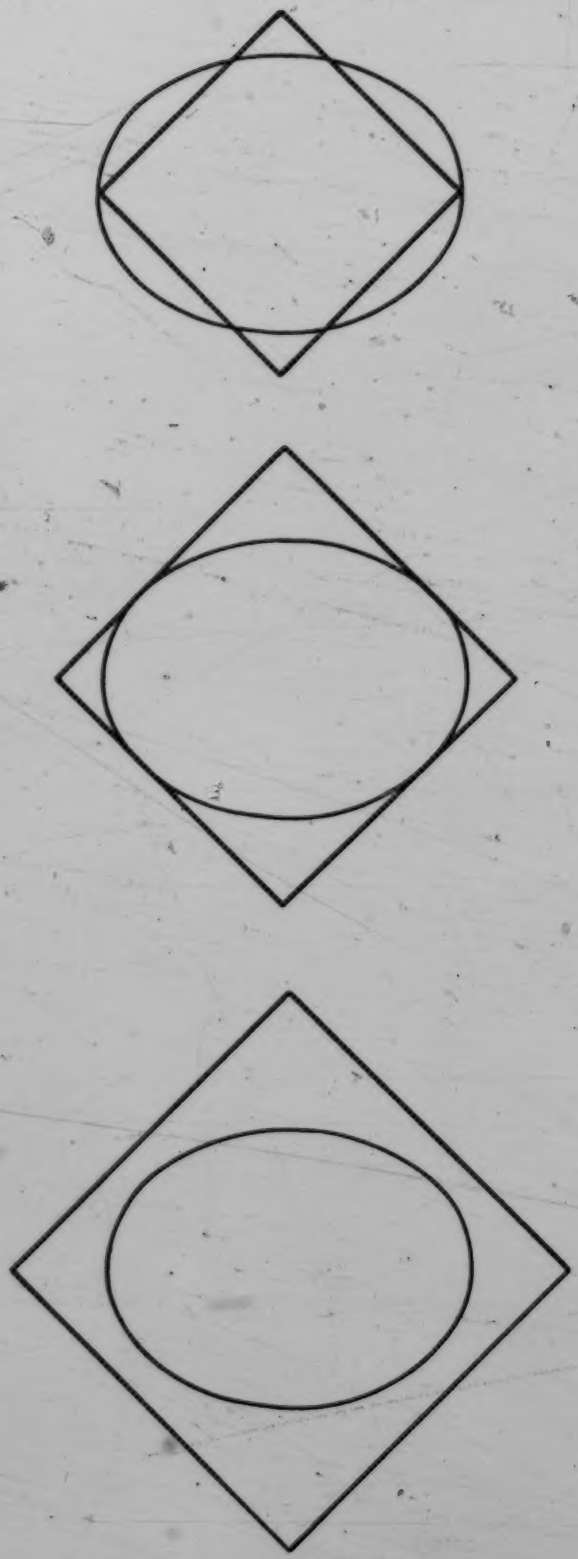

Figure 12

The Relationship of an Ellipse to a Square Hole: Three Cases

a) The boundary of the ellipse in part or completely falls outside the square

b) The boundary of the ellipse touches the square at four points but never falls outside

c) The boundary of the ellipse falls completely within that of the square

ellipsoid is at the threshold of being either retained or passed by the square hole (Figure 12b).

c) The boundary of the ellipse falls completely within that of the square, thus the parent ellipsoid passes through the square hole (Figure 12c).

The relationships among D_s, k_2, A, B, and C in (2), (3), and (4) are determined for case b). For illustration, B is calculated using (3); where D_s is held constant at 1.0 and k_2 varied from 0.001 to 1.0. As k_2 increases, the B axis of the ellipse decreases (Table 5 and Figure 13). At k_2=0.001, B=1.4142 which equals L_d for D_s=1.0. For common k_2 values, 0.55-0.75, B:D_s ranges from 1.24:1 to 1.13:1 respectively. When k_2 reaches 1.0, B=D_s=1.0. This is the special case where the ellipse is in fact a circle which touches the square at the midpoints of the four sides.

2.2.3 Apparent Axial Distributions a and b

The histograms and cumulative frequency distributions generated by the numerical method reveal relationships among ellipsoidal k values, true axial values and apparent axial distributions a and b. Spheres and ellipsoids of rotation, which have received much attention in the literature, have very unusual histograms relative to ellipsoids (k_1 less than 1, k_2 less than 1) (Kellerhals et al, 1975). By means of equations (2), (3), and (4) and Figures 14 a and b which summarize the relationships between true axial values, k values and the means of the apparent axial distributions, inequalities can be constructed. For ellipsoids with k values within the common range, 0.55-0.75, five pairs of k values were selected and the inequalities formed for A, B, C, D_s, $\overline{a}$, $\overline{b}$, and $\overline{ab}$ (mean of $\overline{a}$ and $\overline{b}$). In each case D_s was assigned a value of 1.0. The inequalities and their numerical values (Table 6) lead to the following observations.

Table 5
B Values Calculated by Equation (3),
D_s=1.0, k_2 range, 0.001 to 1.0

D_s	k_2	B
1.0	.001	1.4142
1.0	.01	1.4141
1.0	.02	1.4139
1.0	.03	1.4136
1.0	.04	1.4131
1.0	.05	1.4124
1.0	.06	1.4117
1.0	.07	1.4108
1.0	.08	1.4097
1.0	.09	1.4085
1.0	.10	1.4072
1.0	.20	1.3868
1.0	.30	1.3546
1.0	.40	1.3131
1.0	.50	1.2649
1.0	.60	1.2127
1.0	.70	1.1586
1.0	.80	1.1043
1.0	.90	1.0512
1.0	1.00	1.0000

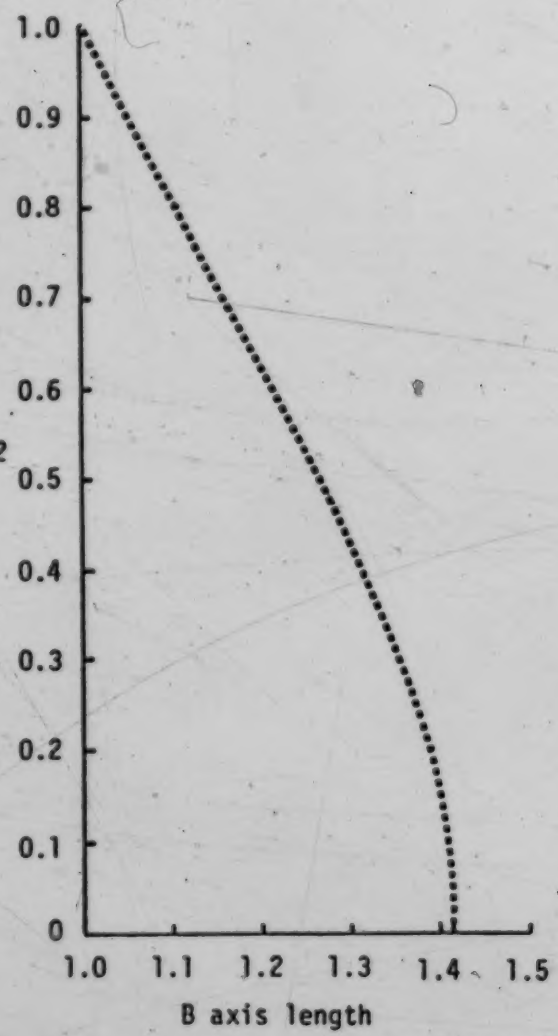

Figure 13
Graph of Table 5 Data

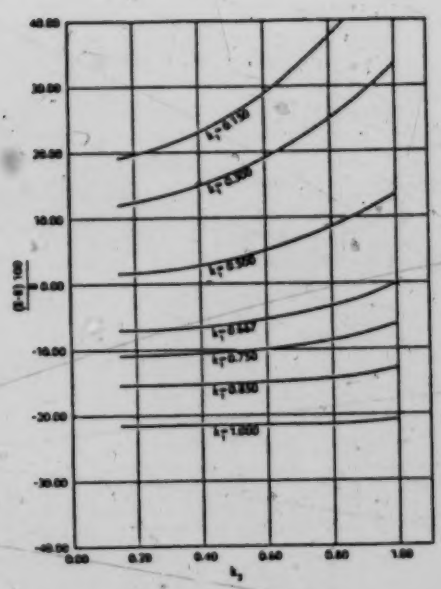

Figure 14a

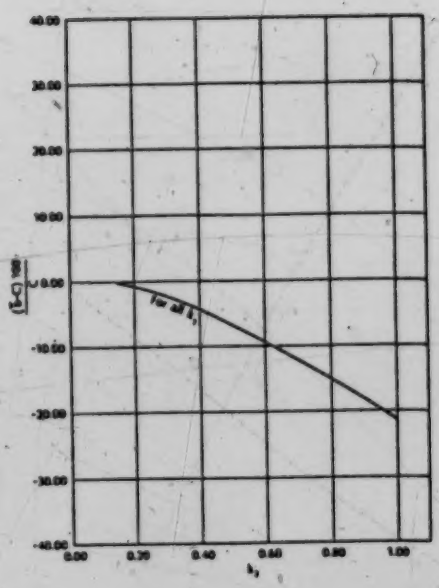

Figure 14b

Difference Between the Sample Mean of Apparent Axes and the Corresponding True Axes (from Kellerhals et al 1975, p.88)

Table 6
Axial Inequalities for Ellipsoids
with Common k Values 0.55-0.75

D_s	k_1	k_2	Inequality						
1.0	.55	.55	A	> $\bar{a}$	> B	> D_s	> $\overline{ab}$	> C	> $\bar{b}$
			2.25	1.25	1.24	1.0	0.94	0.68	0.63
1.0	.65	.65	A	> B	> $\bar{a}$	> D_s	> $\overline{ab}$	> C	> $\bar{b}$
			1.82	1.19	1.15	1.0	0.92	0.77	0.69
1.0	.75	.75	A	> B	> $\bar{a}$	> D_s	> $\overline{ab}$	> C	> $\bar{b}$
			1.51	1.13	1.03	1.0	0.88	0.85	0.73
1.0	.55	.75	A	> $\bar{a}$	> B	> D_s	> $\overline{ab}$	> C	> $\bar{b}$
			2.06	1.18	1.13	1.0	0.96	0.85	0.73
1.0	.75	.55	A	> B	> $\bar{a}$	> D_s	> $\overline{ab}$	> C	> $\bar{b}$
			1.65	1.24	1.12	1.0	0.88	0.68	0.63

1) Two inequality patterns emerge:

$A > \bar{a} > B > D_s > \overline{ab} > C > \bar{b}$ and

$A > B > \bar{a} > D_s > \overline{ab} > C > \bar{b}$

These inequalities are the same except $\bar{a}$ and B are reversed in position. The reason for this is discernable in Figure 14a. It reveals that $\bar{a} > B$ when $k_1 < 0.52$ (for all k_2) and $B > \bar{a}$ when $k_1 \geq 0.667$ (for all k_2). For $0.52 < k_1 < 0.667$, $\bar{a} > B$ for lower k_1 and higher k_2 values, for $B > \bar{a}$ the converse is true. Thus for the five pairs examined it is reasonable to expect k_1, k_2 pairs 0.55, 0.55 and 0.55, 0.75 will exhibit the inequality $\bar{a} > B$.

2) For the five pairs and more generally for any k_1, k_2 pair with values within the common range, B and $\bar{a}$, and C and $\bar{b}$ are closely associated. Within this range

$4.4 \geq \frac{(\bar{a}-B)100}{B} \geq -10.0$ (Figure 14a) and

$-8.0 \geq \frac{(\bar{b}-C)100}{C} \geq -13.8$ (Figure 14b). This latter figure shows the inequality $C > \bar{b}$ is true for all pairs of k values.

3) For the five pairs $B > D_s > C$. Inspection of equations (2), (3) and (4) demonstrates that $B > D_s > C$ whenever ellipsoidal k values are less than 1.0 (see also 2.2.2).

The preceding results were based on grains of a particular shape characterized by one point on the Zingg diagram. The sensitivity of a distribution to variability in shape was tested by forming a combined a-distribution for grains with values clustered around a point on the Zingg diagram. This was compared with the distribution of a, for grains with the central shape characteristic. Kellerhals et al (1975)

found the curves to be very similar and thus concluded that an average shape value was justified.

2.3 Three Empirical Experiments

2.3.0 Introduction

The numerical method simulates the grid-by-number sampling of a randomly selected thin section obtained from an isotropic material composed of identical ellipsoidal grains. Given the axial dimensions of the constituent grains of this uniform material, equations (2), (3), and (4) (2.2.1) and Figures 14a and b (2.2.3) predict the D_s and mean values of apparent axial distributions a and b which would be obtained if this material was actually sampled. While results can be extended for a material in which grains vary in shape (2.2.3), both grain shape and size vary in most clastic sediments. For the numerical method to have practical value it must be shown that it is applicable to the sampling of these nonuniform materials.

2.3.1 Experiment 1

Kellerhals et al (1975, p.85) compare the median sieve diameter predicted by their numerical method with that obtained by sieving, $D_{sieve50}$, for seven sandstone samples. For all samples, grid-by-number (a_t) and grid-by-number (b_t) distributions were obtained from thin sections. Simultaneous grid-by-number and bulk sieve distributions for five of these samples were obtained from Friedman (1958, Figure 7). The two remaining samples, Y_1 and Y_2 were acquired from two artificial sandstone blocks made by cementing mixtures of fluvioglacial sand. These blocks were then cut to produce thin sections.

For Friedman's data, b_{t50} was converted to C_{p50}, a numerical method prediction of C (henceforth: subscript p signifies that the term's value depends both on experimental data and numerical method

predictions). The conversion of b_{t50} into C_{p50} is as follows: Using average $k_2=\frac{b_{t50}}{a_{t50}}$ in Figure 14b, $\frac{(\bar{b}-C)100}{C} = Y$, $C_{p50}= (1.0-Y)(b_{t50})$, (method used by Kellerhals et al, 1975, p.85) $\bar{C}_p$, the mean counterpart of C_{p50} can be calculated in the same way except $\bar{b}_t$ and $\bar{a}_t$ are used. A similar but more precise formula for C_{p50} is $\frac{100b_{t50}}{(Y+100)}$.

Using C_{p50} and (4) the predicted median sieve diameter $d_{sp50}= \frac{C_{p50}}{2k_2}[2(1+k_2^2)]^{\frac{1}{2}}$ was calculated. The mean counterpart of d_{sp50}, $\bar{d}_{sp}$ can be calculated in the same way except $\bar{b}_t$, $\bar{a}_t$, and $\bar{C}_p$ are used. The d_{sp50} of samples Y_1 and Y_2 were calculated in a similar manner except that (3) was employed. This was made possible because k_1, which is necessary to the determination of B from Figure 14a), had been estimated through microscopic measurement of A_t and B_t axes of 100 constituent grains of Y_1 and Y_2.

The results (Table 7) for the seven samples may be summarized as follows.

1) The k_2 values of these samples range from 0.59 to 0.69. This is within the common range of k values.

2) $a_{t50} > d_{sp50} > b_{t50}$

   $a_{t50} > D_{sieve50} > b_{t50}$ except for Cardium Sandstone where $D_{sieve50} > a_{t50}$

3) $D_{sp50} > ab_{t50}$

   $D_{sieve50} > ab_{t50}$ for Y_2, $D_{sieve50} = ab_{t50}$

4) $D_{sieve50}$ and d_{sp50} values compare reasonably well for the seven samples. This may be observed either directly or by comparing the ratios $a_{t50}:d_{sp50}$ and $a_{t50}:D_{sieve50}$ for each sample. The mean value of the former is 1.09:1 and the latter ratio is 1.10:1.

Table 7
Comparison Between Predicted
and Actual Median Sieve Sizes, d_{sp50} and $D_{sieve50}$
(adapted from Kellerhals et al, 1975, Table 1)

Sample	a_{t50} (mm)	b_{t50} (mm)	ab_{t50} (mm)	k_2	d_{sp50} (mm)	$D_{sieve50}$ (mm)	Ratio $a_{t50}:d_{sp50}$	Ratio $a_{t50}:D_{sieve50}$
Y_1	0.414	0.287	0.351	0.69	0.388	0.354	1.07:1	1.17:1
Y_2	0.456	0.316	0.386	0.69	0.427	0.386	1.07:1	1.18:1
Trinity Sandstone I	0.218	0.128	0.173	0.59	0.193	0.200	1.13:1	1.09:1
Trinity Sandstone II	0.167	0.109	0.138	0.65	0.157	0.159	1.06:1	1.05:1
Simpson Sandstone	0.166	0.109	0.138	0.66	0.155	0.144	1.07:1	1.15:1
Tensleep Sandstone	0.142	0.085	0.114	0.60	0.128	0.128	1.11:1	1.11:1
Cardium Sandstone	0.069	0.043	0.056	0.62	0.063	0.072	1.10:1	0.96:1
						Mean	1.09:1	1.10:1

In general d_{sp50} and $D_{sieve50}$ appear to be comparable. Both participate analogously in inequalities, form similar ratios and are close in actual value. Since d_{sp50} was based on the numerical method which assumes a uniform material, and $D_{sieve50}$ was produced by sieving a nonuniform material, their high degree of correspondence supports the hypothesis that the numerical method can be employed effectively in sampling thin section surfaces of nonuniform materials.

2.3.2 Experiment 2

Friedman (1958, 1962) discussed the results of thin section grid-by-number (a_t) and bulk sieve analyses of his 38 sandstone samples. Table 8 (adapted from Friedman, 1962, Table 2a) displays $\overline{a}_t$, $\overline{D}_{sieve}$ and $\overline{a}_t$:$\overline{D}_{sieve}$ for these samples (for Friedman Mean $\overline{x}_\phi = \frac{1}{100} \Sigma$ fm where f = frequency of the different grain-size grades present, and m_ϕ = mid-point of each grain-size grade in phi values).

For all samples $\overline{a}_t > \overline{D}_{sieve}$*. This conforms with both predicted and actual inequalities in Tables 6 and 7 (sole exception being Cardium Sandstone where a_{t50}:$D_{sieve50}$=0.96:1). In order to further clarify the extent to which the numerical method predicts this inequality to arise, at least for uniform materials, and particularly for k_1, k_2 pairs within the common range, three possible cases ($a > D_s$, $a=D_s$ and $D_s > a$) were investigated. Results (Table 9 and Figure 15a) indicate that the k_1, k_2 pairs region where $D_s > \overline{a}$, is very small relative to the $\overline{a} > D_s$ region, and is confined to k_1, k_2 pairs of high value. As well, k_1, k_2 pairs within the common range fall completely within the latter region. Assuming that most of Friedman's sandstone samples have mean k values within the common range, these results confirm the predictive power of

*in 2.3.2 the values of mean terms are in mm.

Table 8
The Ratio $\overline{a}_t:\overline{D}_{sieve}$ Based on Thin Section Grid-by-Number Analysis and Bulk Sieve Analysis
(adapted from Friedman, 1962, Table 2a)

Sample	$\overline{a}_t$ (Ø units)	$\overline{D}_{sieve}$ (Ø units)	$\overline{a}_t$ (mm)	$\overline{D}_{sieve}$ (mm)	Ratio $\overline{a}_t:\overline{D}_{sieve}$
1	2.55	2.68	.171	.156	1.10:1
2	2.70	2.92	.154	.132	1.17:1
3	2.58	2.73	.167	.151	1.11:1
4	2.39	2.60	.191	.165	1.16:1
5	2.56	2.83	.170	.141	1.21:1
6	2.77	2.99	.147	.126	1.17:1
7	2.65	2.81	.159	.143	1.11:1
8	2.70	2.98	.154	.127	1.21:1
9	2.72	2.84	.152	.140	1.09:1
10	2.82	2.98	.142	.127	1.12:1
11	0.90	1.03	.536	.490	1.09:1
12	0.93	1.34	.525	.395	1.33:1
13	0.81	1.24	.570	.423	1.35:1
14	0.74	1.13	.599	.457	1.31:1
15	0.75	1.17	.595	.444	1.34:1
16	2.50	2.71	.177	.153	1.16:1
17	3.64	3.76	.080	.074	1.08:1
18	3.18	3.44	.110	.092	1.20:1
19	3.02	3.36	.123	.097	1.27:1
20	2.85	2.88	.139	.136	1.02:1
21	2.22	2.33	.215	.199	1.08:1
22	2.09	2.17	.235	.222	1.06:1
23	2.30	2.41	.203	.188	1.08:1
24	2.65	2.74	.159	.150	1.06:1
25	2.05	2.14	.241	.227	1.06:1
26	1.70	1.93	.308	.262	1.18:1
27	3.51	3.78	.088	.073	1.21:1
28	3.78	3.87	.073	.068	1.07:1
29	3.97	4.18	.064	.055	1.16:1
30	3.74	3.86	.075	.069	1.09:1
31	3.80	3.94	.072	.065	1.11:1
32	3.51	3.52	.088	.087	1.01:1
33	3.15	3.42	.113	.093	1.22:1
34	2.74	3.03	.150	.122	1.23:1
35	2.18	2.49	.221	.178	1.24:1
36	2.05	2.48	.241	.179	1.35:1
37	2.21	2.39	.216	.191	1.13:1
38	1.88	2.20	.272	.218	1.25:1
				Mean Ratio	1.16:1
				Standard Deviation	0.09

Table 9
Some k_1, k_2 Pairs for which $\bar{a}:D_s$=1:1 or 1.16:1

k_1	k_2	D_s	B from equation (3)	From Figure 14a) $\frac{(\bar{a}-B)100}{B} = X$	$\bar{a}=B(\frac{X}{100}+1)$
0.667	1.00	1.00	1.00	0	1.00
0.75	0.82	1.00	1.09	- 8.5	1.00
0.85	0.66	1.00	1.18	-14.9	1.00
1.00	0.49	1.00	1.27	-21.6	1.00
0.48	1.00	1.00	1.00	+16.0	1.16
0.667	0.57	1.00	1.23	- 5.6	1.16
0.75	0.43	1.00	1.30	-10.6	1.16
0.85	0.25	1.00	1.37	-15.4	1.16

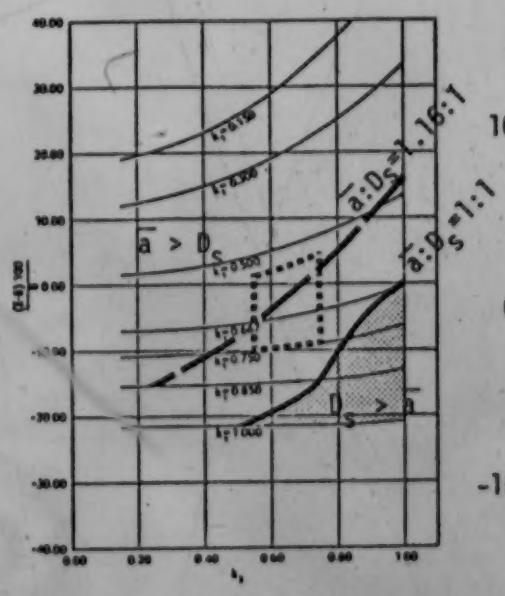

Figure 15a
Regions where $\bar{a} > D_s$ and $D_s > \bar{a}$
(adapted from Kellerhals et al 1975, Figure 5a)

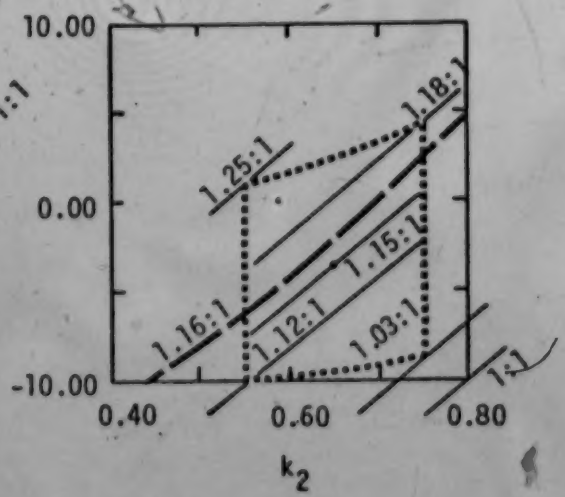

Figure 15b
$\bar{a}:D_s$ Values for k_1, k_2 Pairs Within the Common Range (refer Table 6)

the numerical method for nonuniform materials.

Table 8 indicates that the average $\bar{a}_t:\bar{D}_{sieve}$=1.16:1 (standard deviation 0.09) for the 38 sample ratios. For the purpose of evaluating this ratio with respect to numerical method predictions, the line corresponding to $\bar{a}:D_s$=1.16:1 was drawn (Figures 15a and b). As well, in Figure 15b, additional $\bar{a}:D_s$ ratios for common k_1, k_2 pairs found in Table 6 were plotted. Figure 15b shows that for the $\bar{a}:D_s$ equal width "bands" exist which decrease in value ($\bar{a}$ value decreases) as the k_1 and k_2 values of a pair approach 1.0. For k_1, k_2 pairs with common values, $\bar{a}:D_s$ ranges from 1.25:1 (k_1=k_2=0.55) to 1.03:1 (k_1=k_2=0.75). The $\bar{a}:D_s$= 1.16:1 line falls centrally within the subregion formed by the common range k_1, k_2 pairs. Significantly, the ratios 1.25:1 and 1.07:1, which correspond to the $\bar{a}_t:\bar{D}_{sieve}$ ratios which are one standard deviation on either side of the 38 sample mean, also fall within this subregion. Assuming that the mean k values of most of Friedman's samples fell within the common range, these results strongly support the hypothesis that the $\bar{a}:D_s$ ratios of the numerical method predict the behavior of $\bar{a}_t:\bar{D}_{sieve}$ for nonuniform materials.

2.3.3 Experiment 3

In section 1.5 distributions provided by grid-by-number (B_t) and bulk sieve analysis of exposed gravel bars, were examined. It was observed that grid-by-number (B_t) distributions were coarser than their D_{sieve} counterparts (1.5.1). It was concluded (1.5.4) that there were two reasons for this inequality arising; geometric non-equivalence due to surface paving and the non-equivalence of grain-size measures B and D_s. These possible causes of non-equivalence can be investigated in detail since McGinn's (1971) sampling program differentiates between surface and

subsurface deposits and the Kellerhals et al (1975) numerical method makes quantitative predictions concerning the relationship among B, D_s, and k_2 (2.2.2).

McGinn sampled the surface layer with essentially eight different procedures, including grid-by-number (B_t) and quadrant (area)-by-weight (henceforth: Q is the term denoting the quadrant (area)-by-weight sampling procedure whereby all surface grains $\geq$ 8 mm, within a specified area are removed and sieved; $\overline{Q}$ is the term denoting the mean of the grain-size distribution obtained from Q). The subsurface deposit was also sampled using bulk sieve analysis (henceforth: D_{sieve2} is the term denoting the bulk sieve analysis of the coarse ($\geq$ 8 mm) portion of the subsurface sample; $\overline{D}_{sieve2}$ is the term denoting the mean of the grain-size distribution obtained from D_{sieve2}). The weights of Q and D_{sieve2} were then added to provide the D_{sieve} distribution for each sample.

The advantage of comparing grid-by-number (B_t) and Q is that only surface grains are being sampled, thus population differences due to surface paving are avoided. However, as discussed by Kellerhals and Bray (1971) and McGinn (1971), Q is not geometrically equivalent to either grid-by-number or volume-by-weight and requires the weighting factor $\frac{1}{D}$,(refer to Kellerhals and Bray, 1971, p.1173, 1175 for more detail on this procedure; $\overline{Q}_{sieve}$ is the term denoting the mean of the Q_{sieve} grain-size distribution).

The values $\overline{Q}$, $\overline{Q}_{sieve}$, $\overline{D}_{sieve}$ and $\overline{D}_{sieve2}$* can be compared for both paved and non-paved deposits. If the deposit is paved, it is expected that $\overline{Q}_{sieve} > \overline{D}_{sieve} > \overline{D}_{sieve2}$, whereas if non-paved $\overline{Q}_{sieve}=\overline{D}_{sieve}=\overline{D}_{sieve2}$. In both types of deposits $\overline{Q} > \overline{Q}_{sieve}$ since the weighting factor $\frac{1}{D}$ applied to Q always produces a finer Q_{sieve} distribution.

*in 2.3.3 the values of mean terms are in mm.

Although Q_{sieve} and grid-by-number (B_t) are geometrically equivalent, the numerical method suggests that $\overline{B}_t > \overline{Q}_{sieve}$. More specifically, it predicts that for a uniform material composed of ellipsoids the $B:D_s$ range is 1.4142:1 to 1:1, where $B:D_s$=1.4142:1 as k_2 approaches 0 and $B:D_s$=1:1 for k_2=1.0. The $B:D_s$ range for common k_2 values is 1.24:1 to 1.13:1, where $B:D_s$=1.24:1 for k_2=0.55 and $B:D_s$=1.13:1 for k_2=0.75(2.2.2). Since the numerical method has been applied quite successfully to non-uniform materials in 2.3.1 and 2.3.2 and the grain-size measures of Q_{sieve} and grid-by-number (B_t) are D_s and B respectively, it is expected that the $\overline{B}_t:\overline{Q}_{sieve}$ range for surface layer gravels will be from 1.24:1 to 1.13:1, assuming a common range of k_2 values.

The results of McGinn's (1971, Tables 5 and 8) Wilcoxon Tests for his 30 samples tend to conform to expectation. It was found that $(\overline{Q}=\overline{B}_t) > \overline{D}_{sieve}$ (grid-by-number (B_t) and Q distributions were also similar for median, skewness and kurtosis parameters) and $\overline{Q}_{sieve}=\overline{D}_{sieve}$ (these distributions were also similar for median, skewness and kurtosis parameters). It may be inferred that $(\overline{Q}=\overline{B}_t) > (\overline{Q}_{sieve}=\overline{D}_{sieve})$. The inference that $\overline{B}_t > \overline{Q}_{sieve}$ lends support to the hypothesis that B is a coarser grain-size measure than D_s. The relative coarseness of $\overline{Q}$ and $\overline{B}_t$ compared to Q_{sieve} and D_{sieve} distributions has been predicted above, however, their apparent equivalence is not a necessary outcome of any of these predictions. The equivalence between Q_{sieve} and D_{sieve} distributions implies that the samples may not have been paved.

Geometric and grain-size measure non-equivalence were further examined by calculating the $\overline{B}_t$, $\overline{D}_{sieve}$ and $\overline{Q}_{sieve}$ values for McGinn's samples (raw data from McGinn, 1971, Appendix I) and then combining them to form ratios $\overline{B}_t:\overline{D}_{sieve2}$, $\overline{Q}_{sieve}:D_{sieve2}$ and $\overline{B}_t:\overline{Q}_{sieve}$ (Table 10). As

Table 10
Sample Weight $Q:D_{sieve2}$, $\overline{B}_t:\overline{D}_{sieve2}$
$\overline{Q}_{sieve}:\overline{D}_{sieve2}$ and $\overline{B}_t:\overline{Q}_{sieve}$
(adapted from McGinn, 1971, Appendix I)

Sample	Sample Weight $Q:D_{sieve2}$	$\overline{B}_t$ (mm)	$\overline{Q}_{sieve}$ (mm)	$\overline{D}_{sieve2}$ (mm)	$\overline{B}_t:\overline{D}_{sieve2}$	$\overline{Q}_{sieve}:\overline{D}_{sieve2}$	$\overline{B}_t:\overline{Q}_{sieve}$
1	1.32:1	34.3	22.6	14.9	2.30:1	1.52:1	1.52:1
2	1.28:1	27.9	26.0	14.9	1.87:1	1.74:1	1.07:1
3	1.05:1	24.3	19.7	13.9	1.75:1	1.42:1	1.23:1
4	1.68:1	45.3	29.9	21.1	2.15:1	1.42:1	1.52:1
5	1.61:1	34.3	27.9	19.7	1.74:1	1.42:1	1.23:1
6	1.27:1	39.4	39.4	14.9	2.64:1	2.64:1	1 : 1
7	0.80:1	34.3	27.9	18.4	1.86:1	1.52:1	1.23:1
8	1 : 1	29.9	24.3	16.0	1.87:1	1.52:1	1.23:1
9	0.96:1	34.3	27.9	17.1	2.01:1	1.63:1	1.23:1
10	0.75:1	26.0	17.1	18.4	1.41:1	0.93:1	1.52:1
11	0.50:1	21.1	17.1	14.9	1.42:1	1.15:1	1.23:1
12	0.34:1	39.4	21.1	16.0	2.46:1	1.32:1	1.87:1
13	1.31:1	39.4	39.4	34.3	1.15:1	1.15:1	1 : 1
14	1.50:1	48.5	29.9	32.0	1.52:1	0.93:1	1.62:1
15	0.28:1	32.0	29.9	13.9	2.30:1	2.15:1	1.07:1
16	0.79:1	36.8	24.3	19.7	1.87:1	1.23:1	1.51:1
17	0.28:1	26.0	16.0	14.9	1.74:1	1.07:1	1.63:1
18	0.57:1	29.9	21.1	16.0	1.87:1	1.32:1	1.42:1
19	0.58:1	29.9	21.1	14.9	2.01:1	1.42:1	1.42:1
20	1.45:1	45.3	36.8	36.8	1.23:1	1 : 1	1.23:1
21	1.28:1	45.3	36.8	29.9	1.52:1	1.23:1	1.23:1
22	0.42:1	18.4	13.9	18.4	1 : 1	0.76:1	1.32:1
23	0.69:1	18.4	14.9	14.9	1.23:1	1 : 1	1.23:1
24	1.18:1	32.0	42.2	17.1	1.87:1	2.47:1	0.76:1
25	0.99:1	27.9	32.0	14.9	1.87:1	2.15:1	0.87:1
26	0.97:1	27.9	29.9	16.0	1.74:1	1.87:1	0.93:1
27	0.92:1	34.3	29.9	14.9	2.30:1	2.01:1	1.15:1
28	1.38:1	32.0	34.3	17.1	1.87:1	2.01:1	0.93:1
29	1.11:1	34.3	32.0	16.0	2.14:1	2.00:1	1.07:1
30	1.15:1	36.8	29.9	16.0	2.30:1	1.87:1	1.23:1
Mean Ratio	0.98:1				1.83:1	1.53:1	1.25:1
Standard Deviation	0.40				0.40	0.48	0.25

well, the sample weight ratio $Q:D_{sieve2}$ was calculated. If these ratios show that the surface and subsurface populations were different, even though these suspected differences had been compensated for by using only grains $\geq$ 8 mm, then it is clear that D_{sieve} was a mixture of two distinct populations and the value of $\overline{D}_{sieve}$ was dependent upon their grain-size characteristics and proportions. As such, the comparison of a D_{sieve} distribution with surface sampling procedure distributions grid-by-number (B_t) or Q_{sieve}, cannot be expected to yield equivalent results, even if D_s and B were equivalent grain-size measures.

The ratio data in Table 10 clearly indicates that most of McGinn's samples were paved and thus D_{sieve} was actually a mixture of two distinct populations. The surface and subsurface deposits were combined in approximately equal proportions since the average value of the sample weight ratio $Q:D_{sieve2}$=0.98:1, standard deviation = 0.40. The relative coarseness of the surface is confirmed by the average value of the ratio $\overline{Q}_{sieve}:\overline{D}_{sieve2}$=1.53:1, standard deviation = 0.48. The average values of the ratios $\overline{B}_t:\overline{D}_{sieve2}$=1.83:1. standard deviation 0.40, and $\overline{B}_t:\overline{Q}_{sieve}$=1.25:1, standard deviation = 0.25 further emphasize the population differences. Grid-by-number (B_t) and Q_{sieve}, which are geometrically equivalent surface layer methods, were much closer in value than grid-by-number (B_t) and D_{sieve2}, which were derived from surface and subsurface deposits respectively. The Wilcoxon Test result, $\overline{Q}_{sieve}=\overline{D}_{sieve}$, which initially suggested that the samples were not paved, apparently was a consequence of applying the weighting factor $\frac{1}{D}$ to Q and combining Q with D_{sieve2} values, respectively. At least for McGinn's data, these two distinct value-reducing operations performed on Q, both produced statistically similar grain-size values.

The outcome of the investigation of the ratio $\overline{B}_t:\overline{Q}_{sieve}$ for McGinn's 30 samples bears heavily on the question of the non-equivalence of grain-size measures B and D_s since both grid-by-number (B_t) and Q_{sieve} are surface layer sampling procedures and are geometrically equivalent, but employ different grain-size measures B and D_s. The average value of the ratio $\overline{B}_t:\overline{Q}_{sieve}$=1.25:1, lies just outside the common k_2 value B:D_s range, 1.24:1 to 1.13:1 established by the numerical method, and corresponds to k_2=0.53. It is notable that 11 out of the 30 ratio values fall within this relatively narrow range, 10 of these being 1.23:1. The range of the $\overline{B}_t:\overline{Q}_{sieve}$ values determined by using the standard deviation 0.25, 1.50:1 to 1:1, corresponds quite closely with the predicted B:D_s range, 1.4142 to 1.1. These ratio results uphold the inference based on the Wilcoxon Tests that $\overline{B}_t > \overline{Q}_{sieve}$ implying that B is a coarser grain-size measure than D_s. Furthermore, assuming that the mean k values of most of McGinn's samples fell within the common range, $\overline{B}_t:\overline{Q}_{sieve}$ results compare quite well with numerical method predictions.

The preceding discussion examines why sampling procedure experiments which attempted to show the equivalence between bulk-sieve analysis and grid-by-number utilizing exposed gravel bars, generally found grid-by-number (B_t) distributions to be coarser than those of D_{sieve}. This effect was probably caused by geometric non-equivalence associated with surface paving and the non-equivalence of grain-size measures B and D_s. By comparing only geometrically equivalent surface layer sampling methods and employing the numerical method, the degree to which $\overline{B}_t > \overline{Q}_{sieve}$ was predicted with reasonable success. This outcome confirms the value of the weighting factors associated with the theory of geometric equivalence (grid-by-number is geometrically

equivalent to Q_{sieve}) and the predictive value of the numerical method's equation (3) for nonuniform materials.

2.3.4 Conclusion

Each of the three sampling experiments test a different facet of the numerical method's predictions for nonuniform materials. The success of these predictions strongly supports the conclusion that the numerical method has broad applicability to the solution of problems associated with nonuniform material sampling procedure equivalence.

CHAPTER THREE

TERRACE GRAVEL EXPERIMENT METHODOLOGY

3.1 General Introduction

The apparent EGS of a terrace gravel exposure can be treated as a thin section surface (1.3.5). However, this surface is different from that of a thin section in that both apparent and true axial values of grid selected surface grains can be measured easily. Thus terrace gravels provide a unique opportunity to test certain numerical method predictions not considered in the previous three experiments.

This chapter presents methods associated with the fourth experiment; the grid-by-number sampling of terrace gravels. It describes the study area, the field procedures employed in the collection of the terrace gravel grid samples, and the methods used to analyze the resulting data.

3.2 The Study Area

Whitemud and Weed Creeks are north-flowing tributaries of the North Saskatchewan River. These two neighbouring stream systems, which are found in the vicinity of Edmonton, Alberta (Figure 16), have been the subject of geomorphic investigation by Rains (1969) and Shelford (1974). Their terrace maps as well as Rains' numerous Whitemud terrace stratigraphies, greatly simplified the search for terrace gravels suitable for testing.

A discussion of the surficial geology of both basins assists in clarifying the character of the terrace deposits. In particular, their lithological variability is a direct outcome of a complex regional surficial geology. The present summary follows Westgate's (1969) comprehensive paper on the Quaternary geology of the Edmonton area.

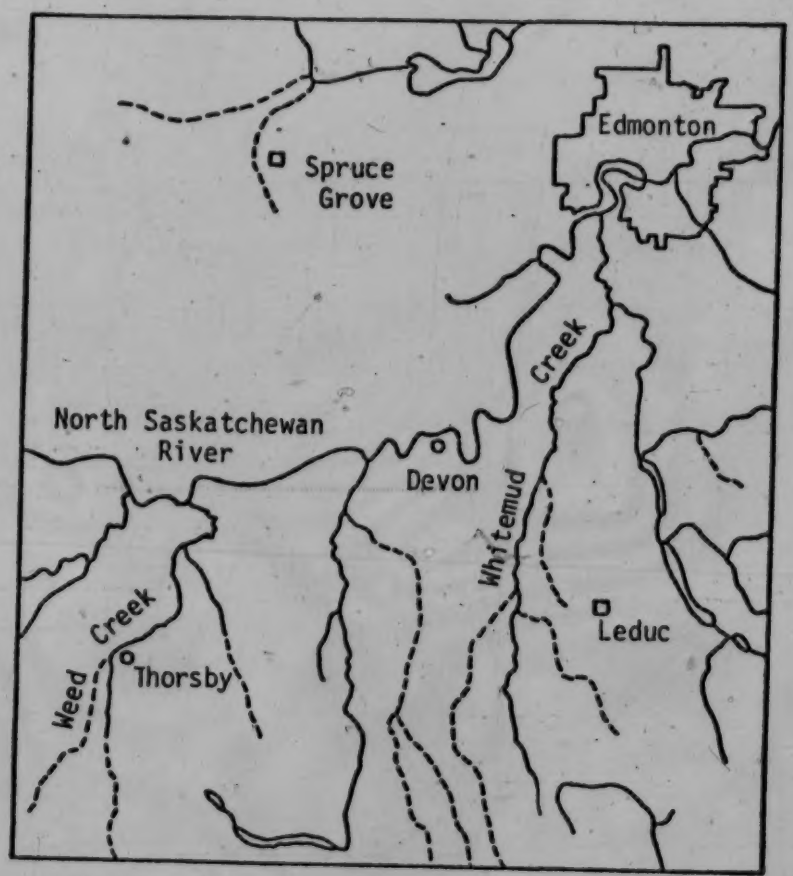

Figure 16

The Study Area, Whitemud and Weed Creeks near Edmonton, Alberta

Bedrock in the Whitemud and Weed Creek drainage basins is predominantly Upper Cretaceous in age, and consists of interbedded bentonitic shales and sandstones, with some coal seams and bentonite beds. Lying unconformably upon the bedrock, and associated with preglacial valleys, fluviatile preglacial Saskatchewan Sands and Gravels are found as terrace and valleyfill deposits. The lithology of this material is primarily quartzose sandstone and chert but also includes arkosic sandstone, jasper and local bedrock. This composition provides strong evidence of Cordilleran origin. Overlying the Saskatchewan Sands and Gravels or sitting directly on the bedrock is a lower grayish brown till. This and another Laurentide till (upper till) are commonly separated by stratified sediments known as Tofield Sand. Both tills bear a sizeable proportion of Canadian Shield igneous and metamorphic rocks. The northern sections of both basins are veneered with lacustrine deposits from the former proglacial Lake Edmonton.

Shortly after the draining of Lake Edmonton, the North Saskatchewan began to cut its valley. Within this postglacial river valley four distinct terrace levels can now be observed indicating that the river has shown variable rates of degradation. The terrace maps of Rains and Shelford revealed analogous terracing patterns in both their tributary valleys. The presence of what are termed the "lower, middle, upper and higher" cyclic terraces convinced them that periods of aggradation and degradation within these tributaries depended upon base level changes of the North Saskatchewan.

The terrace gravels found within the Whitemud and Weed Creek basins are lithologically highly variable. The composition is related to the local abundance and availability of the Horshoe Canyon Formation,

Saskatchewan Sands and Gravels and till-derived materials. Typically, the terrace stratigraphy consists of bedrock overlain by a thin stratum of alluvial, occasionally imbricated gravel grading upwards into fine grained sediments.

3.3 Field Methods

3.3.0 Introduction

This section discusses the factors involved in site selection and methods of grid placement, grain selection and measurement.

3.3.1 Site Selection

The terrace exposures examined were those of the lower and middle terraces of both Whitemud and Weed Creeks. The following criteria were used to determine the site selection.

1) Site Accessibility - Some promising exposures were inaccessible because they were found on quite sheer cut-banks.
2) Dimensions of Gravel Stratum - The exposed terrace gravel stratum had to be large enough to accept the 0.5m square grid, so the exposure's minimum dimension had to be at least 0.5M.
3) Material - Terrace gravel deposits which appeared quite isotropic and homogeneous were preferred. In most gravel strata anistropy due to imbrication was low. Deposits which consisted of substantial quantities of shales and sandstones were avoided because they were in sheets and were usually highly fractured and difficult to extract.

4) Surface - The gravel surfaces selected were near vertical and approximately flat. If it was not flat initially it was modified so as to decrease photographic scale distortion due to distance variations.

3.3.2 Grid Placement, Grain Selection and Measurement

In order to standardize site investigation, a five step procedure was adopted:

Step 1) A 0.5m grid with 100 intersection points was staked firmly in place at the chosen site. Each grid was labelled for purposes of photographic identification (Figure 17a) e.g., WMM3G; Whitemud Creek, middle terrace, site 3, grid G.

Step 2) The grid was observed from a fixed frame of reference located approximately 1.0m directly in front of the grid center (Figure 17b). From this vantage point a number of grains were selected using the grid intersection points. The approximate size, shape and location of the selected surface grains were recorded on a grid map. These systematically gathered grains served as the grain population for this grid.

Two slightly different methods were used to select grains. The first method tends to produce lower n values (number of grains selected per grid) than the second method. It is hypothesized that these variations in n make no difference.

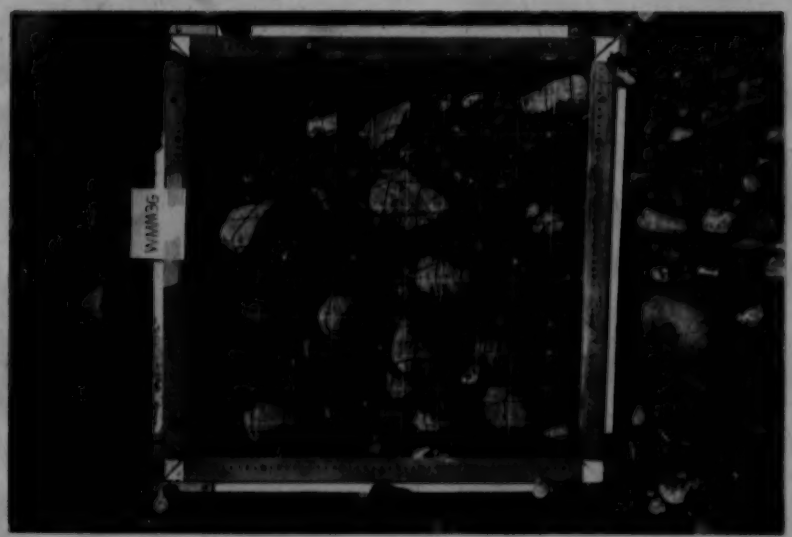

Figure 17a A Grid and Associated Terrace Gravels

Figure 17b A Grid and Its Fixed Frame of Reference

Method 1) A grain whose minor apparent axis was $\geq$ 8mm (see 1.5.2) and lay under a grid intersection point was selected.

Method 2) This method required that the grid intersection points be examined in a specific order. The grid was divided into 10 columns each consisting of 10 grid intersection points. The columns were sampled from left to right. Each column was examined from the top to the bottom. In all cases, if a grain had a minor apparent axis $\geq$ 8mm and lay beneath a grid intersection, it was chosen. If the grain's minor apparent axis was < 8mm, the point was considered barren and another clast was sought by moving either up, right, down or to the left along one of the two grid lines composing the intersection. The search continued as far as the next intersection. Only one grain search was allowed per barren point, the direction of search being varied by 90^{o} clockwise for each successive barren point encountered. If a suitable grain was discovered along the grid line and it was not under the adjacent intersection, it was collected as a representative

of that intersection. In this latter case, as well as when no suitable grain was found at all, the barren point was left without representation.

Step 3) Where useful for clarity purposes the surface was sprayed white (spray paint) and the grid was photographed from the frame of reference (Figures 18a and b).

Step 4) By constant reference to the map the selected grains were carefully removed to prevent face collapse and subsequent loss. In a number of cases where there was a partial face collapse a selected stone could be identified and recovered from the debris because its size and shape (assistance from the grid map) were known and it was partially white due to spraying. The A_t, B_t and C_t axes of these selected grains were then measured by calipers and recorded.

Step 5) Prints of the grid were later examined. Those clasts extracted in the field were located by means of the grid map and the major and minor apparent axes a_t and b_t were measured. The white paint often made the trace outlines of the surface grains more evident.

Since on the prints (approximately 11.5 x 8cm), the millimeter divisions could be discerned on the grid frame metric rulers, it can be inferred that the

Figure 18a Grid and Unsprayed Terrace Gravel Surface

Figure 18b Grid and Sprayed Terrace Gravel Surface

photographic resolution was 1.0mm. Although the grids were generally 1/7 life size on the prints, and therefore the millimeter divisions approximately 0.14mm on these prints, the calipers could measure down to 0.02mm and thus could accurately measure the divisions on the millimeter rule.

3.4 Data Analysis

3.4.0 Introduction

The objective of this experiment is to observe the effect variations in assigning linear dimensions to selected grains have on their respective grain-size distributions, and to compare these results with those predicted by the numerical method. Because identical grains of the surface layer population are employed in a given grid-by-number experiment, differences in a grain-size distribution must be a consequence of treatment (grain-size measurement).

The remainder of this section discusses the test procedures whereby specific predictions of the numerical method are compared with the empirical data. Also, a method for examining the effect of sample number on the results is described.

3.4.1 Primary Data Analysis

The true and apparent axes (A_t, B_t, C_t, a_t, b_t) of each grid-selected grain were measured (3.3.2). Four additional grain-size measures (AB_t, ABC_t, BC_t, ab_t) (1.5.1) were also computed for each grain. The frequency of the data associated with each of these nine grain-size measures was determined by number using 0.25 Ø class intervals. From this grid-by-number data the values for nine cumulative size-frequency distributions were calculated for each grid.

The distributions associated with each grid were plotted on arithmetic probability paper. For each of these curves, Ø values were determined which permitted the computation of the median, mean, standard deviation, skewness and kurtosis parametric values by Folk and Ward statistics (King, 1966).

3.4.2 The Wilcoxon Matched Pairs Signed Ranks Test

The Wilcoxon Test utilizes both direction and magnitude differences within matched pairs to test whether two treatments are different. This paired non-parametric test was used because it does not require the assumption that the populations being examined are normally distributed.

In the Wilcoxon Test, differences are initially ranked without regard to sign. Subsequently, both positive and negative values are totalled and the smallest value noted. This value is compared with the Wilcoxon Table and its significance determined for the selected probability level (in this experiment $\alpha = 0.05$ for two-tailed tests; $\alpha = 0.025$ for one-tailed tests). The rationale of the test is that if two treatments are equivalent, then the sums of the positive and negative ranks should be about equal. If the sums are considerably different then the null hypothesis, H_0, that the treatments do not differ is rejected and H_1, the alternative hypothesis accepted (see Siegel, 1956, p.75-83 for more details).

In this study 20 matched pairs were used in each test, each pair being derived from a different grid experiment. For a given test of two treatment types, all values tested were for the same parameter, e.g., the Ø values of 20 B_{t50}-a_{t50} matched pairs. The method of analysis is similar to that of McGinn (1971, p.17-20); see also 1.5 and 2.3.3.

3.4.3 Testing Procedures A to F

Test Procedure A

The Wilcoxon Test (two-tailed) was used to test all possible combinations of median and mean matched pairs consisting of both true axial and apparent values. The ABC_{t50} and $\overline{ABC}_t$ values were matched with each of the other five true axial medians and means respectively, and tested. As well, the standard deviation, skewness and kurtosis parametric values of five pairs (B_t-ABC_t, B_t-a_t, ABC_t-a_t, BC_t-ab_t, C_t-b_t) were tested.

This initial testing procedure serves to detect general relationships between true and apparent axial distributions. Special emphasis was given to the five pairs because of McGinn's (1971) finding that grid-by-number (B_t) and (ABC_t) distributions were statistically equivalent (1.5.1) and Kellerhals et al (1975, p.84) statement that:

> "Even in the case of nonuniform materials, the observed distribution of a can be expected to resemble the true distribution of B in first approximation, and similarly the observed b-distribution will resemble the true C-distribution."

Test Procedure B

This testing procedure utilized the Wilcoxon Test to examine specific numerical method predictions for grid-by-number (B_t) and (a_t) distributions, and grid-by-number (C_t) and (b_t) distributions. B_{t50} and $\overline{B}_t$ were converted by means of Figure 14a) to obtain a_{p50} and $\overline{a}_p$ values respectively; similarly C_{t50} and $\overline{C}_t$ were converted by means of Figure 14b) to obtain b_{p50} and $\overline{b}_p$ values respectively (henceforth: a_{p50}, $\overline{a}_p$, b_{p50} and $\overline{b}_p$ are terms denoting predicted median and mean apparent axial values calculated as follows:

Example of conversion of B_{t50} into a_{p50}

average $k_1 = \frac{B_{t50}}{A_{t50}}$, average $k_2 = \frac{C_{t50}}{B_{t50}}$

using this average k_1 and k_2 in Figure 14a), $\frac{(\bar{a}-B)100}{B} = X$

$a_{p50}=B_{t50}\ (\frac{X}{100} + 1)$, $\bar{a}_p$ is formed in the same way except $\bar{A}_t$, $\bar{B}_t$ and $\bar{C}_t$ are used.

Example of conversion of C_{t50} into b_{p50}

average $k_2 = \frac{C_{t50}}{B_{t50}}$

using this average k_2 in Figure 14b), $\frac{(\bar{b}-C)100}{C} = Y$

$b_{p50} = C_{t50}(\frac{Y}{100} + 1)$, $\bar{b}_p$ is formed in the same way except $\bar{B}_t$ and $\bar{C}_t$ are used.

The four sets of 20 matched pairs (a_{t50}-a_{p50}, $\bar{a}_t$-$\bar{a}_p$, b_{t50}-b_{p50}, $\bar{b}_t$-$\bar{b}_p$) were then compared using the Wilcoson Test (two-tailed).

Test Procedure C

This testing procedure utilized the Wilcoxon Test to examine the relationship between grid-by-number (C_t) and (b_t) distributions. In contrast to testing procedure B which had similar objectives, b_{t50} and b_t were converted by means of Figure 14b) to obtain C_{p50} and $\bar{C}_p$ (see 2.3.1 for more details on conversion). The two sets of 20 matched pairs (C_{t50}-C_{p50}, $\bar{C}_t$-$\bar{C}_p$) were then compared using the Wilcoxon Test (two-tailed).

Test Procedure D

This testing procedure employed the Wilcoxon Test to investigate the relationship among the four methods of estimating the average k_2 ($\frac{C_{t50}}{B_{t50}}$, $\frac{\bar{C}_t}{\bar{B}_t}$, $\frac{b_{t50}}{a_{t50}}$, $\frac{\bar{b}_t}{\bar{a}_t}$). The Wilcoxon Test (two-tailed) was applied to all six average k_2 estimate combinations, each consisting of 20 matched pairs

$(\frac{C_{t50}}{B_{t50}} - \frac{\bar{C}_t}{\bar{B}_t}, \frac{C_{t50}}{B_{t50}} - \frac{b_{t50}}{a_{t50}}, \frac{C_{t50}}{B_{t50}} - \frac{\bar{b}_t}{\bar{a}_t}, \frac{\bar{C}_t}{\bar{B}_t} - \frac{b_{t50}}{a_{t50}}, \frac{\bar{C}_t}{\bar{B}_t} - \frac{\bar{b}_t}{\bar{a}_t}, \frac{b_{t50}}{a_{t50}} - \frac{\bar{b}_t}{\bar{a}_t})$.

As well, the arithmetic and weighted mean were calculated for each of these average k_2 methods.

Test Procedure E

This testing procedure used the Wilcoxon Test (two-tailed) to examine the realtionship between predicted sieve median and mean values based on either true or apparent axial values. Thus two sets of 20 matched pairs ($D_{sp50} - d_{sp50}$, $\overline{D}_{sp} - \overline{d}_{sp}$) were compared (henceforth: D_{sp50} and $\overline{D}_{sp}$ are terms denoting predicted median and mean sieve values calculated as follows:

average $k_2 = \frac{C_{t50}}{B_{t50}}$ or $\frac{\overline{C}_t}{\overline{B}_t}$

$D_{sp50} = \frac{C_{t50}}{2k_2} [2(1+k_2^2)]^{\frac{1}{2}}$ equation (4); $\overline{D}_{sp} = \frac{\overline{C}_t}{2k_2} [2(1+k_2^2)]^{\frac{1}{2}}$ equation (4)

Calculations required to obtain predicted sieve values d_{sp50} and $\overline{d}_{sp}$ were described in 2.3.1. These required average k_2 estimates $\frac{b_{t50}}{a_{t50}}$ and $\frac{\overline{b}_t}{\overline{a}_t}$ respectively.

Test Procedure F

The purpose of this testing procedure is to determine if the degree of difference between matched pairs which the numerical method predicts are of equal value, is dependent upon either grid sample size n, or the use of median versus mean values.

These particular matched pairs were employed because their predicted relationship is one of equivalence (no difference). In contrast, the numerical method predicts that differences between matched pairs $\overline{B}_t - \overline{a}_t$ or $BC_{t50} - b_{t50}$ for example, are dependent upon the average k values of each grid experiment. In this latter case, differences caused by factors such as sample size may be obscured.

The testing procedure utilized eight sets of 20 matched pairs

$a_{t50} - a_{p50}$, $b_{t50} - b_{p50}$, $C_{t50} - C_{p50}$, $D_{sp50} - d_{sp50}$, $\bar{a}_t - \bar{a}_p$, $\bar{b}_t - \bar{b}_p$, $\bar{C}_t - \bar{C}_p$ and $\bar{D}_{sp} - \bar{d}_{sp}$. The matched pairs were grouped according to the size of the sample and by parameter (median or mean) (Table II).

Table II Matched Pair Groups

n	Median	Mean
20 to 29	group 1 median	group 1 mean
30 to 39	group 2 median	group 2 mean
40 to 49	group 3 median	group 3 mean
50 to 59	group 4 median	group 4 mean
60 to 69	group 5 median	group 5 mean

Groups were compared with respect to their minimum and maximum differences, range of differences and the weighted mean of their differences.

CHAPTER FOUR

TERRACE GRAVEL EXPERIMENT RESULTS AND DISCUSSION

4.1 General Introduction

Chapter Four presents the results of the terrace gravel grid-by-number experiment described in Chapter Three. The degree to which the testing procedures confirm numerical method predictions for this non-uniform material is discussed.

4.2 The Data Used in the Wilcoxon Tests

The Ø5, Ø16, Ø25, Ø50, Ø75, Ø84, and Ø95 values of all true and apparent axial distributions are located in Appendix I. With these Ø values the median, mean, standard deviations, skewness and kurtosis parameters of each distribution can be calculated.* The median and mean Ø values of all true axial distributions are presented in Appendix II. The median and mean Ø values of a_t and b_t apparent axial distributions and numerical method predictions can be found in Table 16, Chapter Four.

4.3 Experimental Results and Discussion

4.3.0 Introduction

The results of testing procedures A to F described in 3.4.3 are presented and examined.

4.3.1 Testing Procedure A

The Wilcoxon Test results (Table 12) indicate that only three of the true and apparent axial matched pairs tested (B_t-ABC_t, ABC_t-a_t, BC_t-ab_t) have significantly similar median or mean values. For the five matched pairs which were tested using all five parameters it is observed:

*(Folk and Ward, 1957)

Table 12
Wilcoxon Test Comparison of True and Apparent
Axial Distribution Parameters

	Median			
	ABC_{t50}	a_{t50}	ab_{t50}	b_{t50}
A_{t50}	H_1	H_1	H_1	H_1
AB_{t50}	H_1	H_1	H_1	H_1
B_{t50}	H_0	H_1	H_1	H_1
ABC_{t50}		H_1	H_1	H_1
BC_{t50}	H_1	H_1	H_0	H_1
C_{t50}	H_1	H_1	H_1	H_1

	Mean			
	$\overline{ABC}_t$	$\overline{a}_t$	$\overline{ab}_t$	$\overline{b}_t$
$\overline{A}_t$	H_1	H_1	H_1	H_1
$\overline{AB}_t$	H_1	H_1	H_1	H_1
$\overline{B}_t$	H_0	H_1	H_1	H_1
$\overline{ABC}_t$		H_0	H_1	H_1
$\overline{BC}_t$	H_1	H_1	H_1	H_1
$\overline{C}_t$	H_1	H_1	H_1	H_1

Axial Measures	Standard Deviation	Skewness	Kurtosis
B_t-ABC_t	H_0	H_0	H_0
B_t-a_t	H_0	H_0	H_1
ABC_t-a_t	H_0	H_0	H_0
BC_t-ab_t	H_0	H_0	H_0
C_t-b_t	H_0	H_0	H_0

Null Hypothesis. H_0: the compared axial distributions do not differ with respect to the tested grain-size parameter at level of significance $\alpha=0.05$

Reject Null Hypothesis. H_1: the compared axial distributions do differ with respect to the tested grain-size parameter at level of significance $\alpha=0.05$

B_t-ABC_t matched pair

The null hypothesis is accepted for all five parameters, thus the two distributions are statistically equivalent. These findings are identical to those of McGinn (1971).

B_t-a_t matched pair

The null hypothesis is accepted for the standard deviation and kurtosis parameters. This indicates that while distributions have similar characteristics one of the grain-size measures produces coarser results.

ABC_t-a_t matched pair

The null hypothesis is accepted for all parameters except that of the median. While this indicates that the distributions based on these two measures are statistically similar the results are slightly confusing since B_t-ABC_t distributions are equivalent. This suggests B_t-a_t distributions are only slightly different with respect to median and mean values.

BC_t-ab_t matched pair

The null hypothesis is accepted for all parameters except that of the mean. Thus the distributions based on these two different measures are quite similar.

C_t-b_t matched pair

The null hypothesis is accepted for standard deviation, skewness and kurtosis parameters. Like the B_t-a_t matched pairs the distributions have similar characteristics but one of these measures produces coarser results.

Considering that the B_t-a_t distribution median and mean values are only slightly different and that the BC_t-ab_t distributions are quite similar, it is probable that the C_t-b_t distributions have only slightly

different median and mean values.

4.3.2 Testing Procedure B

The Wilcoxon Tests indicate that matched pairs a_{t50}-a_{p50}, $\bar{a}_t$-$\bar{a}_p$, b_{t50}-b_{p50} and $\bar{b}_t$-$\bar{b}_p$ are statistically equivalent. This strongly confirms the numerical method's predictive capability.

As discussed in 3.4.3 predicted median and mean apparent axial values are derived from median and mean true axial values by using Figures 14a) and b). In all cases, these figures predicted that $B > \bar{a}$ and $C > \bar{b}$ for the average k_1 and k_2 values used (Tables 13a and b). Table 14 which is based on Tables 13a and b, provides information on the ranges of X and Y.

Since these matched pairs are statistically equivalent it may be inferred that the grid-by-number (B_t) and (C_t) distributions in Testing Procedure A are coarser than the grid-by-number (a_t) and (b_t) distributions, respectively. It appears in approximate terms that the B_t and C_t distributions are 10 percent coarser (Table 14). Wilcoxon Tests (one-tailed) confirm that $B_{t50} > a_{t50}$, $\bar{B}_t > \bar{a}_t$, $C_{t50} > b_{t50}$, and $\bar{C}_t > \bar{b}_t$*.

4.3.3 Testing Procedure C

The Wilcoxon Tests reveal that C_{t50} is equivalent to C_{p50} but that the null hypothesis must be rejected for $\bar{C}_t$ and $\bar{C}_p$.

4.3.4 Testing Procedure D

The Wilcoxon Tests show that of the four average k_2 estimate methods all except $\frac{\bar{C}_t}{\bar{B}_t}$ provide statistically equivalent values. The arithmetic and weighted means support these findings and demonstrate $\frac{\bar{C}_t}{\bar{B}_t}$ derived k_2 values are probably slightly greater than the other three estimates (Table 15). Wilcoxon Tests (one-tailed) uphold this conclusion.

* > here signifies "is coarser than".

Table 13a

C_{p50}, a_{p50}, b_{p50}, D_{sp50} and d_{sp50} Values in mm for the 20 Grids

Grid Experiment	A_{t50} (mm)	B_{t50} (mm)	C_{t50} (mm)	$k_1 = \frac{B_{t50}}{A_{t50}}$	$k_2 = \frac{C_{t50}}{B_{t50}}$	$\frac{(\bar{a}-B)100}{B} = X$	$\frac{(\bar{b}-C)100}{C} = Y$	$a_{p50} = B_{t50}(\frac{X}{100}+1)$	$b_{p50} = C_{t50}(\frac{Y}{100}+1)$	D_{sp50} equation(4) (mm)	a_{t50} (mm)	b_{t50} (mm)	$k_2 = \frac{b_{t50}}{a_{t50}}$	correction factor derived Figure 14b	C_{p50} = corr. f. x b_{t50} (mm)	d_{sp50}, C_{p50} equation(4) (mm)
WCM3A	78.8	64.0	36.8	.81	.58	-12.9	- 8.8	55.7	33.6	51.9	48.5	29.9	.62	1.099	32.9	44.0
WCM3B	48.5	39.4	22.6	.81	.57	-12.9	- 8.5	34.3	20.7	32.3	34.3	21.1	.62	1.099	23.2	31.1
WCM3C	45.3	39.4	19.7	.87	.50	-16.0	- 6.7	33.1	18.4	31.1	34.3	16.0	.47	1.058	16.9	28.1
WCM5A	90.5	59.7	32.0	.66	.54	- 5.8	- 7.7	56.2	29.5	47.7	55.7	27.9	.50	1.067	29.8	47.0
WCM5B	48.5	34.3	19.7	.71	.57	- 7.7	- 8.5	31.7	18.0	28.2	45.3	19.7	.43	1.047	20.6	36.9
WCM5C	64.0	55.7	29.9	.87	.54	-15.8	- 7.7	46.9	27.6	44.6	39.4	21.1	.54	1.077	22.7	33.9
WCM6A	73.5	59.7	45.3	.81	.76	-12.1	-14.1	52.5	38.9	53.0	55.7	39.4	.71	1.124	44.3	54.0
WCM6B	104.0	63.6	36.8	.66	.54	- 5.8	- 7.7	64.6	34.0	54.8	48.5	32.0	.66	1.11	35.5	45.5
WCM6C	59.7	42.2	24.3	.71	.58	- 7.7	- 8.8	39.0	22.2	34.3	36.8	17.1	.46	1.055	18.0	30.5
WM10A	59.7	45.3	32.0	.76	.71	- 9.8	-12.4	40.9	28.0	39.0	42.2	29.9	.71	1.124	33.6	41.0
WM10B	45.3	34.3	19.7	.76	.57	-10.4	- 8.5	30.7	18.0	28.2	36.8	24.3	.66	1.11	27.0	34.5
WM10C	59.7	52.0	27.9	.87	.54	-15.8	- 7.7	43.8	25.8	41.6	32.0	18.4	.58	1.088	20.0	28.2
WM13A	48.5	36.8	24.3	.76	.66	-10.0	-11.0	33.1	21.6	31.1	36.8	26.0	.71	1.124	29.2	35.7
WM13B	52.0	39.4	22.6	.76	.57	-10.4	- 8.5	35.3	20.7	32.3	34.3	16.0	.47	1.058	16.9	28.1
WM13C	55.7	36.8	24.3	.66	.66	- 4.9	-11.0	35.0	21.6	31.1	42.2	22.6	.54	1.077	24.3	36.3
WM13D	39.4	26.0	16.0	.66	.62	- 5.3	- 9.9	24.6	14.4	21.4	26.0	14.9	.57	1.085	16.2	23.1
WM13E	45.3	29.9	19.7	.66	.66	- 4.9	-11.0	28.4	17.5	25.2	27.9	18.4	.66	1.11	20.4	26.1
WM13F	59.7	42.2	24.3	.71	.58	- 7.7	- 8.8	39.0	22.2	34.3	39.4	19.7	.50	1.067	21.0	33.2
WM13G	64.0	45.3	26.0	.71	.57	- 7.7	- 8.5	41.8	23.8	37.2	34.3	21.1	.62	1.099	23.2	31.1
WM13H	59.7	48.5	26.0	.81	.54	-13.0	- 7.7	42.2	24.0	38.7	42.2	21.1	.50	1.067	22.5	35.6
Arithmetic mean				0.75	0.59								0.58			
Weighted mean				0.74	0.59								0.57			

Table.13b

$\bar{c}_p$, $\bar{a}_p$, $\bar{b}_p$, $\bar{b}_{sp}$ and $\bar{d}_{sp}$ Values in mm for the 20 Grids

Grid Experiment	$\bar{A}_t$ (mm)	$\bar{B}_t$ (mm)	$\bar{C}_t$ (mm)	$k_1 = \frac{\bar{B}_t}{\bar{A}_t}$	$k_2 = \frac{\bar{C}_t}{\bar{B}_t}$	$\frac{(\bar{a}-B)100}{B} = X$	$\frac{(\bar{b}-c)100}{c} = Y$	$\bar{a}_p = \bar{B}_t(\frac{X}{100}+1)$	$\bar{b}_p = \bar{C}_t(\frac{Y}{100}+1)$	$\bar{b}_{sp}$ equation(4) (mm)	$\bar{a}_t$ (mm)	$\bar{b}_t$ (mm)	$k_2 = \frac{\bar{b}}{\bar{a}_t}$	correction factor derived Figure 14b	$\bar{c}_p =$ corr.f. $\times \bar{b}_t$ (mm)	$\bar{d}_{sp}$, $\bar{c}_p$ equation(4) (mm)
WCM3A	59.7	45.3	29.9	.76	.66	-10.0	-11.0	40.8	26.6	38.3	42.2	29.9	.71	1.124	33.6	41.0
WCM3B	52.0	39.4	24.3	.76	.62	-10.2	- 9.9	35.4	21.9	32.6	36.8	22.6	.61	1.096	24.8	33.7
WCM3C	48.5	36.8	22.6	.76	.61	-10.3	- 9.6	33.0	20.4	30.7	36.8	18.4	.50	1.067	19.6	31.0
WCM5A	84.4	55.7	34.3	.66	.62	- 5.3	- 9.9	52.7	30.9	46.0	48.5	26.0	.54	1.077	28.0	41.7
WCM5B	48.5	36.8	19.7	.76	.54	-10.5	- 7.7	32.9	18.2	29.4	39.4	19.7	.50	1.067	21.0	33.2
WCM5C	64.0	48.5	29.9	.76	.62	-10.2	- 9.9	43.6	26.9	40.1	39.4	19.7	.50	1.067	21.0	33.2
WCM6A	64.0	48.5	36.8	.76	.76	- 9.4	-14.1	43.9	31.6	43.1	45.3	27.9	.62	1.099	30.7	41.1
WCM6B	84.4	59.7	32.0	.71	.54	- 7.7	- 7.7	55.1	29.5	47.7	45.3	27.9	.62	1.099	30.7	41.1
WCM6C	55.7	42.2	24.3	.76	.58	-10.4	- 8.8	37.8	22.2	34.3	36.8	19.7	.54	1.077	21.2	31.6
WMM10A	52.0	42.2	27.9	.81	.66	-12.5	-11.0	36.9	24.8	35.7	36.8	26.0	.71	1.124	29.2	35.7
WMM10B	42.2	32.0	19.7	.76	.62	-10.2	- 9.9	28.7	17.7	26.4	39.4	22.6	.57	1.085	25.4	35.1
WMM10C	64.0	48.5	34.3	.76	.71	- 9.8	-12.4	43.7	30.0	41.8	34.3	21.1	.62	1.099	23.2	31.1
WMM3A	48.5	36.8	24.3	.76	.66	-10.0	-11.0	33.1	21.6	31.1	36.8	22.6	.61	1.096	24.8	33.7
WMM3B	55.7	39.4	24.3	.71	.62	- 7.6	- 9.9	36.4	21.9	32.6	34.3	17.1	.50	1.067	18.2	28.8
WMM3C	52.0	36.8	26.0	.71	.71	- 6.9	-12.4	34.3	22.8	31.7	39.4	22.6	.57	1.085	24.5	35.1
WMM3D	39.4	29.9	17.1	.76	.57	-10.4	- 8.5	26.8	15.6	24.5	27.9	16.0	.57	1.085	17.4	24.8
WMM3E	45.3	34.3	21.1	.76	.62	-10.2	- 9.9	30.8	19.0	28.3	32.0	19.7	.62	1.099	21.7	29.0
WMM3F	52.0	39.4	22.6	.76	.57	-10.4	- 8.5	35.3	20.7	32.3	39.4	21.1	.54	1.077	22.7	33.9
WMM3G	55.7	39.4	27.9	.71	.71	- 6.9	-12.4	36.7	24.4	34.0	34.3	22.6	.66	1.11	25.1	32.1
WMM3H	64.0	45.3	27.9	.71	.62	- 7.6	- 9.9	44.8	25.1	37.4	36.8	21.1	.57	1.085	22.9	32.7
Arithmetic mean				0.75	0.63								0.58			
Weighted mean				0.74	0.63								0.58			

Table 14

Ranges of $\frac{(\bar{a}-B)100}{B} = X$ and $\frac{(\bar{b}-C)100}{C} = Y$ in Tables 13a and b

Predicted Term	X	Y	Table
a_{p50}	-4.9 to -16.0		13a
$\bar{a}_p$	-5.3 to -12.5		13b
b_{p50}		-6.7 to -14.1	13a
$\bar{b}_p$		-7.7 to -14.1	13b

Table 15

Wilcoxon Tests (two-tailed) and Arithmetic and Weighted Mean Results for Four Average k_2 Estimate Methods

Method of estimating average k_2 and Wilcoxon Test results	$\frac{\bar{C}_t}{\bar{B}_t}$	$\neq \frac{C_{t50}}{B_{t50}}$	$= \frac{b_{t50}}{a_{t50}}$	$= \frac{\bar{b}_t}{\bar{a}_t}$
Arithmetic mean of 20 k_2 values	0.63	0.59	0.58	0.58
Weighted mean of 20 k_2 values	0.63	0.59	0.57	0.58

4.3.5 Testing Procedure E

Wilcoxon Tests indicate that matched pairs $D_{sp50}-d_{sp50}$ and $\bar{D}_{sp}-\bar{d}_{sp}$ are statistically equivalent. As discussed in 3.4.3, D_{sp50} and $\bar{D}_{sp}$ values are dependent upon numerical method predictions associated

with true axial median and mean values, while d_{sp50} and $\bar{d}_{sp}$ are derived from apparent axial median and mean values by the numerical method. The equivalence of these two sets of matched pairs supports numerical method predictive capability for nonuniform materials.

That D_{sp50} is equivalent to d_{sp50} is consistent with testing procedures B (C_{t50} is equivalent to C_{p50}) and C ($\frac{C_{t50}}{B_{t50}}$ and $\frac{b_{t50}}{a_{t50}}$ are equivalent estimates of the average k_2).

Since $D_{sp50} = \frac{C_{t50}}{2k_2}\left[2(1 + k_2^2)\right]^{\frac{1}{2}}$ where $k_2 = \frac{C_{t50}}{B_{t50}}$ (4)

and $d_{sp50} = \frac{C_{p50}}{2k_2}\left[2(1 + k_2^2)\right]^{\frac{1}{2}}$ where $k_2 = \frac{b_{t50}}{a_{t50}}$ (4), it is reasonable that D_{sp50} is equivalent to d_{sp50}.

That $\bar{D}_{sp}$ and $\bar{d}_{sp}$ are statistically equivalent is also consistent with testing procedures B ($\bar{C}_t$ is not equivalent to $\bar{C}_p$) and C ($\frac{\bar{C}_t}{\bar{B}_t} > \frac{\bar{b}_t}{\bar{a}_t}$ as an estimate of the average k_2), but in a more complex manner.

Using the arithmetic and weighted mean results (testing procedure C) in (4); $\bar{D}_{sp}=1.33\ (\bar{C}_t)$, where the average $k_2 = \frac{\bar{C}_t}{\bar{B}_t} = 0.63$

$\bar{d}_{sp}=1.41\ (\bar{C}_p)$, where the average $k_2 = \frac{\bar{b}_t}{\bar{a}_t} = 0.58$.

Since $\bar{D}_{sp}$ and $\bar{d}_{sp}$ are statistically equivalent then;

$1.33\ (\bar{C}_t) = 1.41\ (\bar{C}_p)$

$\bar{C}_t = 1.06\ \bar{C}_p$

Thus, for equivalence to occur between $\bar{D}_{sp}$ and $\bar{d}_{sp}$ it is probable that $\bar{C}_t$ is approximately 6 percent greater than $\bar{C}_p$. A Wilcoxon Test (one-tailed) supports this conclusion by demonstrating that $\bar{C}_t$ is significantly greater than $\bar{C}_p$.

4.3.6 Testing Procedure F

The numerical method predicts that the 8 sets of matched pairs tested in 4.3 should be equivalent. The Wilcoxon Tests show that difference in magnitude and direction for these matched pairs are not significant except for $\overline{C}_t$-$\overline{C}_p$. Table 16 presents testing procedure F's n group data and Table 17, an analysis of each group's minimum and maximum range, and weighted mean matched pair differences. It is observed that:

1) The maximum difference between matched pairs declines from group 1 to group 5. The minimum difference between the matched pairs is 0 for all groups. Only for group 2 mean is the maximum difference greater than that for the median based matched pairs. In general, the range of differences between matched pairs declines from group 1 to group 5.

2) The weighted means of small (.1, .2, .3) and large (.4, .5, .6) differences respectively are fairly similar. In the case of group 5 the median and mean weighted mean differences are less than the others, however, this may not be significant since they are based on the results of only one grid. The weighted means of all difference values (0 to .6) decrease from group 1 to group 5. Except for group 1, the median difference weighted means are greater than their mean counterparts.

3) Large matched pair differences are limited to a minority of grids (Table 18). All groups except groups 3 mean, 5 median and mean possess at least one grid experiment

Table 16
β Values for 8 Sets of Matched Pairs
which are Predicted to be Equivalent

Grid	n	Group	a_{t50} (β)	a_{p50} (β)	b_{t50} (β)	b_{p50} (β)	C_{t50} (β)	C_{p50} (β)	D_{sp50} (β)	d_{sp50} (β)	Group	$\bar{a}_t$ (β)	$\bar{a}_p$ (β)	$\bar{b}_t$ (β)	$\bar{b}_p$ (β)	$\bar{C}_t$ (β)	$\bar{C}_p$ (β)	$\bar{D}_{sp}$ (β)	$\bar{d}_{sp}$ (β)
WCM6A	23		-5.8	-5.7	-5.3	-5.3	-5.5	-5.5	-5.7	-5.8		-5.5	-5.5	-4.8	-5.0	-5.2	-4.9	-5.4	-5.4
WMM10C	24	group 1	-5.0	-5.5	-4.2	-4.7	-4.8	-4.3	-5.4	-4.8	group 1	-5.1	-5.5	-4.4	-4.9	-5.1	-4.5	-5.4	-5.0
WMM10B	27	median	-5.2	-4.9	-4.6	-4.2	-4.3	-4.8	-4.8	-5.1	mean	-5.3	-4.8	-4.5	-4.1	-4.3	-4.6	-4.7	-5.1
WCM5A	29		-5.8	-5.8	-4.8	-4.9	-5.0	-4.9	-5.6	-5.6		-5.6	-5.7	-4.7	-5.0	-5.1	-4.8	-5.5	-5.4
WCM3A	33		-5.6	-5.8	-4.9	-5.1	-5.2	-5.0	-5.7	-5.5		-5.4	-5.4	-4.9	-4.7	-4.9	-5.1	-5.3	-5.4
WCM3B	33		-5.1	-5.1	-4.4	-4.4	-4.5	-4.5	-5.0	-5.0		-5.2	-5.1	-4.5	-4.5	-4.6	-4.6	-5.0	-5.1
WCM6C	34		-5.2	-5.3	-4.1	-4.5	-4.6	-4.2	-5.1	-4.9		-5.2	-5.2	-4.3	-4.5	-4.6	-4.4	-5.1	-5.0
WCM3C	35	group 2	-5.1	-5.1	-4.0	-4.2	-4.3	-4.1	-5.0	-4.8	group 2	-5.2	-5.0	-4.2	-4.4	-4.5	-4.3	-4.9	-5.0
WCM5C	35	median	-5.3	-5.6	-4.4	-4.8	-4.9	-4.5	-5.5	-5.1	mean	-5.3	-5.4	-4.3	-4.8	-4.9	-4.4	-5.3	-5.1
WCM6B	35		-5.6	-6.0	-5.0	-5.1	-5.2	-5.2	-5.8	-5.5		-5.5	-5.8	-4.8	-4.9	-5.0	-4.9	-5.6	-5.4
WMM3A	36		-5.2	-5.1	-4.7	-4.4	-5.2	-5.0	-5.0	-5.2		-5.2	-5.1	-4.5	-4.4	-4.6	-4.6	-5.0	-5.1
WCM5B	40		-5.5	-5.0	-4.3	-4.2	-4.3	-4.4	-4.8	-5.2		-5.3	-5.0	-4.3	-4.2	-4.3	-4.4	-4.9	-5.1
WMM10A	41	group 3	-5.4	-5.4	-4.9	-4.8	-5.0	-5.1	-5.3	-5.4	group 3	-5.2	-5.2	-4.7	-4.6	-4.8	-4.9	-5.2	-5.2
WMM3H	46	median	-5.4	-5.4	-4.4	-4.6	-4.7	-4.5	-5.3	-5.2	mean	-5.2	-5.5	-4.4	-4.7	-4.8	-4.5	-5.2	-5.0
WMM3G	47		-5.1	-5.4	-4.4	-4.6	-4.7	-4.5	-5.2	-5.0		-5.1	-5.2	-4.5	-4.6	-4.8	-4.7	-5.1	-5.0
WMM3E	51		-4.8	-4.8	-4.2	-4.1	-4.3	-4.4	-4.7	-4.7		-5.0	-4.9	-4.3	-4.3	-4.4	-4.4	-4.8	-4.9
WMM3C	53	group 4	-5.4	-5.1	-4.5	-4.4	-4.6	-4.6	-5.0	-5.2	group 4	-5.3	-5.1	-4.5	-4.5	-4.7	-4.6	-5.0	-5.1
WMM3F	57	median	-5.3	-5.3	-4.3	-4.5	-4.6	-4.4	-5.1	-5.1	mean	-5.3	-5.1	-4.4	-4.4	-4.5	-4.5	-5.0	-5.1
WMM3B	58		-5.1	-5.1	-4.0	-4.4	-4.5	-4.1	-5.0	-4.8		-5.1	-5.2	-4.1	-4.5	-4.6	-4.2	-5.0	-4.9
WMM3D	64	group 5 median	-4.7	-4.6	-3.9	-3.9	-4.0	-4.0	-4.4	-4.5	group 5 mean	-4.8	-4.7	-4.0	-4.0	-4.1	-4.1	-4.6	-4.6

Table 17
Analysis of Matched Pair Differences
within Matched Pair Groups

Difference between Matched Pairs (Ø)	Group 1 n=20-29		Group 2 n=30-39		Group 3 n=40-49		Group 4 n=50-59		Group 5 n=60-69	
	Number		Number		Number		Number		Number	
	Median	Mean	Median	Mean	Median	Mean	Median	Mean	Median	Mean
0	4	2	7	5	2	2	6	5	2	3
.1	4	2	2	11	6	8	3	7	2	1
.2		1	10	9	5	2	4	2		
.3	2	4	3	1	1	4	1			
.4	1	4	6		1		2	2		
.5	4	2		2	1					
.6	1	1								
Total No.(.1,.2,.3)	6	7	15	21	12	14	8	9	2	1
Weighted Mean (.1,.2,.3)	.17	.23	.21	.15	.16	.17	.18	.12	.1	.1
Total No.(.4,.5,.6)	6	7	6	2	2	0	2	2	0	0
Weighted Mean (.4,.5,.6)	.50	.46	.40	.50	.45	0	.40	.40	0	0
Total No.(0 to .6)	16	16	28	28	16	16	16	16	4	4
Weighted Mean (0 to .6)	.25	.30	.19	.15	.18	.15	.14	.12	.05	.025

*absence of value indicates difference of this amount not observed in group

Table 18
Grids with Large Differences (.4,.5,.6)
in Table 17

Grid	Group		Large Differences		
WMM10B	group 1	median	.4	.5	
WMM10B	group 1	mean	.4	.5	
WMM10C	group 1	median		.5	.6
WMM10C	group 1	mean	.4	.5	.6
WCM6B	group 2	median	.4		
WCM6C	group 2	median	.4		
WCM5C	group 2	median	.4		
WCM5C	group 2	mean		.5	
WCM5B	group 3	median	.4	.5	
WMM3B	group 4	median	.4		
WMM3B	group 4	mean	.4		

with large differences.

Observation 3) helps to clarify observations 1) and 2) concerning maximum differences, maximum range and weighted means (0 to .6). Lower n groups have the largest differences, ranges and weighted means (0 to .6) because they have a greater proportion of grids with large differences and these have the greatest value (i.e., .6).

In general these results indicate that while small sample size grid tests can be performed such that differences between matched pairs predicted to be equivalent are small, there is a tendency for a relatively high proportion of these tests to exhibit very large matched pair differences. In contrast, a relatively low proportion of the larger sample tests tend to display very large matched pair differences. These results may be due to a decrease of chance variations with increased sample size.

Observation 2) furnishes evidence that matched pairs derived from mean data possess smaller differences. In this case, chance variations associated with mean values may be less than medians because the means utilize more distribution information.

4.3.7 Conclusion

Testing procedures B and C (summarized Table 19) demonstrate that the numerical method can be successfully employed to predict apparent axial measure values from true axial measure values. The converse is also true. Similarly, median and mean sieve diameter numerical method predictions based on actual true and apparent grain-size values are significantly similar (testing procedure E , Table 19).

Testing procedure D reveals three average k_2 estimates

Table 19
Summary of Testing Procedures B, C and E

Testing procedure	Based on true axial measures	Based on apparent axial measures	Statistical relation
	Wilcoxon Test (two-tailed)		
B	a_{p50}	a_{t50}	no difference
	$\bar{a}_p$	$\bar{a}_t$	no difference
	b_{p50}	b_{t50}	no difference
	$\bar{b}_p$	$\bar{b}_t$	no difference
C	C_{t50}	C_{p50}	no difference
	$\bar{C}_t$	$\bar{C}_p$	difference
E	D_{sp50}	d_{sp50}	no difference
	$\bar{D}_{sp}$	$\bar{d}_{sp}$	no difference
	Wilcoxon Test (one-tailed)		
B	B_{t50}	a_{t50}	$B_{t50} > a_{t50}$
	$\bar{B}_t$	$\bar{a}_t$	$\bar{B}_t > \bar{a}_t$
	C_{t50}	b_{t50}	$C_{t50} > b_{t50}$
	$\bar{C}_t$	$\bar{b}_t$	$\bar{C}_t > \bar{b}_t$
E	$\bar{C}_t$	$\bar{C}_p$	$\bar{C}_t > \bar{C}_p$

$\frac{C_{t50}}{B_{t50}}$, $\frac{b_{t50}}{a_{t50}}$, and $\frac{\bar{b}_t}{\bar{a}_t}$ are statistically equivalent. $\frac{\bar{C}_t}{\bar{B}_t}$ provides slightly larger k_2 values. This latter observation combined with the Wilcoxon test result $\bar{C}_t > \bar{C}_p$ is shown to be consistent with the finding that $\bar{D}_{sp}$ and $\bar{d}_{sp}$ are statistically similar (testing procedure E, Table 19).

Generally these results powerfully confirm the usefulness of the numerical method as it is applied here to the nonuniform terrace gravel deposits. For a given grid experiment the findings of testing procedure F indicate that large sample size and the use of mean values tends to yield smaller differences between estimates of equivalent grain-size measure values.

CHAPTER FIVE

SUMMARY AND CONCLUSIONS

5.1 General Introduction

This concluding chapter discusses the numerical method with respect to the four empirical experiments examined in this thesis. Specific attention is given to the techniques, limitations and advantages of sampling gravels using only photographs of their apparent surfaces.

5.2 The Four Empirical Experiments and the Numerical Method

The four empirical experiments, which test numerical method predictions for nonuniform materials, vary with respect to material, sampling situation and sampling procedure (Table 20). These variations permit different aspects of the numerical method to be tested. As observed, the results of each of the four experiments confirm numerical method predictions.

The numerical method like any other method, model or theory will only achieve popular acceptance as its basic capabilities and limitations are clearly defined and thoroughly tested. The four experiments provide a clear indication of the numerical method's broad predictive powers. Duplication or modification of any or all of these experiments would further assist in determining the reliability of the numerical method predictions.

Experiments slightly different from the ones described are also necessary. Kellerhals et al (1975) predict that if chord length measurements, such as the maximum chord length in a predetermined direction are used instead of apparent axial measurements "...the resulting distribution should give directly a close approximation of the D_s distribution.".

Table 20
Variations among the Four Empirical Experiments

Empirical Experiment	Literature Reference	Thesis Reference	Number of Samples	Material	Sampling Situation	Sampling Procedures
1	Kellerhals et al (1975)	2.3.1	7	sandstone & cemented sand mixtures	laboratory analysis	grid-by-number (a_t,b_t); sieve analysis
2	Friedman (1962)	2.3.2	38	sandstone	laboratory analysis	grid-by-number (a_t); sieve analysis
3	McGinn (1971)	2.3.3	30	coarse fluvial gravels	surface layer of exposed gravel bars	grid-by-number (B_t); area-by-weight
4	This work	Chapters Three and Four	20	coarse fluvial gravels	terrace gravel exposures	grid-by-number (A_t, B_t, C_t, a_t, b_t)

Also Kellerhals et al (1975, p.89) discuss the fact that their numerical method predictions have been generated assuming a material is isotropic. Since clastic sediments are often anisotropic, the numerical method results presented in their paper may not be useful for samples with preferred orientation. They propose that this can be corrected for by changing the basic mathematical sampling process fundamental to the numerical method predictions so as to take into account "...the strength of the preferred orientation and the alignment of the thin section(s).". This can be tested.

5.3 Photographic Sampling of Gravel Surfaces

5.3.0 Introduction

Empirical experiments 3 and 4 show that the numerical method can be employed successfully in the photographic grain-size sampling of both apparent OGS and EGS. This final section reviews the evidence supporting this conclusion and discusses the techniques, limitations and advantages of sampling each type of surface photographically.

5.3.1 Photographic Sampling of an Apparent OGS

McGinn (1971) showed in his exposed gravel bar sampling experiments (example of an apparent OGS) that grid-by-number (B_t) and (b_t) distributions were quite similar (1.5.2). In Experiment 3 (2.3.3) using his data, the numerical method predicted with reasonable success the degree by which $\overline{B}_t$ was greater than $\overline{Q}_{sieve}$. It may be inferred from these results that equal success may be obtained if $\overline{B}_t$ was replaced by $\overline{b}_t$ (i.e., $\overline{b}_t > \overline{Q}_{sieve}$). However, as discussed in 1.5.2, the equivalence of grid-by-number (B_t) and (b_t) does depend on the C_t axis of most gravel bar grains being perpendicular to the surface plane.

The numerical method conversion of b_{t50} or $\bar{b}_t$ to a predicted median or mean sieve diameter would be facilitated if an average k_2 value could be derived from the actual measurement of the true axes of 50 to 100 grains within the general area where photographic sampling is taking place. Using equation (3), the predicted median and mean sieve diameters would equal $\frac{b_{t50}}{2}\left[2(1 + k_2^2)\right]^{\frac{1}{2}}$ and $\frac{\bar{b}_t}{2}\left[2(1 + k_2^2)\right]^{\frac{1}{2}}$ respectively. It must be remembered that these median and mean sieve values only apply to surface layer gravels.

5.3.2 Photographic Sampling of an Apparent EGS

In Experiment 4 (Chapters Three and Four) the terrace gravel apparent EGS was treated as a thin section surface (equivalence discussed in 1.3). In almost every case the median and mean values of grain-size measures which were predicted to be equivalent by the numerical method were statistically similar (4.3; Table 19). The predicted median and mean sieve diameters, d_{sp50} and $\bar{d}_{sp}$ can be calculated in the manner described in Experiment 1 (2.3.1). Because average k_2 estimates based on either true or apparent axes tend to be comparable (4.3.4, testing procedure D) true axes of grains need not be measured in the field.

Several problems unique to the photographic sampling of terrace gravel apparent EGS may be encountered.

1) The clasts composing the gravel deposit must be approximately ellipsoidal in shape. Fluviatile quartzite gravel found within the Edmonton area is ideal.
2) The terrace gravel deposit may have a pronounced fabric. As discussed in 5.2 numerical method predictions may have to be adjusted to take into

account preferred orientation.

3) The area within the grid frame may include more than one bed. This should not prove much of a problem as long as it is recognized and grain-size distributions determined for each bed.

4) Since much work is done in a cut-bank setting, it is often impossible to position oneself properly to take the grid photograph. Usually, the photograph is taken from approximately one meter from grid center and the line of sight passes through this center and is perpendicular to the surface plane. A solution to this problem involves placing the camera on a bracket attached to the grid frame (Appendix III).

For terrace gravels, the field and data analysis procedures necessary for the determination of the predicted median and mean sieve diameters, d_{sp50} and $\bar{d}_{sp}$ respectively, are provided in Appendix IV.

5.3.3 General Features of Apparent Surface Photographic Sampling

There are several points which must be taken into account when sampling gravel apparent OGS and apparent EGS. The number of grains collected per sample should be quite large, approximately 50 and the minor apparent axis of a selected clast should be no smaller than 8mm. There may be problems if the gravel is particularly coarse since the frame and grid require a relatively flat surface. In this case, a frame bearing rulers but no grid may be used. The grid can be superimposed later on the photograph and scale determined using the rulers. If grid-by-number results are to be directly comparable to those of bulk sieve

analysis, the axial values of a clast should be counted as many times as it falls under grid intersection points (see Kellerhals and Bray, 1971, p.1168 and conversion factor theory 1.4.4).

5.3.4 Advantages of Photographic Sampling

The grain-size sampling of river bar and terrace gravel deposits by photography has a number of advantages. Time savings may enable more comprehensive sampling programs to be considered. Because of its speed, ephemeral features associated with river channels or beaches may be more easily studied. Field work time-savings could be paralleled by the automated analysis of the photographs. Finally, it may be the only reasonable sampling technique to employ in certain undersea or extraterrestial environments.

BIBLIOGRAPHY

Adams, J. Sieve Size Statistics from Grain Measurement. Journ. of Geol., V.85, pp.209-227, 1977.

Allen, J. R. L. Notes Toward a Theory of Concentration of Solids in Natural Sands. Geol. Mag., V.106, No.4, pp.309-321, 1969.

Folk, R. L. and Ward, W. C. "Brazos River Bar, A Study in the Significance of Grain Size Parameters." Journ. of Sed. Pet., V.27, pp.514-529, 1957.

Friedman, G. M. Determination of Sieve-Size Distribution from Thin-Section Data for Sedimentary Petrological Studies. Journ. of Geol., V.66, pp.394-416, 1958.

_____ Comparison of Moment Measures for Sieving and Thin-Section Data in Sedimentary Petrological Studies. Journ. of Sed. Pet., V.32, pp.15-25, 1962.

Johansson, C. E. Orientation of Pebbles in Running Water. A Laboratory Study. Geografiska Annaler, V. 45, pp. 85-112, 1963.

Kellerhals, R. and Bray, D. I. Sampling Procedures for Coarse Fluvial Sediments. Journ. of the Hydraulics Division, ASCE, V.97, No. HY8, Proc. Paper 8279, pp.1165-1180, August, 1971.

_____ Comments on 'An Improved Method for Size Distribution of Stream Bed Gravel' by Luna B. Leopold. Water Resources Research, V.7, No.4, pp.1045-1047, August, 1971a.

_____ Shaw, J. and Arora, V. K. On Grain Size from Thin Sections. Journ. of Geol., V.83, pp.79-96, 1975.

King, C. A. M. Techniques in Geomorphology. Edward Arnold Ltd., London, 1966.

Leopold, L. B. An Improved Method for Size Distribution of Stream Bed Gravel. Water Resources Research, V.6, No.5, pp.1357-1366, October, 1970.

McGinn, R. A. The Problem of Sampling Coarse Fluvial Gravels. Unpublished M.Sc. Thesis, University of Alberta, Edmonton, 62pp., 1971.

Pashinsky, A. F. Experience of the Study of Alluvial Deposits of the Psezuapse River. Soviet Hydrology, Selected Papers, No.3, pp.276-290, 1964.

Rains, R. B. Some Aspects of the Fluvial Geomorphology of the Whitemud Basin, Central Alberta. Unpublished Ph.D. Thesis, University of Alberta, Edmonton, 215pp., 1969.

Rosenfeld, M. A., Jacobson, L. and Fern, J. C. A Comparison of Sieve and Thin Section Technique for Size Analysis. Journ. of Geol., V.61, pp.114-132, 1953.

Shelford, R. Geomorphology of the Weed Creek Basin. Unpublished M.Sc. Thesis, University of Alberta, Edmonton, 122pp., 1974.

Siegel, S. Non-Parametric Statistics for the Behavioral Sciences. McGraw-Hill, New York, 1956.

Thornes, J. and Hewitt, K. Some Problems in Estimating Size and Shape Parameters of Unconsolidated Particles from Photographs. Paper presented to the British Geomorph. Res. Group, Preston Montford, October, 1967.

Westgate, J. A. The Quaternary Geology of the Edmonton Area, Alberta. Proc. of the Symp. on Ped. and Quat. Res., University of Alberta Edmonton, pp.129-151, 1969.

Wolman, M. G. A Method of Sampling Coarse River Bed Material. Transactions of the American Geophysical Union, V.35, No.6, pp.951-956, December, 1954.

Whitten, D. G. A. and Brooks, J. R. V. A Dictionary of Geology. Penquin Books Ltd., Maryland, USA, 1972.

APPENDIX I

Important Ø Values
of all True and Apparent Axial Distributions

	A_t	AB_t	B_t	ABC_t	BC_t	C_t	a_t	ab_t	b_t
WCM3A									
Ø5	-3.9	-3.8	-3.2	-3.7	-3.2	-3.2	-3.9	-3.6	-3.2
Ø16	-4.4	-4.3	-4.0	-4.0	-4.0	-3.6	-4.3	-4.0	-3.9
Ø25	-5.2	-4.9	-4.8	-4.5	-4.3	-4.0	-4.9	-4.6	-4.2
Ø50	-6.3	-6.2	-6.0	-5.9	-5.7	-5.2	-5.6	-5.4	-4.9
Ø75	-6.9	-6.5	-6.2	-6.3	-6.2	-5.9	-6.3	-6.0	-5.6
Ø84	-7.0	-6.7	-6.4	-6.5	-6.3	-6.0	-6.4	-6.1	-5.8
Ø95	-7.7	-7.3	-7.1	-7.1	-6.9	-6.3	-7.0	-6.5	-6.3
WCM3B									
Ø5	-4.2	-4.2	-3.9	-3.9	-3.9	-3.2	-4.0	-3.6	-3.2
Ø16	-4.8	-4.7	-4.4	-4.4	-4.2	-3.8	-4.2	-3.9	-3.5
Ø25	-5.3	-5.1	-4.8	-4.8	-4.4	-4.0	-4.5	-4.2	-3.8
Ø50	-5.6	-5.4	-5.3	-5.3	-5.0	-4.5	-5.1	-4.7	-4.4
Ø75	-6.4	-6.2	-6.1	-6.0	-5.8	-5.3	-6.0	-5.8	-5.2
Ø84	-6.6	-6.5	-6.2	-6.2	-6.0	-5.6	-6.2	-5.9	-5.6
Ø95	-7.0	-6.8	-6.6	-6.8	-6.6	-6.6	-6.7	-6.5	-6.1
WCM3C									
Ø5	-4.2	-3.9	-3.7	-3.9	-3.7	-3.1	-3.7	-3.4	-3.2
Ø16	-4.6	-4.4	-4.2	-4.2	-4.0	-3.6	-4.2	-3.8	-3.3
Ø25	-5.0	-4.8	-4.6	-4.6	-4.3	-3.7	-4.2	-3.9	-3.5
Ø50	-5.5	-5.4	-5.3	-5.1	-4.8	-4.3	-5.1	-4.9	-4.0
Ø75	-6.5	-6.2	-6.0	-6.0	-5.8	-5.5	-6.1	-5.7	-5.2
Ø84	-6.8	-6.6	-6.2	-6.3	-5.9	-5.7	-6.3	-5.8	-5.4
Ø95	-7.0	-6.8	-6.5	-6.6	-6.3	-5.9	-6.4	-6.0	-5.7
WCM5A									
Ø5	-4.3	-3.9	-3.9	-3.6	-3.6	-3.1	-3.6	-3.5	-3.1
Ø16	-5.6	-5.4	-5.1	-5.1	-4.4	-4.5	-4.6	-4.3	-4.0
Ø25	-5.7	-5.5	-5.2	-5.3	-5.0	-4.6	-5.1	-4.9	-4.3
Ø50	-6.5	-6.1	-5.9	-5.9	-5.6	-5.0	-5.8	-5.4	-4.8
Ø75	-6.7	-6.6	-6.3	-6.4	-6.1	-5.5	-6.3	-5.9	-5.1
Ø84	-7.0	-6.8	-6.4	-6.5	-6.2	-5.8	-6.4	-6.0	-5.3
Ø95	-7.4	-7.1	-6.9	-6.6	-6.4	-6.3	-6.9	-6.1	-5.9

Important Ø Values
of all True and Apparent Axial Distributions

	A_t	AB_t	B_t	ABC_t	BC_t	C_t	a_t	ab_t	b_t
WCM5B									
Ø5	-3.9	-3.7	-3.1	-3.4	-3.1	-3.1	-3.8	-3.3	-3.1
Ø16	-4.4	-4.2	-4.0	-4.0	-3.7	-3.1	-4.2	-3.6	-3.2
Ø25	-4.8	-4.4	-4.1	-4.2	-4.1	-3.3	-4.4	-3.9	-3.5
Ø50	-5.6	-5.5	-5.1	-5.1	-4.8	-4.3	-5.5	-5.0	-4.3
Ø75	-6.5	-6.3	-6.0	-6.0	-5.8	-5.2	-6.0	-5.8	-5.0
Ø84	-6.8	-6.7	-6.5	-6.4	-6.0	-5.6	-6.3	-6.0	-5.4
Ø95	-7.4	-7.1	-7.0	-6.7	-6.3	-6.0	-7.0	-6.3	-5.8
WCM5C									
Ø5	-4.9	-4.5	-4.2	-4.3	-3.9	-3.7	-3.7	-3.5	-3.1
Ø16	-5.0	-5.1	-4.9	-4.8	-4.5	-3.9	-4.3	-4.1	-3.5
Ø25	-5.2	-5.2	-5.0	-5.0	-4.7	-4.5	-4.8	-4.4	-3.7
Ø50	-6.0	-5.9	-5.8	-5.6	-5.4	-4.9	-5.3	-5.1	-4.4
Ø75	-6.5	-6.3	-6.0	-6.0	-5.7	-5.3	-5.9	-5.6	-4.9
Ø84	-6.9	-6.6	-6.2	-6.3	-6.1	-5.8	-6.2	-5.6	-5.1
Ø95	-7.3	-7.2	-7.1	-7.0	-6.8	-6.4	-6.6	-6.3	-6.0
WCM6A									
Ø5	-3.8	-3.8	-3.6	-3.6	-3.3	-3.1	-3.1	-3.1	-3.0
Ø16	-4.4	-4.4	-4.2	-4.2	-4.2	-3.9	-3.9	-3.7	-3.2
Ø25	-5.6	-5.4	-4.9	-5.2	-4.7	-4.4	-4.5	-4.1	-3.5
Ø50	-6.2	-6.2	-5.9	-5.9	-5.7	-5.5	-5.8	-5.6	-5.3
Ø75	-6.9	-6.6	-6.4	-6.5	-6.2	-6.2	-6.6	-6.1	-5.8
Ø84	-7.5	-7.3	-6.6	-7.1	-6.6	-6.3	-6.8	-6.6	-6.1
Ø95	-7.6	-7.5	-7.2	-7.3	-7.0	-7.0	-7.2	-6.8	-6.5
WCM6B									
Ø5	-4.4	-4.2	-3.9	-4.0	-3.8	-3.1	-3.7	-3.7	-3.1
Ø16	-5.2	-5.1	-4.8	-4.8	-4.4	-3.6	-4.6	-4.3	-3.6
Ø25	-5.6	-5.3	-5.1	-5.0	-4.6	-4.2	-5.0	-4.5	-4.2
Ø50	-6.7	-6.4	-6.1	-6.1	-5.8	-5.2	-5.6	-5.4	-5.0
Ø75	-7.1	-6.8	-6.4	-6.6	-6.3	-5.9	-6.3	-5.9	-5.6
Ø84	-7.2	-7.0	-6.7	-6.7	-6.5	-6.2	-6.4	-6.3	-5.9
Ø95	-7.4	-7.3	-7.0	-7.0	-6.9	-6.8	-6.8	-6.5	-6.2

Important Ø Values
of all True and Apparent Axial Distributions

	A_t	AB_t	B_t	ABC_t	BC_t	C_t	a_t	ab_t	b_t
WMM6C									
Ø5	-3.7	-3.4	-3.1	-3.4	-3.1	-3.1	-3.4	-3.4	-3.0
Ø16	-4.4	-4.3	-3.9	-4.0	-3.8	-3.2	-3.9	-3.8	-3.1
Ø25	-4.5	-4.4	-4.3	-4.2	-3.9	-3.4	-4.2	-4.0	-3.4
Ø50	-5.9	-5.7	-5.4	-5.4	-5.1	-4.6	-5.2	-4.8	-4.1
Ø75	-6.9	-6.7	-6.4	-6.3	-6.1	-5.6	-5.9	-5.5	-5.2
Ø84	-7.2	-6.9	-6.9	-6.6	-6.2	-5.9	-6.5	-6.2	-5.6
Ø95	-8.1	-8.0	-7.8	-7.6	-7.3	-6.9	-7.3	-6.8	-6.5
WMM10A									
Ø5	-4.2	-3.9	-3.5	-3.7	-3.3	-3.1	-3.6	-3.3	-3.1
Ø16	-4.8	-4.6	-4.5	-4.4	-4.2	-3.8	-3.9	-3.8	-3.4
Ø25	-5.1	-4.9	-4.7	-4.8	-4.4	-4.2	-4.4	-4.3	-3.8
Ø50	-5.9	-5.8	-5.5	-5.6	-5.2	-5.0	-5.4	-5.2	-4.9
Ø75	-6.4	-6.2	-6.0	-6.0	-5.9	-5.6	-6.1	-5.8	-5.6
Ø84	-6.5	-6.4	-6.3	-6.1	-6.1	-5.7	-6.3	-6.0	-5.7
Ø95	-6.9	-6.9	-6.6	-6.3	-6.4	-6.2	-6.7	-6.5	-6.1
WMM10B									
Ø5	-3.6	-3.5	-3.2	-3.1	-3.2	-3.1	-3.8	-3.6	-3.1
Ø16	-4.4	-4.0	-3.9	-3.9	-3.7	-3.2	-4.3	-3.9	-3.4
Ø25	-4.6	-4.4	-4.0	-4.4	-3.8	-3.5	-4.5	-4.2	-3.8
Ø50	-5.5	-5.2	-5.1	-4.9	-4.6	-4.3	-5.2	-5.1	-4.6
Ø75	-6.3	-6.0	-5.5	-5.8	-5.5	-5.4	-6.1	-5.9	-5.4
Ø84	-6.4	-6.3	-6.0	-6.0	-5.8	-5.5	-6.4	-6.0	-5.6
Ø95	-6.6	-6.5	-6.2	-6.4	-6.1	-5.9	-6.9	-6.4	-6.2
WMM10C									
Ø5	-4.6	-4.3	-4.3	-4.1	-3.8	-3.5	-3.4	-3.1	-3.1
Ø16	-5.0	-4.8	-4.6	-4.7	-4.5	-4.2	-3.9	-3.7	-3.2
Ø25	-5.3	-5.0	-4.8	-4.9	-4.6	-4.4	-4.3	-4.0	-3.5
Ø50	-5.9	-5.8	-5.7	-5.6	-5.4	-4.8	-5.0	-4.7	-4.2
Ø75	-6.8	-6.5	-6.5	-6.3	-6.1	-5.7	-6.3	-5.9	-5.6
Ø84	-7.0	-6.8	-6.6	-6.8	-6.5	-6.3	-6.5	-6.1	-5.8
Ø95	-7.3	-7.1	-6.9	-7.0	-6.7	-6.4	-6.9	-6.7	-6.4

Important Ø Values
of all True and Apparent Axial Distributions

	A_t	AB_t	B_t	ABC_t	BC_t	C_t	a_t	ab_t	b_t
WMM3A									
Ø5	-4.2	-4.0	-3.6	-3.7	-3.6	-3.1	-3.7	-3.4	-3.1
Ø16	-4.4	-4.2	-3.9	-4.0	-3.8	-3.4	-3.9	-3.6	-3.2
Ø25	-4.6	-4.4	-4.3	-4.3	-4.0	-3.8	-4.2	-3.7	-3.7
Ø50	-5.6	-5.5	-5.2	-5.2	-4.9	-4.6	-5.2	-5.1	-4.7
Ø75	-6.4	-6.1	-6.0	-5.9	-5.7	-5.4	-5.9	-5.6	-5.3
Ø84	-6.8	-6.8	-6.5	-5.4	-6.1	-5.8	-6.4	-6.0	-5.5
Ø95	-7.6	-7.3	-7.3	-6.4	-7.1	-6.9	-7.1	-6.8	-6.3
WMM3B									
Ø5	-3.7	-3.7	-3.6	-3.6	-3.4	-3.1	-3.6	-3.5	-3.1
Ø16	-4.5	-4.3	-4.1	-4.1	-3.9	-3.6	-4.0	-3.8	-3.2
Ø25	-4.8	-4.7	-4.4	-4.4	-4.2	-3.9	-4.1	-4.0	-3.5
Ø50	-5.7	-5.5	-5.3	-5.3	-5.1	-4.5	-5.1	-4.8	-4.0
Ø75	-6.6	-6.4	-6.0	-6.1	-5.8	-5.4	-5.8	-5.4	-4.8
Ø84	-7.1	-6.8	-6.5	-6.6	-6.2	-5.6	-6.3	-5.9	-5.1
Ø95	-7.8	-7.5	-7.2	-7.3	-6.8	-6.5	-7.1	-6.5	-6.0
WMM3C									
Ø5	-3.8	-3.7	-3.4	-3.4	-3.2	-3.1	-3.4	-3.5	-3.1
Ø16	-4.7	-4.6	-4.3	-4.2	-4.0	-3.6	-4.4	-4.3	-3.6
Ø25	-5.1	-5.0	-4.7	-4.8	-4.5	-4.0	-4.9	-4.7	-4.2
Ø50	-5.8	-5.7	-5.2	-5.4	-5.0	-4.6	-5.4	-5.1	-4.5
Ø75	-6.4	-6.1	-5.9	-5.9	-5.7	-5.5	-5.9	-5.6	-5.0
Ø84	-6.6	-6.4	-6.1	-6.1	-6.1	-5.8	-6.1	-5.7	-5.4
Ø95	-6.9	-6.7	-6.5	-6.6	-6.3	-6.3	-6.4	-6.2	-5.9
WMM3D									
Ø5	-4.0	-3.8	-3.2	-3.7	-3.2	-3.1	-3.6	-3.4	-3.1
Ø16	-4.3	-4.1	-3.9	-3.9	-3.7	-3.2	-3.8	-3.6	-3.1
Ø25	-4.6	-4.4	-4.1	-4.2	-3.9	-3.3	-3.9	-3.7	-3.2
Ø50	-5.3	-5.0	-4.7	-4.7	-4.3	-4.0	-4.7	-4.4	-3.9
Ø75	-6.0	-5.8	-5.4	-5.5	-5.2	-4.8	-5.4	-5.1	-4.8
Ø84	-6.3	-6.2	-6.0	-5.9	-5.5	-5.1	-5.8	-5.4	-5.1
Ø95	-6.8	-6.7	-6.5	-6.5	-6.2	-5.8	-6.5	-6.1	-5.5

Important Ø Values
of all True and Apparent Axial Distributions

	A_t	AB_t	B_t	ABC_t	BC_t	C_t	a_t	ab_t	b_t
WMM3E									
Ø5	-3.7	-3.6	-3.2	-3.4	-3.2	-3.1	-3.7	-3.6	-3.1
Ø16	-4.3	-4.1	-3.9	-3.9	-3.7	-3.2	-4.0	-3.8	-3.2
Ø25	-4.6	-4.4	-4.1	-4.1	-3.8	-3.5	-4.2	-4.0	-3.4
Ø50	-5.5	-5.3	-4.9	-5.0	-4.5	-4.3	-4.8	-4.5	-4.2
Ø75	-6.3	-6.2	-5.9	-6.0	-5.8	-5.5	-5.8	-5.5	-5.3
Ø84	-6.6	-6.5	-6.4	-6.3	-6.0	-5.8	-6.1	-5.9	-5.5
Ø95	-7.1	-6.9	-6.8	-6.8	-6.4	-6.1	-6.5	-6.3	-5.9
WMM3F									
Ø5	-4.2	-4.0	-3.8	-3.8	-3.5	-3.1	-3.9	-3.8	-3.1
Ø16	-4.6	-4.4	-4.1	-4.2	-3.8	-3.2	-4.3	-4.0	-3.5
Ø25	-4.8	-4.6	-4.4	-4.4	-4.1	-3.7	-4.4	-4.2	-3.7
Ø50	-5.9	-5.7	-5.4	-5.5	-5.2	-4.6	-5.3	-4.9	-4.3
Ø75	-6.5	-6.3	-6.0	-6.0	-5.8	-5.4	-6.0	-5.5	-5.1
Ø84	-6.7	-6.6	-6.3	-6.3	-6.0	-5.7	-6.2	-5.8	-5.3
Ø95	-7.3	-7.1	-7.0	-6.9	-6.5	-6.3	-6.8	-6.3	-6.0
WMM3G									
Ø5	-4.0	-4.2	-3.9	-3.9	-3.7	-3.2	-3.7	-3.5	-3.2
Ø16	-4.6	-4.4	-4.1	-4.2	-4.0	-3.7	-4.0	-3.8	-3.5
Ø25	-4.7	-4.5	-4.3	-4.4	-4.1	-3.8	-4.3	-4.1	-3.6
Ø50	-6.0	-5.7	-5.5	-5.5	-5.2	-4.7	-5.1	-4.7	-4.4
Ø75	-6.5	-6.3	-6.1	-6.1	-5.8	-5.3	-6.1	-5.5	-5.1
Ø84	-6.7	-6.5	-6.4	-6.2	-6.0	-6.1	-6.3	-6.0	-5.5
Ø95	-7.1	-6.9	-6.7	-6.7	-6.5	-6.3	-6.7	-6.4	-6.2
WMM3H									
Ø5	-4.4	-4.3	-4.0	-4.2	-3.8	-3.5	-3.9	-3.6	-3.1
Ø16	-4.8	-4.7	-4.4	-4.5	-4.1	-3.8	-4.1	-3.9	-3.2
Ø25	-5.1	-4.9	-4.6	-4.6	-4.3	-4.0	-4.3	-4.2	-3.8
Ø50	-5.9	-5.8	-5.6	-5.4	-5.2	-4.7	-5.4	-5.1	-4.4
Ø75	-6.3	-6.3	-6.2	-5.9	-5.8	-5.6	-5.9	-5.6	-5.4
Ø84	-6.7	-6.5	-6.5	-6.1	-6.0	-5.8	-6.1	-6.0	-5.6
Ø95	-7.4	-7.0	-6.8	-6.8	-6.6	-6.4	-6.8	-6.4	-6.2

APPENDIX II

Median and Mean Ø Values for all True Axial Distributions

GRID	A_{t50} (Ø)	AB_{t50} (Ø)	B_{t50} (Ø)	ABC_{t50} (Ø)	BC_{t50} (Ø)	C_{t50} (Ø)	$\overline{A}_t$ (Ø)	$\overline{AB}_t$ (Ø)	$\overline{B}_t$ (Ø)	$\overline{ABC}_t$ (Ø)	$\overline{BC}_t$ (Ø)	$\overline{C}_t$ (Ø)
WCM3A	-6.3	-6.2	-6.0	-5.9	-5.7	-5.2	-5.9	-5.7	-5.5	-5.5	-5.3	-4.9
WCM3B	-5.6	-5.4	-5.3	-5.3	-5.0	-4.5	-5.7	-5.5	-5.3	-5.3	-5.1	-4.6
WCM3C	-5.5	-5.4	-5.3	-5.1	-4.8	-4.3	-5.6	-5.5	-5.2	-5.2	-4.9	-4.5
WCM5A	-6.5	-6.1	-5.9	-5.9	-5.6	-5.0	-6.4	-6.1	-5.8	-5.8	-5.4	-5.1
WCM5B	-5.6	-5.5	-5.1	-5.1	-4.8	-4.3	-5.6	-5.5	-5.2	-5.2	-4.8	-4.3
WCM5C	-6.0	-5.9	-5.8	-5.6	-5.4	-4.9	-6.0	-5.9	-5.6	-5.6	-5.3	-4.9
WCM6A	-6.2	-6.2	-5.9	-5.9	-5.7	-5.5	-6.0	-6.0	-5.6	-5.7	-5.5	-5.2
WCM6B	-6.7	-6.4	-6.1	-6.1	-5.8	-5.2	-6.4	-6.2	-5.9	-5.9	-5.6	-5.0
WCM6C	-5.9	-5.7	-5.4	-5.4	-5.1	-4.6	-5.8	-5.6	-5.4	-5.3	-5.0	-4.6
WMM10A	-5.9	-5.8	-5.5	-5.6	-5.2	-5.0	-5.7	-5.6	-5.4	-5.4	-5.2	-4.8
WMM10B	-5.5	-5.2	-5.1	-4.9	-4.6	-4.3	-5.4	-5.2	-5.0	-4.9	-4.7	-4.3
WMM10C	-5.9	-5.8	-5.7	-5.6	-5.4	-4.8	-6.0	-5.8	-5.6	-5.7	-5.5	-5.1
WMM3A	-5.6	-5.5	-5.2	-5.2	-4.9	-4.6	-5.6	-5.5	-5.2	-4.9	-4.9	-4.6
WMM3B	-5.7	-5.5	-5.3	-5.3	-5.1	-4.5	-5.8	-5.5	-5.3	-5.3	-5.1	-4.6
WMM3C	-5.8	-5.7	-5.2	-5.4	-5.0	-4.6	-5.7	-5.6	-5.2	-5.2	-5.0	-4.7
WMM3D	-5.3	-5.0	-4.7	-4.7	-4.3	-4.0	-5.3	-5.1	-4.9	-4.8	-4.5	-4.1
WMM3E	-5.5	-5.3	-4.9	-5.0	-4.5	-4.3	-5.5	-5.3	-5.1	-5.1	-4.7	-4.4
WMM3F	-5.9	-5.7	-5.4	-5.5	-5.2	-4.6	-5.7	-5.6	-5.3	-5.3	-5.0	-4.5
WMM3G	-6.0	-5.7	-5.5	-5.5	-5.2	-4.7	-5.8	-5.5	-5.3	-5.3	-5.1	-4.8
WMM3H	-5.9	-5.8	-5.6	-5.4	-5.2	-4.7	-6.0	-5.7	-5.5	-5.3	-5.1	-4.8

APPENDIX III

Grid Camera Bracket

The bracket consists of a shaft which is attached by means of a hinge midway along the bottom of the grid frame. When the grid frame is in a near vertical position, the shaft is slung by means of two equi-length wires connected to the top corners of the frame such that the end of the shaft is located approximately over the center of the grid. A small camera is placed in a holder which is bolted to the shaft near the end. The holder-camera arrangement is approximately one meter from grid center and aligned so that the line of sight passes through the center and is perpendicular to the surface plane. By means of a cable shutter release or timer, this grid frame-camera system may be held over terrace gravel deposits, and consistently centered, in-focus, photographs taken (Figures 17b, 19).

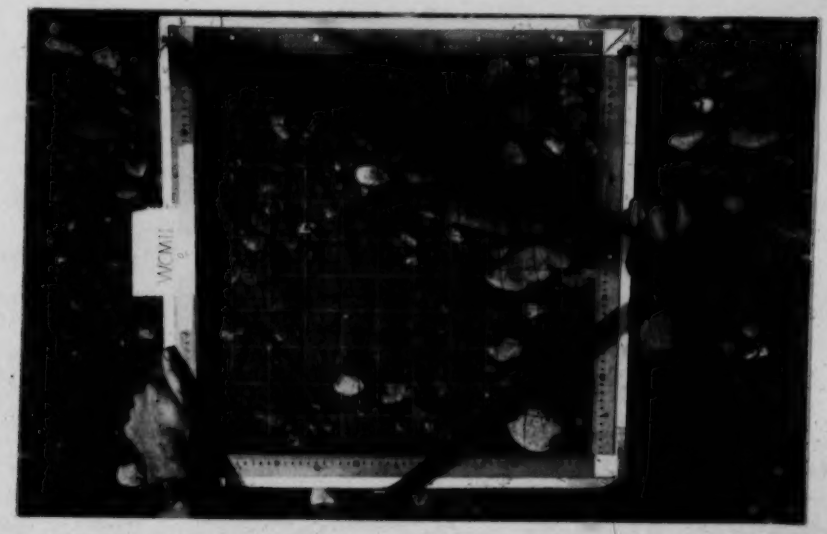

Figure 19 Grid Photograph Taken by means of Grid Camera Bracket and Cable Shutter Release

APPENDIX IV

Field and Data Analysis Procedures Used to Obtain the Predicted Median and Mean Sieve Diameters, d_{sp50} and $\overline{d}_{sp}$

1) Site Selection

   a) The clasts associated with the terrace gravel deposit should be approximately ellipsoidal in shape.

   b) Because numerical method predictions are for an isotropic material, terrace gravel deposits which appear quite isotropic and homogeneous are preferable.

   c) Grain-size analysis should be performed for only one bed.

2) Terrace Gravel Grid Placement and Photography

   a) The gravel surface should be modified so as to be approximately flat in order to decrease photographic scale distortion due to distance variations.

   b) For ease of photography use the grid camera bracket described in Appendix III.

   c) For clarity purposes the gravel surface may be sprayed white or colour film used.

   d) If the terrace gravels are extremely coarse the frame with rulers but no grid may be used. The grid pattern may be superimposed on the print.

   e) Each grid should be labelled in some way.

3) Grain Selection on the Prints

   a) 50 to 100 grains should be selected. This may require more than one grid photograph.

b) Select grains $\geq$ 8mm. found under the grid intersection points. If a clast lies under two intersection points it must be counted twice (Kellerhals and Bray, 1971).

4) Grain Measurement from the Prints

a) Measure the apparent major axis a_t, and apparent minor axis b_t, of each selected grain with calipers.

b) Determine the scale factor from the grid rulers and apply to the apparent axes values.

5) Primary Data Analysis

a) The frequency of the apparent major and minor axis data respectively is determined by number using 0.25 Ø or 0.50 Ø class intervals.

b) The cumulative size-frequency distribution is plotted on arithmetic probability paper.

c) The Ø 16, Ø 15 and Ø 84 values of the distributions in b) are noted. The Ø 50 values of the apparent major and minor distributions are the values of a_{t50} and b_{t50}, respectively. The Folk and Ward mean $\frac{Ø\ 16 + Ø\ 15 + Ø\ 84}{3}$ of the apparent major and minor distributions yields the mean values $\bar{a}_t$ and $\bar{b}_t$, respectively.

6) The Numerical Method Median and Mean Sieve Values

The following presents the method of computing the predicted median sieve diameter, d_{sp50}.

a) Convert a_{t50} and b_{t50} values from Ø units to mm.

b) Calculate C_{p50}:

Using $k_2 = \frac{b_{t50}}{a_{t50}}$ in Figure 14b, $\frac{(\overline{b} - C)100}{C} = Y$,

$C_{p50}=(1.0-Y)(b_{t50})$

$\overline{C}_p$ is calculated in the same way except $\overline{b}_t$ and $\overline{a}_t$ are used.

c) Calculate d_{sp50}:

$$d_{sp50}=\frac{C_{p50}}{2k_2}\left[2(1+k_2^2)\right]^{\frac{1}{2}}$$

where $k_2=\frac{b_{t50}}{a_{t50}}$

$\overline{d}_{sp}$ is calculated in the same except $\overline{b}_t$, $\overline{a}_t$ and $\overline{C}_p$ are used.